Escola Tècnica Superior d'Enginyers
de Camins, Canals i Ports de Barcelona
UNIVERSITAT POLITÈCNICA DE CATALUNYA

PROJECTE O TESINA D'ESPECIALITAT

Títol

Influence of concrete flow on the mechanical properties of ordinary and fibre reinforced concrete

Influència del flux a les propietats mecàniques del formigó convencional i reforçat amb fibres

Autor/a

Elena Vidal Sarmiento

Tutor/a

Tutor intern: Antoni Marí Bernat
Tutor extern: Terje Kanstad (Norwegian University of Science and Technology, NTNU)

Departament

Enginyeria de la Construcció

Intensificació

Intensificació en Anàlisis i Projectes d'Estructures

Data

24 de gener de 2011

Department of Structural Engineering
Faculty of Engineering Science and Technology
NTNU- Norwegian University of Science and Technology

ACCESSIBILITY

MASTER THESIS <2010-2011>

SUBJECT AREA: Concrete technology	DATE: 21/01/2011	NO. OF PAGES: 119

TITLE:

Influence of concrete flow on the mechanical properties of ordinary and fibre reinforced concrete

Innvirkning av betongens strømning på mekaniske egenskaper av vanlig og fiberarmert betong

BY:

Elena Vidal Sarmiento
Civil engineering student
Technical University of Catalonia (UPC)
elena.vidal.sarmiento@hotmail.com

SUMMARY:

Self compacting concrete is often defined as a composite that possesses not only a very high workability, which results in a not necessary compaction, but also that resists segregation and maintains stable composition throughout transport and placing. However, two of the inner properties of SCC, fluidity and stability, seem, in a primary analysis, to be opposed. This research has tried to investigate how these two properties interact. More particularly, what is the influence of the flow of concrete in its stability. However, this potential instability caused by flow could transcend further than the fresh state, affecting also the hardened properties.

RESPONSIBLE TEACHER: Terje Kanstad

SUPERVISOR(S): Terje Kanstad (NTNU) and Antoni Marí Bernat (UPC)

CARRIED OUT AT: Structural department, NTNU

Preface

Self-compacting concrete (SCC) is an important and significant advance within concrete technology which is having a major impact on concrete practice. The study of its fresh behaviour contributes to complete the prediction of its final mechanical properties. In this context, this project has the purpose to investigate the influence of concrete flow on the mechanical properties of ordinary and fibre reinforced concrete.

This research has been carried out at the Structural Department of the Norwegian University of Science and Technology (NTNU). The work has been a part of a large research program denoted as COIN (Concrete Innovation Centre) managed by SINTEF, the largest independent research organization in Scandinavia, with a strong participation from the Structural Department.

The collaboration between the author's home university, Universitat Politècnica de Catalunya (UPC), and the NTNU through the Erasmus exchange program made possible the development of this work.

Acknowledgements

I would like to show my gratitude to all the people who help me in an academic and personal way during the development of this thesis. Therefore, I will express my sincere thanks in English and *Catalan*.

Firstly, I thank my supervisors at NTNU, Pr. Mette Geiker and Pr. Terje Kanstad, for bring me the opportunity to participate in this challenging research. I received all the necessary support and a warm working environment from them. I wish to thank the Structural Department the financial resources invested in my project, in terms of unlimited access to materials and to the laboratory. I appreciate the help from the Concrete Laboratory, particularly from Ove Loraas and Steinar Seehuus, for their time and collaboration with me.

I very much appreciate the active contribution of Giedrius Zirgulis to the experimental part of my research. I owe him special thanks for working side by side with me and for his friendship. I also thank Sindre Sandbakk his help and patience in resolving my doubts.

Agraeixo al meu tutor de l'Escola de Camins, Antoni Marí, la seva col·laboració i entusiasme a l'inici d'aquest projecte. D'altra banda, aprecio la tasca de les Oficines de Relacions Internacionals per facilitar la mobilitat d'estudiants, com ha estat el meu cas.

Per últim, vull agrair a la meva família els seus ànims al llarg d'aquests anys, per ensenyar-me que el que més valor té és ser feliç i per ser el meu model de constància i dedicació. Un especial agraïment al Xavi, amb qui he compartit una llarga carrera de cinc anys de la que espero no titular-me mai.

Table of contents

List of figures

List of tables

Summary

Influence of concrete flow on the mechanical properties of ordinary and fibre reinforced concrete

Elena Vidal Sarmiento, supervised by Terje Kanstad (NTNU), Mette Rika Geiker (NTNU and DTU) and Antoni Marí (UPC)

Self compacting concrete is often defined as a composite that possesses not only a very high workability, which results in a not necessary compaction, but also that resists segregation and maintains stable composition throughout transport and placing. However, two of the inner properties of SCC, fluidity and stability, seem, in a primary analysis, to be opposed. That research has tried to investigate how these two properties interact. More particularly, what is the influence of the flow of concrete on its stability. However, this potential instability caused by flow could transcend further than the fresh state, affecting also the hardened properties.

An initial experimental part had the aim to study the loss of uniformity caused by flow by means of the segregation experiment. Three mixes were studied, representing each mix one of the three groups: a self compacting concrete, a self compacting concrete with the aggregate grading modified for a potential higher segregation and, finally, a steel fibre reinforced self compacting concrete (SFRSCC). Almost identical results were assessed for the three mixes: the coarse aggregate distribution was constant along the length of the mould. In the case of the SFRSCC, also the fibre volume fraction exhibited a uniform distribution. Therefore, no segregation was observed for the three mixes studied, neither when the mix flowed into a 1,2 m long mould, nor when a longer mould of 2,96 m was used.

The second part dealt with the distribution and orientation of fibres within SFRSCC elements. A uniform distribution of fibres is of crucial interest to guaranty the uniform response of the element and the absence of weaker sections that could cause structural problems. The results showed that no differences of the fibre orientation and distribution along the beam were caused by flow. Only a general tendency to distribute more fibres on the bottom part and to align in a planar orientation was observed.

The final experimental part studied the potential influence of flow on the mechanical properties, more particularly, on the residual flexural strength of SFRSCC elements. The tested specimen, consisting of a 2,96 m long beam casted from one end, was sawn into three parts, so that three specimens composed of concrete with potentially different flow effects according to its proximity to the casting point were obtained. The mechanical properties of these specimens were studied through bending tests. After testing the thirds, the lack of differences on the flexural tensile strength between the third closer and the third further to the casting point proved that no influence of the flow of concrete was found in that mechanical property.

The consideration of all the results obtained during the experimental research points in the direction that concrete had the enough stability during flow to exhibit uniform mechanical properties in the hardened state, unaffected by flow.

Key words: self compacting concrete, fresh concrete, rheology, dynamic segregation, fibre reinforcement, fibre orientation, residual flexural tensile strength.

Resum

Influència del flux de formigó a les propietats mecàniques del formigó convencional i reforçat amb fibres

Elena Vidal Sarmiento, supervisada per Terje Kanstad (NTNU), Mette Rika Geiker (NTNU i DTU) i Antoni Marí (UPC)

El formigó autocompactable es defineix com un formigó que posseeix no només una alta treballabilitat, que es tradueix en la no necessitat de compactació, però també que resisteix la segregació i manté estable la seva composició durant el transport i el formigonatge. Tot i això, dues de les propietats bàsiques del formigó autocompactable, la fluïdesa i l'estabilitat, semblen, en un primer anàlisi, estar oposades. Aquesta recerca tracta d'investigar com aquestes dues propietats interaccionen. Més particularment, quina és la influencia del flux de formigó a la seva estabilitat. D'altra banda, aquesta possible inestabilitat causada pel flux podria transcendir més enllà del seu estat fresc, afectant també les propietats del formigó endurit.

La primera part experimental d'aquesta recerca té per objectiu estudiar la pèrdua d'uniformitat causada pel flux per mitjà de l'experiment de segregació. Tres mescles van ser estudiades, representant cadascuna d'elles: un formigó autocompactable, un formigó autocompactable amb l'àrid modificat per a una possible major segregació i, finalment, un formigó autocompactable reforçat amb fibres d'acer (SFRSCC). Gairebé idèntics resultats es van obtenir per les tres mescles: la distribució d'àrid era constant al llarg del motllo. Pel cas de SFRSCC, també la fracció volumètrica de fibres va mostrar una distribució uniforme. Per tant, no es va trobar segregació a les mescles estudiades, tant pel cas en què les mescles fluïen en un motllo de 1,2 m de llargada, com pel cas d'un motllo de 2,96 m.

La segona part tracta la distribució i orientació de fibres als elements estructurals (bigues) de SFRSCC. La distribució uniforme de les fibres té una gran importància per garantir una resposta uniforme de l'element i l'absència de seccions més dèbils que puguin causar problemes estructurals. El resultats van mostrar la inexistència de diferències a la orientació i distribució de les fibres al llarg de la biga, causades pel flux del formigó. Només una tendència general a distribuir fibres a la part inferior i d'alinear-se amb una orientació planar va ser observada.

L'últim apartat experimental estudia la possible influència del flux sobre les propietats mecàniques dels elements de SFRSCC. L'element d'estudi, consistent en una biga de 2,96 m de llargada formigonada des d'un extrem, es va serrar en tres parts, de manera que es van obtenir tres elements formats per formigó amb possibles efectes del flux d'acord amb la proximitat al punt de formigonatge. Les propietats mecàniques dels tres elements es van estudiar per mitjà del l'assaig a flexió. Un cop els tres elements van ser assajats, l'absència de diferències a la resistència residual a tracció entre l'element corresponent al terç més proper i l'element corresponent al terç més llunyà al punt de formigonatge demostrava que el flux no tenia una influència directa sobre les propietats mecàniques pel cas estudiat.

La consideració conjunta de tots els resultats obtinguts durant la part experimental assenyalen que el formigó assajat posseïa la suficient estabilitat durant el flux per exhibir unes propietats mecàniques uniformes, no afectades pel flux.

Paraules clau: formigó autocompactable, formigó fresc, reologia, segregació dinàmica, reforçament amb fibres, orientació de les fibres, resistència residual a tracció.

Chapter 1

Introduction

1.1. General context

The concept of self-compacting concrete (SCC) appeared for first time in the research of underwater concrete and the filling of other inaccessible areas. The development of water-reducing superplasticizers meant that high-workabilty and high-strength concrete could be achieved without excessive cement content (Gaimster & Dixon, 2003). The availability of new types of admixtures started the development of SCC in Japan in the mid-1980s. In the last decade, SCC has been developed further and, although the overall production is still relatively small compared to conventional concrete, it is especially popular in Europe. In 2005, 70% of the precast concrete in the Netherlands was SCC, while 30% of the ready mix concrete produced in Denmark was SCC (Geiker 2008).

The increasing application of this material resides in its numerable benefits respect with the vibrated compacted concrete (Gaimster and Dixon 2003):

- Increased productivity levels leading to shortened concrete construction time
- Lower concrete construction costs
- Improved working environment
- Improvement in environmental loadings
- Improved *in situ* concrete quality in difficult casting conditions
- Improved surface quality

However, the applicability of the SCC reaches further than casting elements with constricted reinforcement or difficult casting conditions. The application of the SCC in the fibre reinforcement field is not only supported by the aforementioned inner properties of this concrete, but also by a better response to structural loads respect with VCC (Døssland 2008).

1.2. Research objective

A main property of SCC is the filling ability, i.e. the ability of the fresh mix to flow under its own weight and completely fill all the spaces in the formwork. It is the characteristic often referred to as “flow” or “fluidity”. However, this is not the only property that features this material. A mix with high water content would have a considerable filling ability in despite of not being self-compacting. Therefore, a second main property needs to be mentioned to understand the behaviour of a SCC mix. The segregation resistance refers to the ability of a fresh mix to maintain its original uniform

distribution of the constituent materials during transport, placing and compaction. It has the same meaning as the "stability" of a fresh mix. Then, self-compacting concrete needs to embrace, on the same time, fluidity and stability.

The objective of this research is to investigate how these two properties interact. More particularly, what is the influence of the flow of concrete on its stability. With this purpose, several questions need to be answered:

- Will the distribution of aggregate after the casting process be uniform, or a nonuniform distribution will be obtained as a result of the dynamic segregation?
- Will fibres distribute uniformly along a specimen length, or lower fibre content will be present at the furthest part to the casting point influenced by flow?
- Will flow align fibres in a preferred direction?
- Will a specimen exhibit different mechanical properties along its length due to a nonuniform distribution of its constituent materials (aggregate and fibres) promoted by flow?

The answer and quantification of these questions are the targeted expectations of this research.

1.3. Research methodology

The experimental part of this research was divided into four sections. The first part had the aim to investigate the possible segregation of concrete due to flow during the casting process and its consequent loss of uniformity by means of the segregation experiment. Three mixes were studied, representing each mix one of the three groups: a self compacting concrete, a self compacting concrete with the aggregate grading modified for a potential higher segregation and, finally, a fibre reinforced self compacting concrete. The segregation experiment consisted of isolating sub regions of fresh concrete after casting from one end of the mould. After the cleaning, the coarse aggregate fraction was separated and its volume fraction obtained for all the sub sections. The same procedure was also carried out with fibres for the SFRSCC samples.

The second part dealt with the distribution of fibres within SFRSCC elements. The study of the fibre distribution concerned not only the investigation of the dispersion of fibres over the cross-section, but also within the length of the element. A 2,96 m long beam, with 0,25% fibre content, was casted from one end of the formwork. Three slices were sawn from this original specimen. The number of fibres over the slice cross-sections was determined by manual counting over each sawn surface. Over every counting surface, different sub regions were defined for the registration of the number of fibres depending on the height.

In the third part, the study of the fibre orientation was carried out. A long beam (2,96 m) was casted from one end, allowing the concrete to flow for filling the framework. Two slices of this beam were studied for the orientation factor measurement. The measure of the fibre orientation through the orientation factor required the determination of two main parameters: the number of fibres over the concrete cross-section, N, and the fibre

volume fraction, v_f. The number of fibres over the concrete cross-section was determined by manual counting over each sawn surface, while the fibre volume fraction was determined by crushing the slice into small fragments. Afterwards, manual crushing together with the help of a magnet enable to isolate the steel fibres from the crushed concrete. The weight of fibres, correlated with its density and the volume of the slice, provided the result of the fibre volume fraction.

Finally, the fourth part (Chapter 6) investigated the variation of the mechanical properties of a FRSCC long element, consisting on a 2,96 m long beam casted from one end. The hardened element was sawed into three parts, so that three specimens composed of concrete with potentially different flow effects according to its proximity to the casting point were obtained. The mechanical properties of these specimens were studied through bending tests. Moreover, three standard specimens not subjected to flow conditions and three subjected to flow conditions were tested in order to characterize the concrete and compare them with the sawn specimens. The standard specimens were tested according to the European Standard EN 14651, while the sawn specimens were tested with a four-point bending test. The results of the three sawn specimens were compared in order to draw conclusions about the flow influence on this mechanical property.

1.4. Outline of the report

The thesis is divided into three main parts. The first one represents the study of the previous investigations through the specialized literature. A second central part deals with the experimental research, which groups the segregation test, the study of the fibre distribution and orientation and the bending test. Finally, the concluding remarks summarize the main results and conclusions obtained in this research.

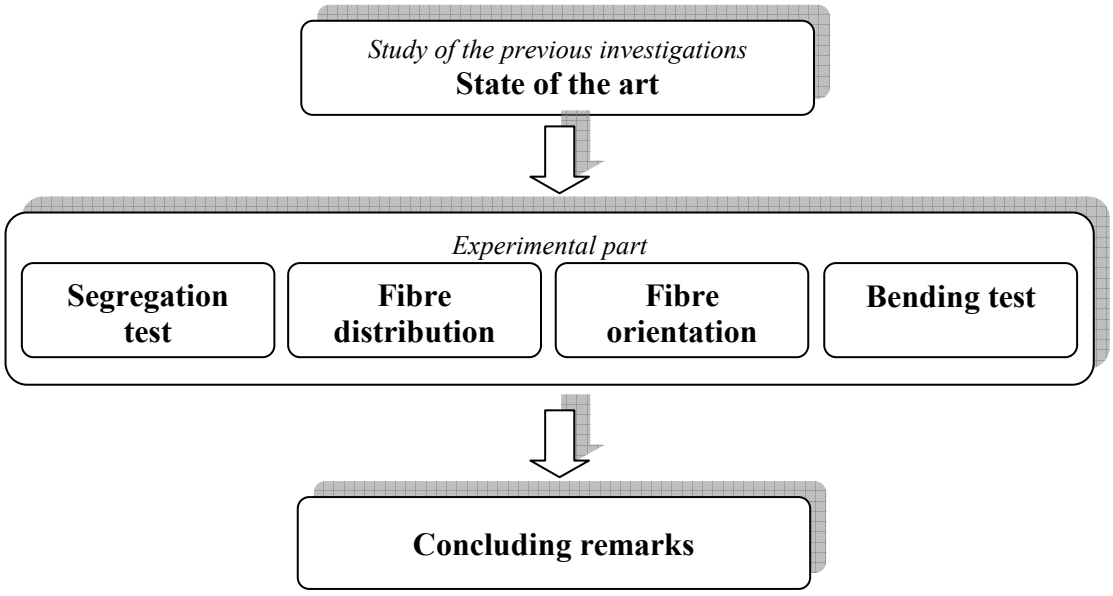

Figure 1. Structure of the report

Chapter 2

State of the art

2.1. Introduction

Self-compacting concrete (SCC) can be considered one of the main materials in the construction field. SCC flows into the formwork under its own weight and, differently from the conventional concrete, SCC achieves the compaction without need of vibration. As a result of this property, many advantages can be mentioned. The improvement on the working environment during construction, the productivity, and the potential improvement of the homogeneity and quality of the concrete are some examples. The named benefits of the use of this material are subjected to the fulfilment of a certain standard of its three key properties: filling ability, passing ability and segregation resistance. However, a proper SCC mix must embrace a compromise between two opposite objectives directly connected with the key properties: fluidity and stability.

The increasing use of this material has entailed a thorough research about its properties and its multiple applications. In this context, the application of fibre reinforcement to SCC is pointed as one of the more advantageous. The benefits of self compactability are added to an improvement of the mechanical properties of fibre reinforced specimens compared with vibrated compacted ones. This mechanical improvement is often explained by a favourable fibre orientation. However, the inclusion of fibres on a SCC mix has an effect on its workability: high fibre content creates a stiff internal structure which counteracts the flow. On the other hand, it is generally accepted that high fibre content improves the structural properties of fibre reinforced specimens. Thereby, another challenge is finding the suitable design between fibre content required to enable easy handling of the fresh concrete and that required for the maximum efficiency in the hardened state.

2.2. Flow influence on SCC properties

2.2.1. Introduction to rheology

Rheology is the branch of science dealing with deformation and flow of matter. The scope of rheology is therefore very wide. However, in the engineering practice, it is mainly used to describe the behaviour of materials which do not follow the “ideal” laws of deformation and flow (simple, elastic, Newtonian), (De Schutter, Bartos, Domone, & Gibbs, 2008).

Plain concrete is a composite material consisting of aggregate, cement paste and a small amount of voids filled by air or water. The cement paste, which itself is a composite, coats and separates the particles of aggregate, forming the "lubricating" layer which reduces the friction between them and facilitates their movement and rearrangement. A complex interaction between the paste and the aggregate then controls the flow of concrete mix and provides the mix with a certain level of workability.

Rheological equations which link the basic rheological characteristics and parameters of a fresh concrete mix rely on several assumptions, namely that fresh concrete is:

- A homogeneous material of a uniform composition
- An isotropic material
- A continuum, with no discontinuities between any two points within the material

Flow characteristics of SCC can be described by rheology. Several rheological models have been proposed for describing the flow of the cement suspensions. A Bingham behaviour of the fresh concrete is the case of the most common shear rates occurring during handling and placing of concrete. The Bingham model is based on the following relationship between the stress (τ) and the shear rate ($\dot{\gamma}$):

$$\tau = \tau_0 + \mu\dot{\gamma} \quad (1)$$

where the two basic rheological parameters are the yield stress (τ_0) and the plastic viscosity (μ).

The first parameter, the yield stress, is defined as the stress that should be overcome to initiate flow from rest, and below which the flow stops during casting (Roussel, et al. 2010). While the second parameter, the plastic viscosity, is a measure of the resistance of the concrete against an increased speed of movement (Flatt and Y.F. 2001).

Vibrated compacted concretes, with low workability, generally exhibit high yield stresses. In contrast with this, typical SCCs, with high flowabilty, are featured by low yield stresses, close to the Newtonian behavior, which corresponds with a zero value of the yield stress.

2.2.2. Key characteristics of fresh self-compacting concrete

There are three key properties that help to understand the ability of a SCC to flow into the framework under its own weight, even around complicated reinforcement arrangements. These properties are: filling ability, passing ability and segregation resistance. Adequate levels of all three properties must be reached for fresh concrete to be self-compacting and to remain so during transport and placing.

2.2.2.1. Filling ability

Filling ability is the ability of the fresh mix to flow under its own weight and completely fill all the spaces in the formwork. It is the characteristic often referred to as "flow" or "fluidity". It indicates how far a fresh SCC mix might flow, and how well it

would fill formwork and spaces of varying degrees of complexity. The filling ability must be high enough, the mix must be fluid enough, to permit any air introduced in the mixing process, or trapped during placing, to escape and leave behind an adequately compact concrete (De Schutter, et al. 2008).

To enable this to occur, the interparticle friction of the materials must be reduced. This can be achieved in two ways: first, by the inclusion of superplasticizers and, second, by optimizing the packing of fine particles by the introduction of fillers or segregation controlling admixtures (Gaimster and Dixon 2003).

2.2.2.2. Passing ability

According to (De Schutter, et al. 2008), the passing agility determines how well the fresh mix will flow through confined and constricted spaces, narrow openings and between reinforcement. The determination of the passing ability helps to evaluate the level of risk that the flow of the fresh mix will be impaired or even fully blocked by coarse aggregate, which will become wedged or form arches between bars or within narrow openings.

Passing ability is linked to filling ability and segregation resistance. In order for concrete to pass freely through reinforcement, it is necessary for the coarse aggregate particles to rearrange their positions within the mix, maintain a degree of separation and not interlock and block the gaps. It has been observed that in a mix with low filling ability the coarse aggregate particles have difficulty in doing so. Such a mix has poor passing ability, even without an excessive content of coarse aggregate. Both an adequate filling ability and passing ability are required for a fresh mix to be adequately self-compacting and suitable for a given application.

However, as it is described in (Geiker 2008), even if requirements in filling ability and segregation resistance are fulfilled, insufficient passing ability and blocking can develop easily when:

- the size of aggregate is large relative to the size of the opening
- the total content of the aggregate is high
- the shape of the particles deviates from spherical, for example crushed aggregate

Moreover, (Gaimster and Dixon 2003) points out that the more congested the structure is, in terms of reinforcement, the higher the volume of paste required compared with the amount of coarse aggregate.

Although passing ability is normally associated with aggregate, also fibres from a fibre reinforced concrete can cause blockade when passing through confined spaces. It is generally accepted than a minimum opening of twice the fibre length is required for avoiding problems associated with blocking.

2.2.2.3. Resistance to segregation

Segregation resistance is the ability of a fresh mix to maintain its original uniform distribution of the constituent materials during transport, placing and compaction. It has the same meaning as the "stability" of a fresh mix. Sedimentation takes place during flow due to stress gradients, it is called dynamic segregation, or, as settlement due to gravity, what is called static segregation (Geiker 2008).

Segregation in vibrated compacted concrete (VCC) is often present as honeycombing in the hardened concrete, revealed after formwork has been removed. Honeycombed concrete displays large, usually irregular voids between particles of coarse aggregate. Other forms of segregation include "bleeding". Bleeding occurs when water separates from the mix during placing and rises to the upper, horizontal surface of the cast element, where a thin layer of paste with very high water/cement ratio is formed.

Segregation can still occur in a SCC which possesses adequate filling and passing abilities. However, it is unlikely to show in the usual form of honeycombed or uncompacted hardened concrete. The segregation takes the form of a nonuniform distribution of aggregate, particularly of coarse aggregate. The nonuniform distribution of the coarse aggregate can be present in three main ways:

- Coarse aggregate may settle at the bottom of the formwork and be sparsely present at the top. This fact is associated with static segregation.
- Coarse aggregate can be nonuniformly distributed along the formwork length. A higher concentration of aggregate is placed close to the casting point than further to that point. This is associated with dynamic segregation.
- It can concentrate aggregate in locations where passage during casting is more difficult. In either case, the homogeneity of the concrete is reduced.

Segregation is caused by the differences in gravity of the constituent materials and depends on hydrodynamics and inter-particle forces. These terms have an influence on the rheological properties and, on the same time, they are also responsible for the segregation resistance. For example, the value of the yield stress of the cement paste determines if sedimentation of the coarsest elements of the concrete may occur: sedimentation is avoided when the gravity forces, generated by the density difference between an individual coarse grain and the cement paste, are too small to overcome the yield stress of the cement paste (Roussel, et al. 2010). On the other hand, if a particle is sinking, the viscosity of the paste will offer resistance to this movement. As a result, the lower is the plastic viscosity of the paste, the higher the sedimentation rate.

Modern cementitious materials such SCC may contain particles from alternative powders far smaller than cement particles. That results in an increase of the influence of Brownian motion over inter-particle forces. By reducing the amount of flocs which are prone to sedimentation, cement suspensions should become more stable. This is why the addition of fine particles has been proposed to facilitate robustness with regard to sedimentation. In addition, viscosity modifying admixtures (VMA) are sometimes added to fresh concrete to achieve cohesion and sedimentation resistance

A much less studied segregation, within the group of FRSCC, is the segregation of fibres caused by static segregation or by flow influence. This, together with the study of the coarse aggregate distribution, will be part of the experimental research of this project.

2.2.3. Flow induced heterogeneities

Regardless the passing ability, an ideal SCC mix has two opposite objectives: fluidity, i.e. the ability of filling the formwork; and stability, i.e. the ability of avoiding components to separate during casting. Therefore, the mix design results a compromise between these two qualities. In order to study this combination between these two key properties of SCC, some investigations have carried out numerical flow simulations, avoiding the expensive and time consuming experimental researches.

In (Spangenberg, et al. 2010), the aim of the research was fixed on obtaining maps of coarse aggregate distribution through and at the end of the casting process, using numerical simulations of the casting process coupled with numerical simulations of the segregation of the coarsest particles. Once the coarse aggregates distribution was known, by means of semi-empirical correlations, maps of local properties in the hardened state of the structural element were obtained.

According to the results for the particle distribution, during the casting, the density difference between the coarse particle and the continuous phase promoted a slow migration of the particles towards the bottom of the formwork. Consequently, at the end of the casting, a higher aggregate volume fraction was predicted compared with the bottom part.

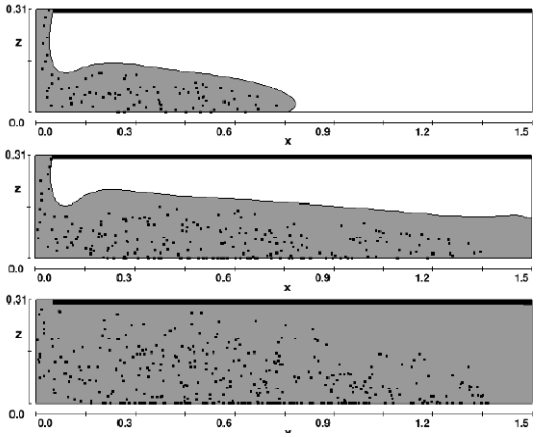

Figure 2. Particle distribution through the casting process. Only the right half of the 3m long specimen is shown. Vertical and horizontal distances are in m. Source: (Spangenberg, et al. 2010)

The properties in the hardened state that were studied in this research were the elastic modulus, the compressive strength and the drying shrinkage. The results showed that the variations induced by segregation in the elastic modulus and the compression strength were of the order of 10%. Finally, the variation induced by segregation in the drying shrinkage was of 25% and could induce a strong concentration of shrinkage in specific zones of the beam, which could in turn induce some cracking.

2.2.4. Measurements to describe the state of fresh concrete

Two general terms are used to describe the state of fresh concrete. The first one, workability, is defined as the amount of work done to overcome the internal friction between individual particles in the concrete necessary to produce full compaction. A concrete which can be readily compacted is said to be workable. The second term, consistence, is the firmness of form of a substance or the ease with which it will flow. Although some literature has established the difference between these two concepts (Neville, 2003), in the field of SCC it is frequent to refer both concepts to the ease by which fresh concrete can be placed.

As there is no test that measures directly the workability as defined earlier, numerous attempts have been made to correlate workability with some easily determinable physical measurements. A widespread test used for describing the fresh state of a SCC is the slump-flow test. This test was developed from the common slump test, widely used for VCC. Instead of the vertical settlement of the truncated cone of concrete after removal of the mould when VCC is tested, in this test the sample collapses and the concrete flows out in all directions. The test therefore measures the diametric spread of the sample after flow stoppage (Figure 3).

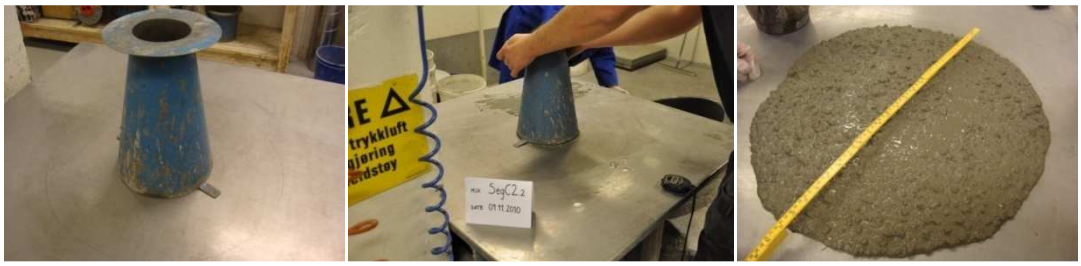

Figure 3. Slump-flow test

A sample of 6 l is mixed to fill the standard conical mould (height 300 mm, base diameter 200 mm, top diameter 100 mm). The test is performed over a smooth metal baseplate with maximum flatness. All the surfaces must be previously pre-wetted and the mould must be lifted vertically in a single action within approximately 30 s of filling the mould. Once the concrete has stopped, the largest diameter of the spread and its perpendicular diameter are measured. A visual check of the spread is generally carried out.

The rate or speed of flow of the fresh concrete is also of interest in characterization of the fresh concrete state. In this way, the time it took for the concrete sample of the slump-flow test to remould itself from the original shape of the truncated cone into a circular layer can be determined, usually in addition to the measurement of the slump-flow spread. The flow rate is expressed as the time taken from the moment the mould is being lifted to the flowing concrete to reach a circle of 500 mm in diameter, concentrically with the position of the mould. It is often referred to as time t_{500}.

There are numerous other methods which refer directly to the aforementioned key properties of concrete. Filling ability is normally characterized by the slump-flow test, but J-ring test (De Schutter, et al. 2008) is also widely used because it gives, on the same time, a value for the passing ability. Passing ability can also be assessed by the L-

box test (Nguyen, Roussel and P. 2006). Finally, the sieve segregation test is the commonly used test for the segregation resistance. The tests mentioned do not represent any definitive list, but are, among others, the most common in current use.

On the other hand, as there is a proposed linear relationship between shear stress and shear rate (equation 1), in order to obtain the characterization of this relationship at least two points $(\tau_1, \dot{\gamma}_1)$ and $(\tau_2, \dot{\gamma}_2)$ have to be assessed. Alternatively, some workability tests are focused on measuring the yield stress and the plastic viscosity. Firstly, rheometers allow the measurement of these two independent parameters that are needed to describe the rheological behaviour of fresh concrete. However, different rheometers do not give the same absolute values of the measured rheological parameters even with a given set of tested concretes. Civil engineers still do not have a tool to measure quickly and easily the rheological parameters of a given concrete and that is probably why empirical "stoppage test", such as the slump flow, are still so widespread. In these methods, after lifting the mould, if the shear stress in the tested sample becomes smaller than the yield stress, flow stops.

The value of the time t_{500} is related to the viscosity (μ) of the fresh mix. The shorter the time t_{500}, the higher will be the flow rate of SCC during placement and, consequently, the plastic viscosity. On the other hand, the spread of the slump-flow test is connected with the yield stress and several attempts can be found in literature in order to relate its values. On this way, (Roussel and Coussot 2005) divided the flow into two regimes: the "slump regime" (H>>R) and "spread regime" (R>>H) where H and R are the final height and radius of the sample. For the two regimes very different theoretical approaches to the yield stress may be used.

When performing the slump-test, in the slump regime the sample height and diameter are of the same order of magnitude. Contrary, in the spread regime the flow thickness of the sample is, in general, much smaller than the radial spread of the sample. An analytical solution assesses the expression for the yield stress as a function of the spread radius R and the volume of the sample Ω:

$$\tau_0 = \frac{225\rho g \Omega^2}{128\pi^2 R^5} \quad (2)$$

Where τ_0 is the yield stress and ρ the density of the concrete.

The case of SCC is included on the spread regime. However, according to (Roussel 2007) the validity of this correlation between yield stress and spread of the slump-flow test is subjected to fulfil the following conditions:

- The surface tension effects must be negligible
- The inertia effects must be negligible
- The tested volume must be representative of the mixture
- The thickness of the sample must be at least five times the size of the largest particle for the equations to be applicable. Otherwise, the material can not be considered as a homogenous fluid.

The three firsts conditions are generally fulfilled. Nevertheless, the thickness of the sample at flow stoppage does not enable us to consider the flow of a homogeneous mixture. Although two mixes have the same yield stress, one can have a lower spread in the slump-flow test due to a higher content of the coarsest aggregate. The thickness at stoppage should be around five times the maximum diameter of the aggregate to be representative of the rheological behaviour, and the volume needed for that should be 300 litres, which is a not applicable consideration.

A new alternative way to measure the yield stress of a given SCC is presented in (Roussel 2007). It is called LCPC-box test and it is based on the fact that in a conical flow redundant information is given as the shape of the material at stoppage is the same on every diameter. Therefore, this new test is based on a channel flow of fixed dimensions, using also a 6 l sample. As the flow is nearly unidirectional, the thickness of the sample at stoppage for the same sample volume is greater than in the slump-flow test. The prescribed dimensions of the box are shown in Figure 4.

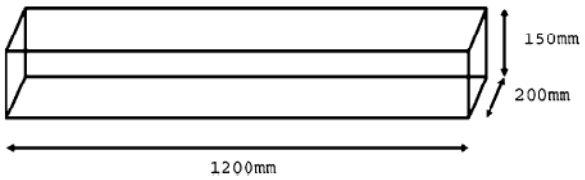

Figure 4. LCPC-box geometry. Source: (Roussel 2007)

The test procedure consists in pouring slowly the sample by means of a bucket from one extreme end of the box. The emptying of the bucket should take about 30 s. After flow stoppage, the spread length (L) in the box is assessed as the average of the maximum spread length and the lateral wall spread length. Also the thickness of the sample at the extremity of the box (h_0) is measured.

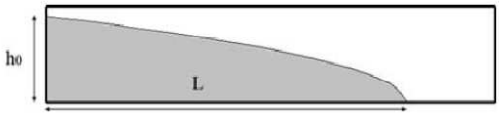

Figure 5. Shape at stoppage in the LCPC-box. Source: (Roussel 2007)

The analysis in (Roussel 2007) predicts the shape at stoppage of a given volume of fluid flowing slowly. The volume is expressed as:

$$V = l_0 \int_0^{h_0} x dh = \frac{l_0^3}{4A}\left(ln(1+u_0) + \frac{u_0(u_0-2)}{2}\right) \quad (3)$$

Where:

$$A = \frac{2\tau_0}{\rho g l_0} \text{ and } u_0 = \frac{2h_0}{l_0} \quad (4)$$

l_0 is the width of the channel, $l_0 = 20\ cm$. The spread length L at stoppage is then:

$$L = \frac{h_0}{A} + \frac{l_0}{2A} ln\left(\frac{l_0}{l_0 + 2h_0}\right) \quad (5)$$

Both equations can be used to assess the value of the yield stress with the measured parameters described by the test.

2.2.5. Factors affecting workability

Rheology of the fresh concrete strongly depends on the volume fraction of the aggregate. In order to support a finite amount of stress without flow, a mix must possess an internal network of particles with attractive interactions either via direct contacts or via colloidal forces. This internal network depends on the solid fraction. There exists a critical solid fraction value, ϕ_{perc}, below which the suspension does not display any yield stress. However, the need to determine the workability of the self-compacting concrete as a flowable material requires widening the factors to consider.

Mix proportion is one of the main factors concerning workability. It refers to three basic amounts: the paste content of the mix, the aggregate-cement ratio and the water-cement ratio (Nerville 2003). An increase on the water content decreases both yield stress and plastic viscosity parameters, and it implies an improvement on workability (Collepardi 1997). However, only about half of the water needed to obtain sufficient workability is needed for the hydration of the cement. Unreacted water appears as pores which decrease both strength and durability. To limit the water content in SCC, super-plasticizers are used (Geiker 2008). On the other hand, the paste content (V_{paste}) should be enough to fill the voids between the aggregate particles and create an enveloping layer, thick enough to ensure the required deformability and segregation resistance of the concrete. Minimum paste content is then required and it is generally assessed by determining the maximum packing density of the aggregate.

Maximum size, grading, shape and texture of the aggregate also affect workability. An increase of the coarse aggregate decreases the yield stress while viscosity experiences no considerable changes. Using a gravel type of aggregate instead of a crushed coarse type decreases the viscosity. In addition, water-cement ratio (w/c) and grading have to be considered together: the higher w/c, the finer the grading required for the highest workability. The more angular and elongated the particles are, the higher the viscosity (and yield stress) and less fluid the suspension.

Also the addition of fly ash in rates of 20% has a beneficial effect on workability. On the contrary, condensed silica fume decreases the plastic viscosity, while the yield stress remains almost unaffected.

Rheology depends on the flow history of the material. For example, the yield stress of the concrete left at rest increases with time (workability loss). Some of the structural changes responsible for the evolution of rheological properties are reversible: their effects are erased by mixing or by any type of strong shearing. These reversible changes, often dominant on short observation times, are generally described as thixotropy. Other changes are irreversible and thus contribute to the long term evolution of material properties (Roussel, et al. 2010).

Finally, workability of concrete strongly depends on temperature. The increase of the yield stress of a cement paste with time is accelerated when the temperature increases.

2.3. Flow influence on FRSCC properties

2.3.1. Application of the fibre reinforcement on self-compacting concrete

The positive effects of fibre reinforced concrete (FRC) regarding increased productivity and better working conditions can be further improved by using self-compacting concrete. With SCC the heavy vibration work is avoided. Furthermore, SCC improves the quality and appearance of the concrete.

But far from these advantages, the use of SCC over VCC is justified by a better response to loads. A large research (Døssland 2008) studied the failure of two series of beams reinforced with steel fibres and bars, the first with fibre reinforced compacted concrete (FRVCC), the second with fibre reinforced self-compacting concrete (FRSCC). Every series included different fibre types and fibre volumes. In this way, the objective of the testing was studying the effect of the fibre content and the concrete type, VCC or SCC. On the first hand, the results illustrated that the moment capacity increased with increasing the fibre content. On the second hand, the result of the 1% fibre content beam, compared with the reference beam without fibre, showed that the moment capacity was increased 45% for the VCC and 98% for the SCC.

According to this research, the large difference in moment capacity between the VCC and SCC beams could primarily be explained by a favourable fibre orientation. The number of fibres counted in the longitudinal direction of the beams, i.e. the favourable orientation, was on average 77% higher than the number of fibres in an ideal situation with evenly distributed isotropic oriented fibres. Yet, the capacity increase due to fibres for the SCC beams compared to the VCC beams was even larger than 77%. Another factor that enhanced the difference between the VCC and SCC beams was the increased post-cracking stress due to improved fibre-matrix bonding in the SCC. The reason for this improved fibre-matrix bonding was related both to the matrix strength and the concrete composition. Since SCC has higher matrix content and contains more silica, it is likely that the pore structure is more refined, something that improves the fibre-matrix bonding.

2.3.2. Workability of fibre reinforced self-compacting concrete

As it is exposed on the previous section, high fibre content improves the structural properties of a FRC specimen. Thereby, another challenge is finding the suitable design between fibre geometry required to enable easy handling of the fresh concrete and that required for the maximum efficiency in the hardened composite. High fibre content creates a stiff internal structure which counteracts the flow. Moreover, fibres which are too long tend to “ball” in the mix which, again, creates workability problems. The practical fibre content is thus limited since a sudden decrease of workability occurs at certain fibre content depending on the mixture composition and the applied fibre type.

The study of the fresh fibre reinforced concrete (Vikan 2008) lists the main reasons for the effect of fibres on the workability:

- The shape of fibres is more elongated compared with aggregates and promote interlocking. The surface area of fibres is, moreover, higher resulting in an increased water demand.
- Flexible fibres fill the space between particles while stiff fibres push apart large particles and increase the porosity of the granular skeleton
- The surface characteristics of the fibres differ from that of cement and aggregates.

The packing density of a granular skeleton determines the amount of cement paste that is required to fill the interstices. It has been studied that the concrete packing density decreases linearly with increasing fibre content. The degree to which the packing density decreases depends on the aspect ratio (length/diameter) of the fibres.

The packing density, and thus the optimal fibre content, has been found to depend on the relative content of sand and coarse aggregate in the concrete. The optimum fibre content was defined as the content of steel fibres beyond which fibre balling took place. The established relation was independent of the ratios of aggregate to cement and water to cement, which means that balling occurred at a given fibre content independently of the concrete composition.

2.3.3. Mechanical properties of the fibre reinforcement

The main objectives of engineering in attempting to modify the properties of concrete by the inclusion of fibres are as follows:

- To improve the rheology of the material in the fresh state.
- To improve the tensile or flexural strength.
- To improve the impact strength or toughness.
- To control cracking and the mode of failure by means of post-cracking ductility.
- To improve durability.

It is generally accepted that the inclusion of any type of short fibre at practical fibre content will not significantly alter the load at which cracking occurs in hardened concrete. Therefore, the main benefits of the inclusion of fibres in the hardened concrete relate to the post-cracking state, where the fibres bridging the cracks contribute to the increase in strength, failure strain and toughness of the concrete. Then, this increase in the performance of the composite in the post-cracking state is controlled mainly by the volume of fibres, the physical properties of fibres and matrix, and the bond between the two of them.

The post-crack flexural performance is the most important part of the commercial uses of steel fibre concrete enabling reductions of thickness to be made in sections subjected to flexure or loading points. A typical stress-deflection curve for beams is shown in Figure 6. Impact strength and toughness, defined as energy absorbed to failure, are greatly increased. The increased toughness results from the increased area under the load-deflection curve in flexure.

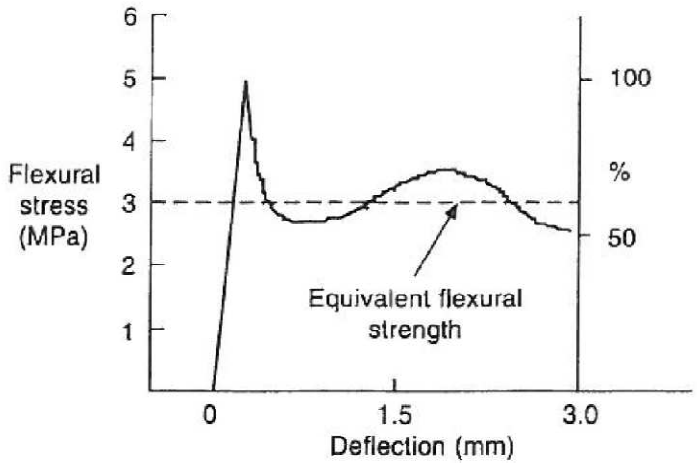

Figure 6. Typical stress-deflection curve for SFRC used to determine equivalent flexural strength in the post-crack state. Source: (Hannant 2003)

From the point of view of specification and control testing, there are additional complexities compared with conventional concrete. Neither the cube strength nor the maximum flexural strength is greatly changed by the addition of fibres at normal fibre dosage and, therefore, other methods have been devised for design purposes to guarantee if the element fulfils the requirements.

A method which is gaining acceptance is to assess the equivalent residual flexural tensile strength, where the term residual refers to the post-crack, by measuring the load-deflection curve up to 3 mm deflection for 150 mm by 150 mm by 600 mm long beams tested on 1/3th point bending.

2.3.3.1. Effects of the testing direction on the flexural behaviour of steel fibre-reinforced concrete

In (Toutanji and Bayasi 1998) a wide research about the effects of the manufacturing techniques on the flexural behaviour of steel fibre-reinforced concrete is presented. This report deals with both effects of curing environments and that of testing direction relative to casting direction.

According to the report, upon placement of steel fibrous concrete, the fibres tend to settle towards the bottom part of the beam. During flexural testing, depending on the relative location of testing direction compared to casting direction, fibres settlement may affect test results. Depending on the flowability of the fibrous mixture, fibre settlement may be extensive, moderate or mild, and the results affected accordingly. Some guidelines, like the European Standard EN 14651, specify that testing direction to be perpendicular to casting direction for thick specimens. This eliminates the effect of fibre settlement. However, this fibre settlement effect could be utilized to enhance the flexural behaviour of steel fibre concrete in some application fields.

The results of this research show that steel fibre reinforced concrete (SFRC) specimens with relatively high flowability, tested in the direction perpendicular to casting direction, exhibited reductions in flexural first-crack strength, residual flexural strength and flexural toughness of 14%, 22% and 33%, respectively, compared to specimens

tested in the direction parallel to casting direction. On the other hand, specimens with relatively moderate and low flowability, tested in the direction perpendicular to casting direction, exhibited insignificant reductions in flexural first-crack and residual strength. However, significant reductions of 20% and 14% in flexural toughness were noted for mixtures with moderate and low flowability, respectively.

2.3.3.2. Scale effects on testing FRC elements

In 2005, the NTNU conducted a series of experimental researches with reinforced beams of different thicknesses (50, 75, 100 and 150 mm). The research (Hegseth, et al. 2008) had the aim to study the scale effect on elements reinforced with steel fibres (0,7 vol %) or with synthetic fibres (1 vol %). The beams were obtained from vertical wall elements with dimensions 600 mm x 600 mm x thickness. After the sawing, four beams of 600 mm x 150 mm x thickness were resulting from each wall element. Three beams of each thickness were tested for bending.

The proceeding for the testing and the analysis of the results was carried out according to the Norwegian guidelines (NSBT). It consisted in a four-point bending test, with two loading points spaced at one third of the span, being the span 450 mm.

The residual flexural tensile strength was obtained for that research as the mean value of the residual strength corresponding to a crack mouth opening displacement ($CMOD$) of 0,5 mm and 2,5 mm.

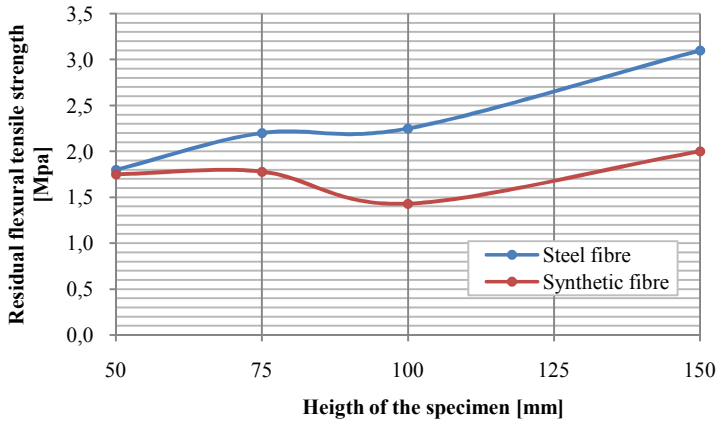

Figure 7. Variation of the residual flexural tensile strength with the height of the specimen. Source: (Hegseth, et al. 2008)

Figure 7 shows that steel fibres had a residual flexural strength proportionally dependant on the height of the specimen. A possible cause for this scale effect is that if we are using the same size of fibres (length and diameter), they will have more difficulties for being uniformly distributed in a smaller cross section than in a bigger one. Therefore, in a smaller specimen there are more probabilities to find areas without any reinforcement, which represent weak points for the post-cracking behaviour. On the other hand, the results for the synthetic fibres did not exhibit any correspondence with the height of the specimen.

2.3.4. Distribution and orientation of fibres

2.3.4.1. Methods for measuring the fibre distribution and orientation

The existing techniques to characterize the orientation of steel fibres may be categorized in destructive or non-destructive methods and based on direct or indirect measurements. The destructive techniques are generally based on evaluating the fibre orientation and distribution on limited size specimens, generally part of a large-scale element, like thin slices. Moreover, regarding the complexity, time-consumption and cost of these techniques, they have been mostly limited to research purposes (Laranjeira 2010). These points out the need to develop reliable, time and cost effective, non-destructive methods for the on-site monitoring of fibre dispersion on large-scale elements, which could be easily implemented into quality control procedures (Ferrara, Grünewald and Dehn 2010).

A popular example of a destructive and indirect measurement of fibre orientation is manual counting, a method which relates the number of fibres in a cross-section with the average orientation of fibres by means of a theoretical expression. Because of the average fibre orientation has been found to be proportional to the post-cracking strength of SFRC, many investigation have also been evaluating indirectly fibre orientation through mechanical testing (Laranjeira 2010). In the direct measurements within the destructive group, fibre orientation can be obtained through techniques such as the image analysis, X-Ray method or computerized tomography.

Recently, there have been significant advances in the development of non-destructive methods. Examples of these methods are the alternating current-impedance spectroscopy (AC-IS), the open coaxial transmission line, the dielectric waveguide antennas and methods based on electrical resistivity. These methods have the great advantage of avoiding the uncertainties that exist between small and large-scale elements.

Finally, numerical modelling of fresh concrete flow has been recently recognized as an effective tool. Computational Fluid Dynamic approaches and Discrete Element methods have been successfully applied to model the fresh concrete behaviour. For these methods, fibres can be modelled as clusters of solid spheres (Ferrara, Grünewald and Dehn 2010).

2.3.4.2. Causes of the preferred fibre orientation

Several aspects can be pointed as causes for a preferred fibre orientation. The interaction between the fibre and the formwork, known as wall-effect, and the fresh state properties of the concrete are identified as the most affecting influences for a FRSCC. Other factors, like vibration, can be of great importance in the study of the fibre orientation for VCC.

Wall-effects
Fibers are supposed to rotate freely in all direction when they are in bulk, i.e. not affected by any boundary condition. On the contrary, when fibres are in the proximities

of the mould side, the rotation is limited and it is not possible to find fibres perpendicular to a wall at a distance lower than half of the fibre length. Furthermore, hydrodynamics and direct mechanical interactions between fibres are considered to strongly influence the orientation over a distance of the order of a fibre length from the walls of the mould (Martinie and Roussel 2010).

Fresh state properties
The existence of a critical stress to be overcome to induce flow, i.e. the yield stress, allow the distinction of two orientation regimes, limited by what is known as plug flow areas:

- Outside the plug flow areas, deformations induced by flow contribute to the fibre alignment. The high shear rates are generally localized at the interface with the mould due to non-slip boundary conditions. This shear stress decreases from its maximum value, in the interface with the mould, until reaching the material yield stress value, at a critical distance from the wall z_c.
- At higher distances to the wall, what is defined as the plug-flow area, the material behaves like a solid. This central area is shifted with the fluid at the velocity of the interface with the sheared part. Therefore, a fibre initially inside a plug-flow area keeps its initial orientation.

Different behaviours can be expected for ordinary rheology concrete than for SCC. Ordinary rheology concrete, with a yield stress of order of a couple thousands of Pa, has a low value of z_c and, therefore, a thin layer around the mould where fibres align quickly with flow direction. The rest of the material flows like a granular paste sliding on that layer, but without modifying fibre alignment. On the other hand, SCC has a yield stress of several tens of Pa and, then, a higher value of z_c, which means that a bigger part will be affected by the fiber orientation and only a small area will keep the fibre initial orientation. In conclusion, fibres are on average less oriented in the case of ordinary rheology concrete than in the case of SCC (Martinie and Roussel 2010).

2.3.4.3. Current approach to determine the fibre orientation

As we have mentioned before, a widespread method to determine the fibre orientation is by means of the manual counting of the number of fibres in the specimen cross section, N. This method is based on the evaluation of a non-dimensional parameter known as orientation factor, α, which can be found as follows:

$$\alpha = \frac{n_f \ A_f}{v_f} = \frac{N \ A_f}{A_c v_f} \quad (6)$$

where:
n_f is the number of fibres per concrete unit surface
A_f is the cross-section of a fibre
v_f is the fibre volume fraction
N is the number of fibres in the concrete cross-section
A_c is the concrete cross-section

Two different methods are used to determine the fibre volume fraction of the element whose orientation factor wants to be found. The first one, a destructive and direct method, is based on crushing the element and manual separation of fibres. The second method is based on the theory of Thorenfeldt (Døssland 2008), which assumes that the volume of fibres in a sawn block can be estimated by counting the fibres over three sawn surfaces perpendicular to each other and applying the relation:

$$v_f = \left(N_1 + \frac{9}{16}N_2 + \frac{7}{16}N_3\right)\frac{A_f}{A_c} \quad (7)$$

where N_1, N_2 and N_3 are the number of fibres for each surface.

The interest of the calculation of this factor is because three values of this factor where found to be correlated with the three ideal orientation situations:

- Uni-directed fibres: $\alpha = 1{,}00$
- Plane orientation: $\alpha = 0{,}64$
- Isotropic orientation: $\alpha = 0{,}50$

The proximity of the calculated orientation factor to one of these three values, enables to draw conclusion about the dominant fibre alignment.

2.3.4.4. Effect of the fibre distribution and orientation on the mechanical properties

Differently from the ordinary reinforcement, where bars are deliberately located, fibres are generally distributed throughout the concrete cross section. Consequently, many fibres are inefficiently located for resisting tensile stresses resulting from applied loads. Also, many fibres are observed to extend across cracks at angles other than 90° or may be less than the required embedment length for development of adequate bond. Only a small percentage of the fibre content may thus be efficient in resisting tensile or flexural stresses and this efficiency will be very much dependant on their orientation and distribution.

A homogeneous dispersion of fibres along the length of FRSCC elements is crucial for a reliable structural performance. As we have seen in section 2.3.3, the main benefits of the inclusion of fibres in the hardened concrete relate to the post-cracking state, but this increase in the performance of the composite in the post-cracking state is controlled, among other things, by the volume of the fibres. If this volume of fibres is not uniformly distributed along the length of the specimen, the post-cracking strength could be different depending on the cross section analyzed.

Some guidelines include the effect of the fibre orientation on the design of the structural elements. The Norwegian *Proposed guidelines for design, construction and inspection of steel fibre reinforced concrete structures* assesses the residual strength with the expression (8). The basis of these equations can be found in (Døssland 2008).

$$f_{ct,residual} = \eta\, v_f\, \sigma_{f,average} \quad (8)$$

where:
$f_{ct,residual}$ is the residual flexural tensile strength
η is the capacity factor
v_f is the volume fibre content
$\sigma_{f,average}$ is the average post-cracking fibre stress

The capacity factor η indicates how much of the fibre forces are effective, i.e. normal to the crack plane. This parameter can be related with the orientation factor α (equation 6) by means of the following expressions:

$$\eta = 2/3\ \alpha \qquad \text{when} \quad 0{,}3 < \alpha < 0{,}5 \tag{9}$$

$$\eta = 4/3\ \alpha - 1/3 \qquad \text{when} \quad 0{,}3 < \alpha < 0{,}5 \tag{10}$$

The capacity factor corresponding to the three ideal orientation regimes, whose experimental values of the orientation factor were seen in the previous section, are:
- Uni-directed fibres: $\eta = 1$
- Plane orientation: $\eta = 1/2$
- Isotropic orientation: $\eta = 1/3$

When deviations from a standard test specimen are found, the residual flexural strength can be estimated by the follow correction:

$$f_{t,res} = f_{t,eq}\ (v_{f,struct}/v_f\ )(\eta_{struct}/\ \eta\ ) \tag{11}$$

where:
$f_{t,res}$ is the residual flexural tensile strength of the structural element
$f_{t,eq}$ is the residual flexural tensile strength of a standard test specimen
v_f is the fibre volume of a standard test specimen
$v_{f,struct}$ is the fibre volume of the structural element
η is the capacity factor of a standard test specimen
η_{struct} is the capacity factor of the structural element

Or expressed with an adjusted coefficient K dependent on the orientation factor α:

$$f_{t,res} = f_{t,eq}/K \tag{12}$$

where:
$$K = (4\alpha - 1)/\ (4\alpha_{struct}\ - 1) \qquad \text{for}\ \ 0{,}5 < \alpha_{struct} < 0{,}8 \tag{13}$$

$$K = (4\alpha - 1)/\ (2/3\alpha_{struct}) \qquad \text{for}\ \ 0{,}3 < \alpha_{struct} < 0{,}5 \tag{14}$$

in which:
α is the orientation factor for a standard test specimen
α_{struct} is the orientation factor for the structural element

It is interesting to mention that this adjustment needs to be done when deviation from a standard test specimen is detected. Unfortunately, nowadays guidelines do not specify how this deviation should be identified.

2.4. Concluding remarks

Self compacting mixes have two opposite objectives: fluidity, i.e. the ability of filling the formwork; and stability, i.e. the ability of avoiding components to separate during casting. According to some researches, when a fluid concrete flows during the casting process, the density difference between the coarse particle and the continuous phase promote a slow migration of the particles towards the bottom of the formwork. Apart from this, a nonuniform distribution of the aggregate along the length of the specimen is present and, consequently, variations in the mechanical properties within the specimen appear.

Several are the test commonly performed to study the fresh behaviour of concrete. Often, the results of the tests are referred to the rheological parameters of the mix. Although slump-flow test is the most commonly used test for SCC, the LCPC-box is presented as a new alternative that avoids some of the drawbacks and limitations of this precedent test.

The increasing use of FRSCC has entailed a thorough research about its properties. In its fresh state, the practical fibre content is limited since a sudden decrease of workability occurs at certain fibre content. This optimum fibre has been of main interest for several researches. In the hardened state, the main interest of the inclusion of fibres relate to the post-cracking state, where fibres bridging the cracks contribute to the increase in strength, failure strain and toughness of the concrete. However, many fibres are inefficient for resisting tensile stresses resulting from applied loads, either because of their distribution or their orientation. For that reason, several methods for studying the fibre orientation and distribution, like the manual counting, are currently in use.

Chapter 3

Segregation experiment

3.1. Introduction

The segregation experiment was performed in order to investigate the possible segregation of the concrete due to flow during the casting process and its consequent loss of uniformity. Three mixes were studied representing each mix one of the three groups: a self compacting concrete, a self compacting concrete with the aggregate grading modified for a potential higher possibility to segregate and, finally, a fibre reinforced self compacting concrete. The result of the distribution of the aggregate volume fraction along the length of the mould was the aim of the research, for what conclusions about the possible segregation were drawn.

3.2. Research parameters

The characterization of the concrete was the first step before performing the intended experiment. This characterization involved the determination of some basic properties of this material: density, air content and rheological properties.

The density and air content were tested according to the European Standard test described in *EN 12350 Testing fresh concrete*, Part 6 and Part 7, respectively. The rheological properties of the concrete were studied with two main tests:

- The first one, the slump-flow test provides two parameters: the spread, which refers to the average between two perpendicular diameters, and the t_{500}, which is correlated with the plastic viscosity.
- The second one, the LCPC-box test described in (Roussel 2007), measures the thickness of a 6 l sample poured from one end of the box at the extremity where the concrete is poured, and the spread length. With expression (3)-(5), these measured parameters are correlated with the yield stress.

In conclusion, the concrete is characterized through the values of: density, air content, diametric spread, t_{500} and yield stress.

On the other hand, the research parameter of the concerned experiment is the volume fraction of the aggregate or the fibres. In order to obtain this value, both weight of the concrete sample and the aggregate (fibres) need to be first measured and then correlated to their volume by means of the densities.

3.3. Properties of the materials

This section refers to the constituent materials used throughout the investigation for the concrete mixes. Table 1 shows the main characteristics of cement, aggregate, superplasticizer and fibres.

Table 1. Characteristics of the constituent materials

	Reference	**Characteristics**
Cement	Norcem Standard Cement FA	Portland Cement Type CEM II/A-V 42,5R
Aggregate	Årdal 0-4 mm Årdal 0-8 mm Årdal 8-11,2 mm Årdal 11,2-16 mm Årdal 8-16 mm	Water absorption: Årdal 0-4 mm, Årdal 0-8 mm: 0,8 % Others: 0,5 % Grading: See Appendix 1
Superplasticizer	Glenium 151	
Fibres	Dramix® 65/35	Circular cross section and hooked ends Length: 35 mm Diameter: 0,54 mm Aspect ratio: 65

3.4. Preparation of the specimens

With the segregation experiment we wanted to study three different mixes. The first mix consisted of a self compacting concrete with an intended high flowability. The second mix, denoted with SegC, was also a self compacting concrete mix but designed for being potentially more segregating than the previous one. This characteristic resulted in a gap in the aggregate grading affecting the $4-8\,mm$ fraction of aggregate.

The process of mix design was an arduous task in this research. A total number of 16 mix proportioning were tested in order to get three stable and flowable mixes, one for each mentioned group. All the recipes and results obtained for the mixes tested are reported in the Appendix 2.

3.4.1. Mix design for the SCC

We developed the mix by starting with a potential mix and then proceeding on a trial-and-error basis. The required properties for the design concerned exclusively fresh properties, in particular, a yield stress of 50 Pa, which is a common order of magnitude for standard SCC in housing construction that may be prone to segregation during casting.

Two basic parameters were modified in this trial-and-error system for getting the right mix design: the paste content and the water-binder ratio (w/b). Also the superplasticizer content was modified and its final amount depended on the observations of the concrete consistence during the mixing process. All the mix proportioning are widely described, as well as the results of the mixes, in Appenix 1. Table 2 summarizes the mixes that were tested according to this three parameters and Figure 8 shows the results obtained

for the basic rheological parameters, i.e. the yield stress and t_{500} as a measure of the plastic viscosity.

Table 2. Paste content and water-binder classification of the SCC mixes

		Paste content [l/m^3]			
		380	**390**	**400**	**420**
w/b	**0,40**	SCC8 (1%SP)	SCC6 (0,9%SP)	SCC4 (0,7%SP) SCC5 (1%SP)	SCC10 (1%SP)
	0,42	SCC9 (1%SP)	SCC7 (1%SP)		
	0,45			SCC3 (0,8%SP)	SCC11 (0,7%SP)
	0,52			SCC2 (0,4%SP)	

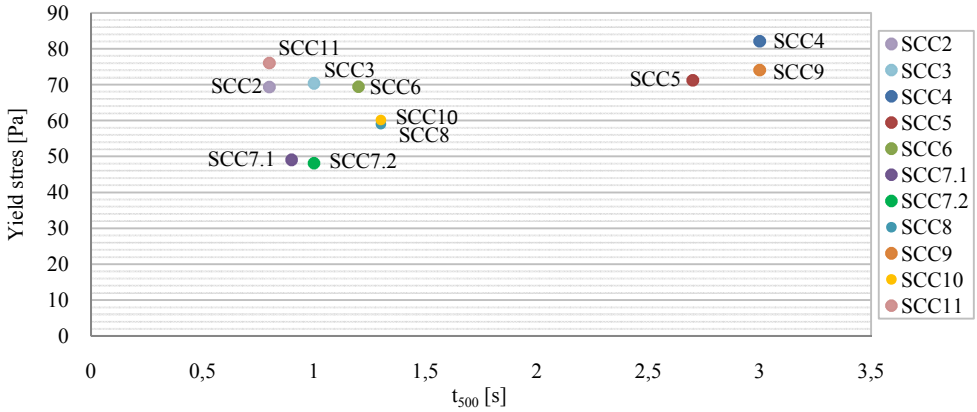

Figure 8. Results for the yield stress and t_{500} of the SCC mixes

With the results obtained we decided to choose SCC7 mix proportioning for the segregation experiment. During the process of mix design we obtained the values represented as SCC7.1 and SCC7.2. On these cases the yield stress was near the desirable value of 50 Pa. Table 3 summarizes the mix proportioning of this mix.

Table 3. SCC7 mix proportioning. SCC7.3

Water/binder	by wt	0,42
Silica/concrete	% by wt	6,0
Filler/concrete	% by wt	5,0
Paste content	l/m^3	390
Water/powder	by wt	0,35
Powder	kg/m^3	579,4
Water/cement	by wt	0,47

Cement	kg/m^3	428,2
Microsilica	kg/m^3	25,7
Filler	kg/m^3	21,4
Free water	kg/m^3	201,4
Absorbed water	kg/m^3	11,2
Aggregate 0 - 8 mm	kg/m^3	991,5
Aggregate 8 - 16 mm	kg/m^3	661,0
Superplastizicer	kg/m^3	4,3
	% from C	1,0

At the beginning of the mix design tests for SCC1-SCC11, the moisture content of the aggregate was tested in order to adjust the necessary addition of water. While the coarse aggregate 8-16 mm was totally dried, a value of 1.7% was obtained for the finest aggregate, 0-8 mm (see Appendix 1). Unfortunately, this value was wrong because of the sample tested came from the surface part of the stockpile and, as a result, less moisture content was registered. Table 4 shows the differences of values.

Table 4. Comparison between moisture content values measured for 0-8 mm aggregate

	Origin of the sample	**Measured value of moisture**
Moisture content used during mix design process	Surface of the stockpile	1,7 %
Real moisture content	Average of different samples	2,0 %

As the mix design was done with a wrong moisture content of the aggregate, lower than its real value, the mixes tested during this process had a higher content of water than what the initial recipe reported (Table 3). That is why the mix proportioning was readjusted to its actual value, as it is shown in Table 5.

Table 5. SCC7 mix proportioning. SCC7.1 and SCC7.2

Water/binder	by wt	0,426
Silica/concrete	% by wt	6,0
Filler/concrete	% by wt	5,0
Paste content	l/m^3	393
Water/powder	by wt	0,35
Powder	kg/m^3	579,0
Water/cement	by wt	0,48

Cement	kg/m^3	428,2
Microsilica	kg/m^3	25,7
Filler	kg/m^3	21,4
Free water	kg/m^3	204,3
Absorbed water	kg/m^3	11,2
Aggregate 0 - 8 mm	kg/m^3	987,0
Aggregate 8 - 16 mm	kg/m^3	658,0
Superplastizicer	kg/m^3	4,3
	% from C	1,0

3.4.2. Density, air content and rheological properties of the SCC7 mix design

Three batches were performed with the SCC7 proportioning. SCC7.1 and SCC7.2 were two batches of 8 l each tested for obtaining the concrete density, t_{500} and spread in the LCPC-box experiment. SCC7.3 was a 46 l batch necessary for obtaining the previously mentioned parameters and performing the segregation experiment.

For that mix, SCC7.3, moisture content of sand was again measured. A value of 2% was obtained and the mix was prepared based strictly on the initial recipe (Table 3), due to the mistake of the wrong moisture adjustment was still unknown. As a result, this batch contained less water compared with the previous ones and considerable different rheological properties were observed. Table 6 shows this variation.

Table 6. Density, air content and rheological properties of SCC7.1, SCC7.2 and SCC7.3

	SCC7.1	**SCC7.2**	**SCC7.3**
Batch [l]	8	8	46
Purpose of the mix	Mix design	Mix design	Segregation experiment with the LCPC-box
Density [kg/m^3]	2338	2339	2352
Air content [%]	-	-	1,7
τ_0 [Pa]	49,1	48,1	61,3
Spread slump-flow [mm]	69,5	68,5	57,5
t_{500} [s]	0,9	1	2,35

3.4.3. Mix design for the SegC

The main idea for the second segregation experiment was testing a mix with a gap in the aggregate grading. This gap affected the 4-8 mm fraction of aggregate. For that purpose,

we used a 0-4 mm aggregate instead of the 0-8 mm that we used on the previous experiment, both grading distributions were comparable.

We developed the mix by starting with a potential mix and then proceeding on a trial-and-error basis. In that case, the potential mix was based on the mix we tested on the previous segregation experiment, i.e. SCC7. Two mixes were tested, SegC1 and SegC2. While SCC7 had 40% 0-8 mm aggregate and 60% 8-16 mm aggregate, SegC2 was designed for 59% of 0-4 mm aggregate and 41% of the 8-16 mm aggregate, without modifying any other parameter. Because of a difference in the grading, the fraction less than 0,125 mm was lower using the new aggregate 0-4 mm. To compensate that difference in the finest particle, SegC1 was designed with a higher amount of filler (11% filler-cement ratio, instead of 5%). Figure 9 shows the difference of the aggregate grading between SCC7 and SegC.

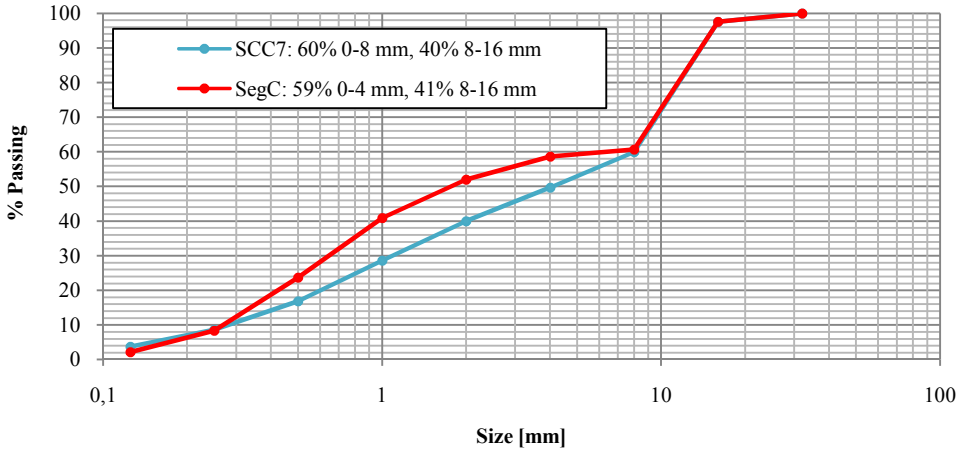

Figure 9. Aggregate size distribution for SCC7 and SegC

Figure 10 shows the LCPC-box test for measuring the yield stress. As it can be seen, SegC1 had a lack of flowability, while SegC2 had a much better behavior.

Figure 10. LCPC-box test for SegC1 (left) and SegC2 (right)

With the results obtained we decided to choose SegC2 mix proportioning for the segregation experiment. Table 7 summarizes the mix proportioning of this mix.

Table 7. SegC2 mix proportioning

Water/binder	by wt	0,42
Silica/concrete	% by wt	6,0
Filler/concrete	% by wt	5,0
Paste content	l/m^3	390
Water/powder	by wt	0,35
Powder	kg/m^3	590,9
Water/cement	by wt	0,47

Cement	kg/m^3	440,1
Microsilica	kg/m^3	26,4
Filler	kg/m^3	22,0
Free water	kg/m^3	207,0
Absorbed water	kg/m^3	6,2
Aggregate 0 - 4 mm	kg/m^3	959,0
Aggregate 8 - 16 mm	kg/m^3	666,4
Superplastizicer	kg/m^3	4,4
	% from C	1,0

The moisture content of the aggregate 0-4 mm was measured, obtaining a value of 3%. Further difficulties were not found concerning the water adjustment for that case.

3.4.4. Density, air content and rheological properties of the SegC2 mix design

Three batches were performed with SegC2 proportioning. SegC2.1 was an 8 litres batch that we used during the mix design tests, obtaining the concrete density, air content, t_{500} and spread in the LCPC-box experiment. SegC2.2 was a 54 litres batch necessary for obtaining the previously mentioned parameters and performing the segregation experiment. Finally, SegC2.3 was a mix used for the segregation experiment with a large mould. It was tested for the air content, density and slump-flow test. If more time had been available, other tests like the LCPC-box test for a 6 l sample could have been performed in order to obtain the value of the yield stress.

The only difference between the three mixes was the amount of superplastizer used. As we mentioned before, the superplasticizer was added depending on the observations of the concrete consistence during the mixing process. A 0,9% was thought to be enough for SegC2.2. In SegC2.3 the amount of 0,8% of cement was added instead of the maximum value of 1,0% used because the use of a bigger mixer, which provides higher energy to the mix, was thought to require less superplasticizer for achieving the same workability. Table 8 shows the differences in the rheological properties.

Table 8. Density, air content and rheological properties of SegC2.1, SegC2.2 and SegC2.3

	SegC2.1	**SegC2.2**	**SegC2.3**
Batch [l]	8	54	159
Purpose of the mix	Mix design	Segregation experiment with the LCPC-box	Segregation experiment with a larger mould
Density [kg/m^3]	2303	2301	2339
Air content [%]	-	2,7	2,0
τ_0 [Pa]	58,0	85,5	-
Spread [mm]	680	585	495
t_{500} [s]	1,3	2,0	3,1

Both the spread and the t_{500} were considerable lower for SegC2.3, which means that the mix was less flowable than expected. Probably, the reduction of the superplasticizer amount was not necessary for that occasion.

3.4.5. Mix design for the FRSCC

The main idea for this third segregation experiment was the inclusion of fibres in the mix. This way, the possibility of the dynamic segregation of fibres and coarse aggregate was analyzed for the case of a Fibre Reinforced Self Compacting Concrete.

Similarly to the other cases, we developed the mix by starting with a potential mix and then proceeding on a trial-and-error basis. Two basic parameters were modified in this trial-and-error system for getting the right mix design: the paste content and the water-binder ratio. Also the superplasticizer content was modified and its final amount depended on the observations of the concrete consistence during the mixing process. Table 9 summarizes the mixes that were tested according to these three parameters.

Table 9. Paste content and water-binder classification of the FRSCC mixes

		Paste content [l/m^3]	
		380	**390**
w/b	**0,42**		FIB3 (1% SP)
	0,45	FIB2 (0,91%SP)	
	0,52	FIB1 (0,46%SP)	

FIB1 and FIB2 mixes were tested with a volume fraction of 0,5% fibres. These mixes were tested for obtaining the concrete density, air content, t_{500} and spread in the LCPC-box experiment. The results showed the mixes were unstable and not enough workability was achieved (Figure 11). Further information about mix proportioning and results of these tests can be found in Appendix 1.

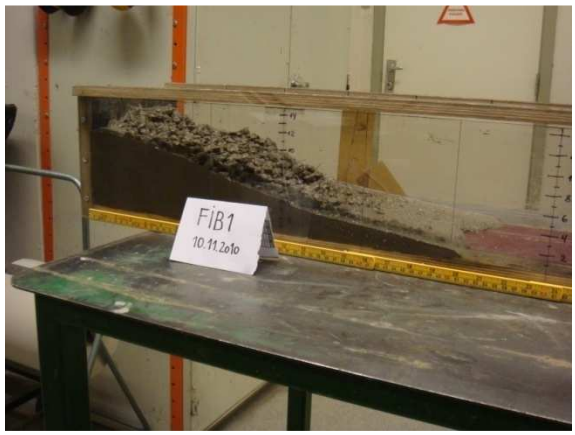

Figure 11. LCPC-box test for FIB1

Finally, FIB3 was designed based on the SCC7 mix proportioning, which was used for the first segregation experiment, but with the addition of fibres. This way, a more accurate comparison of results between a SCC and a FRSCC could be reached. For achieving the desired rheological properties of the mix, different volume fractions of fibres were tested, regarding that an increase on the content of fibres concerns an improvement on the hardened state but, on the same time, a loss of workability. According to that, $FIB3_{0,25}$, $FIB3_{0,35}$, $FIB3_{0,50}$ and $FIB3_{0,75}$ were designed with fibres volume fraction of 0,25, 0,35, 0,30 and 0,75, respectively.

While $FIB3_{0,25}$ and $FIB3_{0,35}$ were tested for density, slump-flow test and LCPC-box experiment, $FIB3_{0,50}$ and $FIB3_{0,75}$ were exclusively tested for slump-flow test. Despite that the spread obtained with the slump-flow test is not the suitable parameter to correlate with the yield stress, it may be used as a first approximation of the loss of workability for comparing these mixes (Figure 12).

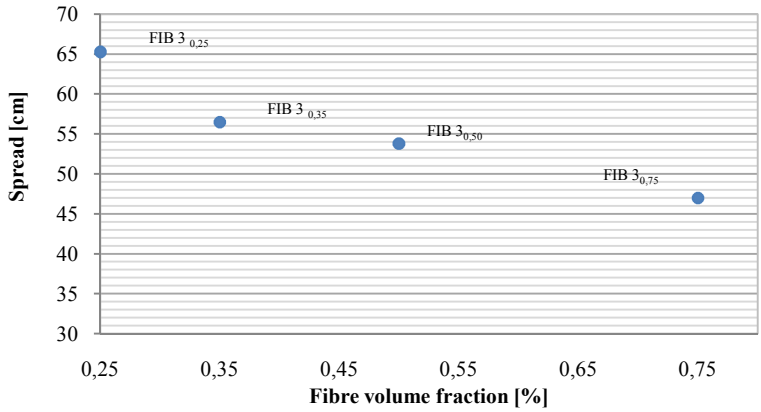

Figure 12. Variation of the measured spread of the slump-flow test with the fibre content

Figure 13 shows the results of the LCPC-box tests for the mixes $FIB3_{0,25}$ and $FIB3_{0,35}$.

Figure 13. LCPC-box test for $FIB3_{0,25}$ (left) and $FIB3_{0,35}$ (right)

With the results obtained, we decided to select $FIB3_{0,25}$ mix proportioning for the segregation experiment as it was the more flowable mix. Table 10 summarizes its mix proportioning.

Table 10. Mix proportioning for $FIB3_{0,25}$

Water/binder	by wt	0,426
Silica/concrete	% by wt	6,0
Filler/concrete	% by wt	5,0
Paste content	l/m^3	393
Water/powder	by wt	0,35
Powder	kg/m^3	578,9
Water/cement	by wt	0,48

Cement	kg/m^3	428,6
Microsilica	kg/m^3	25,7
Filler	kg/m^3	21,4
Free water	kg/m^3	204,5
Absorbed water	kg/m^3	11,1
Aggregate 0 - 8 mm	kg/m^3	982,4
Aggregate 8 - 16 mm	kg/m^3	654,9
Superplastizicer	kg/m^3	4,3
	% from C	1,0
Fibres	kg/m^3	19,5

3.4.6. Density, air content and rheological properties of the $FIB3_{0,25}$ mix design

Two batches were performed with the $FIB3_{0,25}$ proportioning. The first one was an 8 litres batch that we used during the mix design tests, obtaining the concrete density, air content, t_{500} and spread in the LCPC-box experiment. The second one was a 54 litres batch necessary for obtaining the previously mentioned parameters and performing the segregation experiment with the LCPC-box.

A third mix was considered for the segregation experiment with a larger mould. However, after mixing, the concrete showed different consistence with respect to the previous mixes. Two aspects have been detected as causes of that fact:

- A higher content of the coarsest aggregate (>16 mm)

  Because of the store conditions in the concrete laboratory, a different coarse aggregate was used in that case. Normally, the coarse aggregate we were using was the mixture of 50% of the 8-11,2 mm fraction and 50% of the 11,2-16 mm fraction. However, on that occasion, the coarse aggregate came from an 8-16 mm stockpile.

  According to the grading provided by the supplier the difference between using one or the other coarse aggregate was the shown in Figure 14.

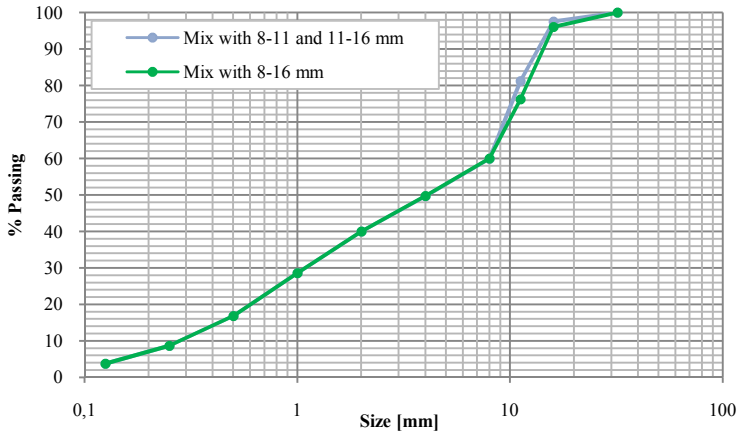

Figure 14. Differences in the grading between a mix with 8-11 mm and 11-16 mm, and a mix with 8-16 mm aggregate. Information from the supplier

After the washing and weighing of the coarse aggregate during the segregation experiment, a different grading distribution was observed from the grading provided by the supplier. As a result, the real difference between using different stockpiles resulted in a considerable different grading for the coarse aggregate fraction, as it can be seen in Figure 15.

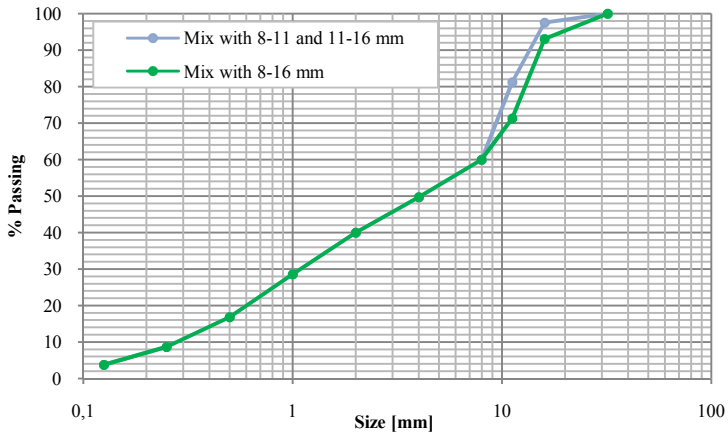

Figure 15. Differences in the grading between a mix with 8-11 mm and 11-16 mm, and a mix with 8-16 mm aggregate. Information measured

Moreover, pictures were taken comparing the fraction 11,2-16 mm from the two different stockpiles. A considerable higher number of particles over the 16 mm diameter were found in the 8-16 mm stockpile used for this third mix.

Figure 16. Difference of the 11,2-16 mm fraction between the two stockpiles used for FIB3

This fact reflects the importance of planning in advance the amounts and the accesses to the materials to use in order to avoid using different reserves that can potentially hide different characteristics.

- A wrong adjustment of the moisture content of the fine aggregate

The proceeding for obtaining the mix design of the FRSCC was made with a wrong value of the moisture content of the fine aggregate 0-8 mm that was described previously in section 3.4.1. The result of this fact was that the total water content said in the initial mix proportioning recipe was lower than what was actually used for the precedent mixes due to consider a lower moisture content of sand.

For this mix, a new reserve of 0-8 mm sand was used, so that moisture content of sand was again measured. A value of 3 % was obtained and the mix was prepared based strictly on the initial recipe with 0,420 water-cement ratio. As a result, this batch contained less water compared with the previous ones. Table 11 shows the differences of water-binder and paste content due to this wrong water content adjustment.

Table 11. Differences of water-binder ratio and paste content between $FIB3_{0,25}$ and FIB4

Mix identification	Water-binder ratio [#]	Paste content [l/m^3]
$FIB3_{0,25}$, SCC7 and others	0,426	393
Current mix, defined as FIB4	0,420	390

The combination of both facts, are pointed as the causes of a FRSCC not comparable with the FRSCC defined as $FIB3_{0,25}$, used for the LCPC-box segregation experiment. Nevertheless, results were still of great value for our study, because the dynamic segregation was studied independently of the results for $FIB3_{0,25}$. Table 12 shows the mix proportioning in which FIB 4 was based on.

Table 12. FIB 4 mix proportioning

Water/binder	by wt	0,42
Silica/concrete	% by wt	6,0
Filler/concrete	% by wt	5,0
Paste content	l/m^3	390
Water/powder	by wt	0,35
Powder	kg/m^3	590,9
Water/cement	by wt	0,47

Cement	kg/m^3	428,3
Microsilica	kg/m^3	25,7
Filler	kg/m^3	21,4
Free water	kg/m^3	201,5
Absorbed water	kg/m^3	11,2
Aggregate 0 - 8 mm	kg/m^3	987,3
Aggregate 8 - 16 mm	kg/m^3	658,2
Superplastizicer	kg/m^3	4,3
	% from C	1,0
Fibres	kg/m^3	19,5

This mix was used for the segregation experiment with a larger mould, but also for casting two beams of 2,96 m length for the next experimental sections of the research, i.e. studying fibre distribution and orientation and the mechanical properties in the hardened state. In total, a volume of $540\ l$ were mixed. The concrete obtained was tested for density, air content and slump-flow test. The results are summarized in Table 13 together with $FIB3_{0,25}$.1 and $FIB3_{0,25}$.2.

Table 13. Density, air content and rheological properties of $FIB3_{0,25}$.1, $FIB3_{0,25}$.2 and FIB4

	$FIB3_{0,25}$.1	**$FIB3_{0,25}$.2**	**FIB4**
Batch [l]	8	54	540
Purpose of the mix	Mix design	Segregation experiment with the LCPC-box	Segregation experiment with a large mould, study of the fibre distribution and orientation and study of the mechanical properties
Density [kg/m^3]	2354	2341	2338
Air content [%]	-	1,7	2,8
τ_0 [Pa]	72,24	49,26	-
Spread [mm]	630	675	455
t_{500} [s]	1,4	1,0	No reached the 500 mm spread

Although FIB4 had a considerable different workability, during the casting process of the two beams and the segregation experiment the concrete flowed along the 2,96 m of length without difficulties.

3.4.7. Mixing of concrete

The following mixing protocol was adopted. First aggregates, cement, filler and silica were dried-mixed for one minute. Then, water was added and mixed further for one

minute. After two minutes rest, the superplasticizer was added and, finally, concrete was mixed for one additional minute. For the FRSCC, fibres were added after the resting time, the same as the superplasticizer.

The mixing process was performed with vertical axis mixers. However, four mixers were used with different mixing capacities according to the required batch. Figure 17 shows, from left to right, the mixer used for 8-9 litres batch; the mixer used for 22, 46 and 54 litres; the mixer used for 159 litres; and, finally, the mixer used for the 540 litres batch.

Figure 17. Mixers used during the mixing in the concrete laboratory (NTNU)

3.5. Method and testing procedure

3.5.1. Methodology with the LCPC-box

The segregation experiment consists of filling a mould with a SCC mix and measure the volume of concrete and coarse aggregate in different sub regions, in order to obtain the aggregate volume fraction for different distances to the casting point.

The filling process is carried out from one end of the mould, where the funnel is placed. The funnel needs to have the same filling height during all the casting process in order to guarantee a uniform inlet velocity, which should be between 0,24 and 0,48 l/s. The concrete flows along the mould (Figure 18) and the filling stops when the concrete reaches the top of the mould at the end where the funnel is placed. The specific geometry of the funnel is not important, however, the inlet of the funnel needs to be wide enough to avoid getting blocked by the aggregate or by the fibres, but, on the same time, narrow enough to guarantee the aforementioned values of filling velocity. Three different funnels were used. The first one had a squared inlet of $100\ mm\ x\ 100\ mm$, which was too big for guaranteeing a reduced filling velocity. The second one had a circular inlet of $65\ mm$ diameter, which was suitable for a SCC without fiber reinforcement. This second inlet was completely blocked when the FRSCC was casted, so that a third funnel with a circular inlet of $80\ mm$ diameter was used for that concrete.

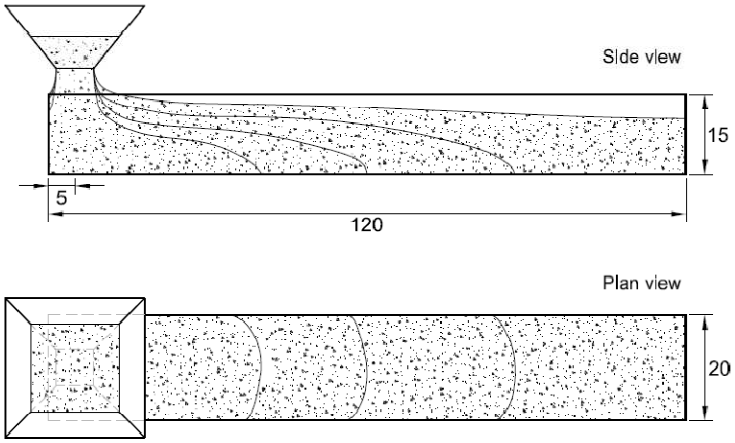

Figure 18. Filling process for the segregation experiment with the LCPC-box. Dimensions in cm

The mould for what the segregation experiment was designed was the LCPC-box (Roussel 2007). This mould (Figure 4) was build for first time at NTNU for this research. The side walls were made of methacrylate (Plexyglas) and their transparency allowed the recording of the flow propagation. A special rough material was used to cover the bottom surface for a non-sliding condition during the flow.

Figure 19. Filling process of the segregation expreriment with SegC2.2

After the flow stoppage, twelve sub regions of 10 cm length were isolated by means of thin plates (Figure 20). The concrete placed in each sub region was weighed and cleaned in order to keep only the coarse aggregate ($8 - 16\,mm$). This aggregate was kept in the oven at 105°C during 3-5 hours, depending on the volume, until it had lost all the moisture and, consequently, the weight was constant. The dried aggregate was sieved and weighed for the fraction $8 - 11{,}2\,mm$ and $11{,}2 - 16\,mm$. Finally, these weights were correlated to volume and the aggregate volume fraction was determined for each sub region.

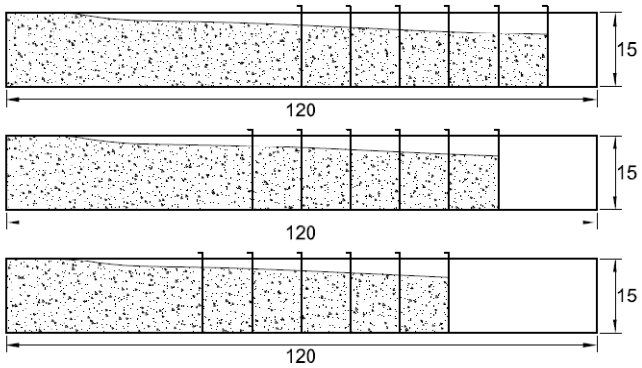

Figure 20. Isolation of the sub regions in the segregation experiment with the LCPC-box. Dimensions in cm

Figure 21. Isolation of the sub regions in the segregation experiment for SCC7.3

Figure 21 shows the pictures taken during the first segregation experiment, in which only two plates were used to isolate the regions. For the rest of the experiments a total number of 6 plates were used (as shown in Figure 20) in order to minimize the pressure in the plate when the previous sub region was emptied.

Finally, the dried coarse aggregate and the sieves are shown in Figure 22.

Figure 22. Dried aggregate 8-16 mm and sieving process

3.5.2. Methodology with a longer mould

With this new segregation experiment we wanted to investigate about the possibility of the dynamic segregation of fibres and coarse aggregate increasing the distance of flow, i.e. considering a longer mould. Figure 23 shows its dimensions.

As the segregation experiment was designed for being performed in the LCPC-box, several differences need to be mentioned:

- A plywood mould was used (Figure 25). As a first consequence, no transparent walls allowed observations of the flow shape during the casting process or at flow stoppage. Secondly, the non-slid condition on the bottom surface was not verified.

- The filling conditions that were obtained thanks to a funnel, which kept the filling height constant during the casting process for the LCPC-box experiment, were not reproduced in that case, where a skip containing the entire 150 l batch discharged from one point.

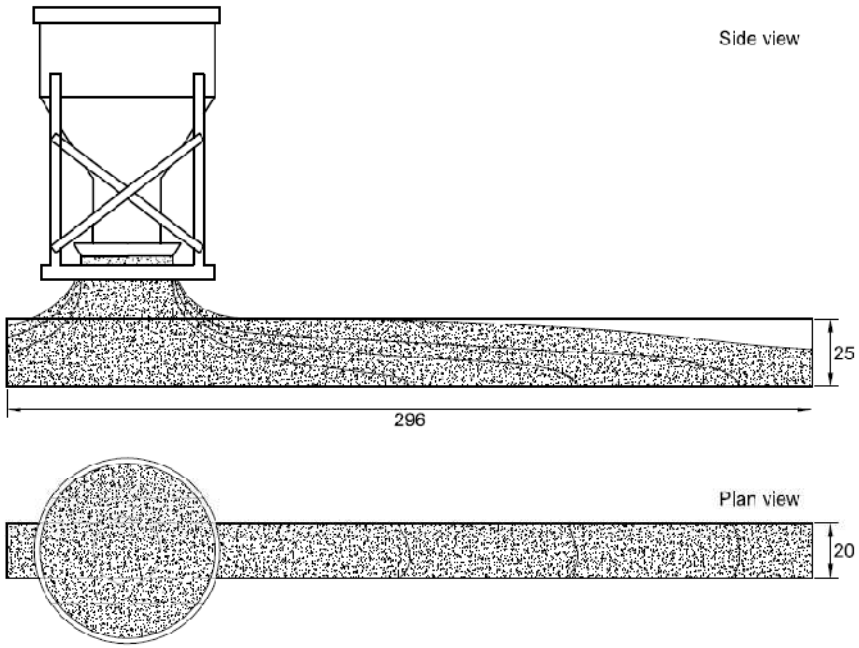

Figure 23. Filling process for the segregation experiment with the large mould. Dimensions in cm

The proceeding of cleaning the concrete from each sub region was laborious and time consuming. When time is running, the fresh concrete loses its workability and the hardening process develops. For that reason only six sub regions of 10 cm length were analyzed in that test (Figure 24).

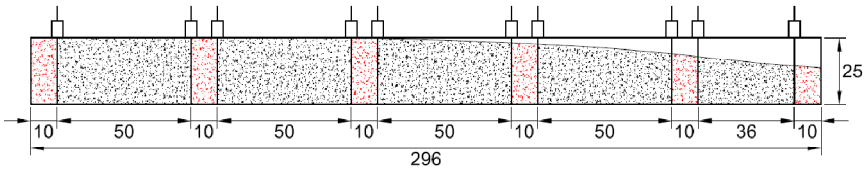

Figure 24. Isolation of the sub regions in the segregation experiment with the large mould. Dimensions in cm

Figure 25. Filling process and isolation of the sub regions for the segregation experiment with FIB4

The concrete placed in each sub region was tested following the same methodology described for the experiment with the LCPC-box. Figure 25 shows some representative pictures of the test.

3.6. Results, analysis and discussion

A summary of the segregation experiments realized in that research is shown in Table 14 in order to draw the general idea before the results are exposed.

Table 14. Summary of the segregation experiments tested

	Mixes		
Segregation experiment with the LCPC-box	SCC7.3	SegC2.2	$FIB3_{0.25}.2$
Segregation experiment with the large mould	-	SegC2.3	FIB4

The reason why the segregation experiment with the large mould was not studied for the SCC group was that the results obtained for SegC2.3 were enough to draw conclusions also for this concrete. A special mention is pointed in the results of SegC2.3.

3.6.1. Results for the self compacting concrete

The segregation experiment with the LCPC-box was performed according to section 3.5.1 for the mix denoted as SCC7. Figure 26 shows the shape of the concrete at the flow stoppage, while Figure 27 represents the distribution of the coarse aggregates 8-16 mm along the length of the mould.

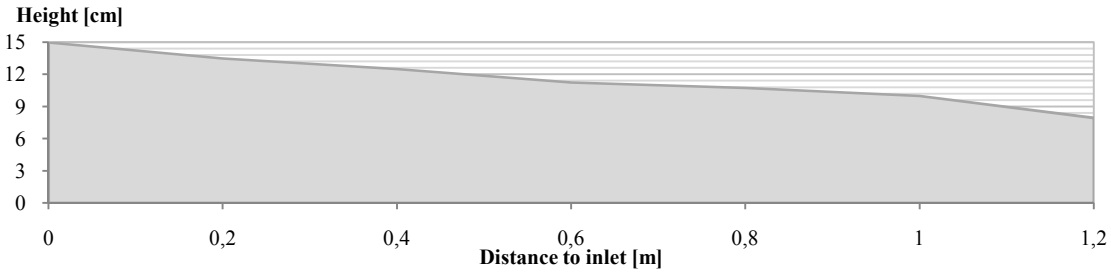

Figure 26. Shape of the concrete after casting for SCC7

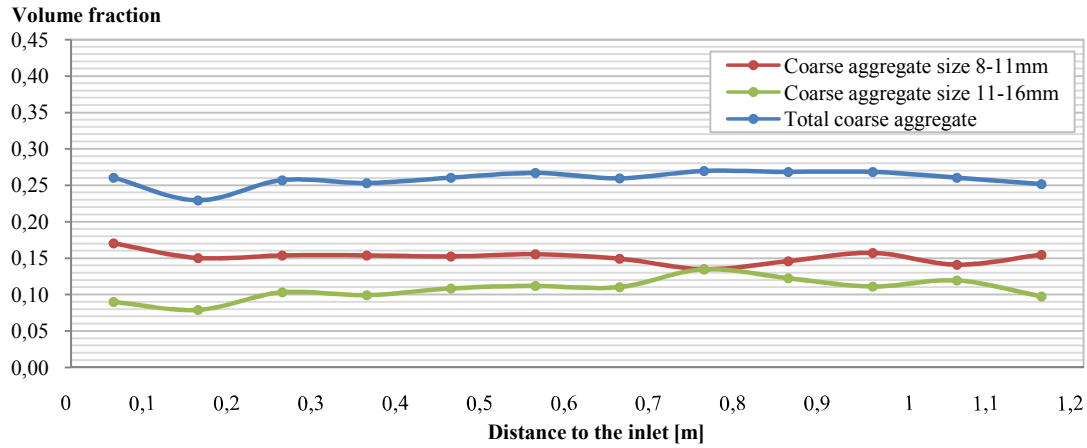

Figure 27. Aggregate distribution by volume fraction for SCC7

The curve of the total coarse aggregate was significantly constant and just a reduced variation was registered for the second sub region. In consequence, no segregation of the coarse aggregate due to flow was observed.

3.6.2. Results for the self compacting concrete with a gap in the aggregate grading

SegC2.2 was tested for the segregation experiment with the LCPC-box. The following results concerning the shape of concrete when static and the distribution of the coarse aggregates 8-16 mm are shown in Figure 28 and Figure 29.

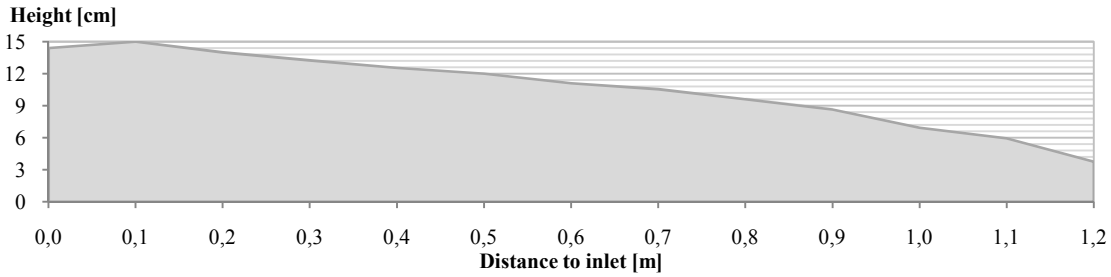

Figure 28. Shape of the concrete after casting for SegC2.2

In that case, a minimum height of 3,75 cm was measured at the end of the mould placed furthest to the inlet. The comparison of that value with a 7,95 cm determined for the previous test (Figure 26) shows that this current mix was less flowable compared with SCC7.

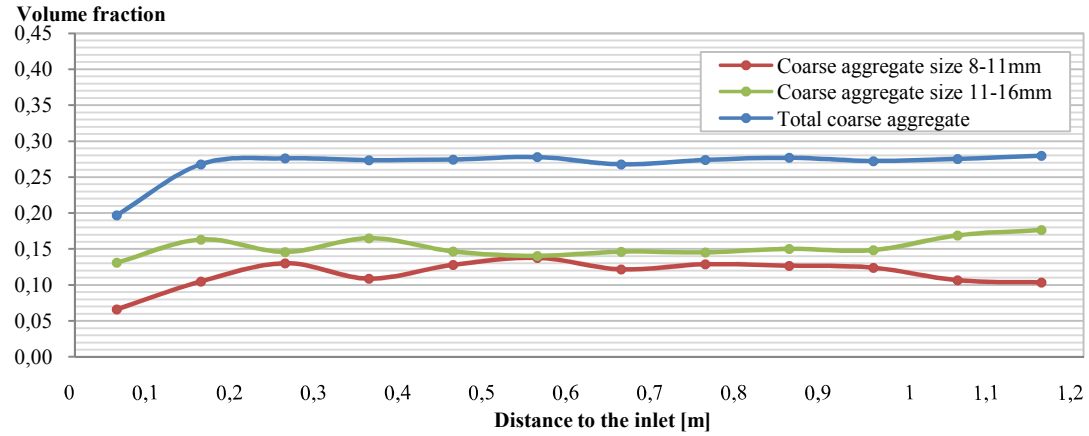

Figure 29. Aggregate distribution by volume fraction for SegC2.2

The results showed that no segregation due to flow was observed as it is shown in Figure 29. Only the first sub region had a lower volume fraction of aggregate and a higher volume fraction of 11-16 mm aggregate was observed for the two last sub regions.

With the results obtained we decided to investigate about the possibility of the dynamic segregation of the coarse aggregate increasing the distance of flow, i.e. considering a longer mould. The segregation experiment described in section 3.5.2 was realized with the mix SegC2.3 and the distribution of the coarse aggregates 8-16 mm was studied in 6 sub regions of 0,10 m long distributed at different distances from the casting point. Figure 30 shows the results obtained.

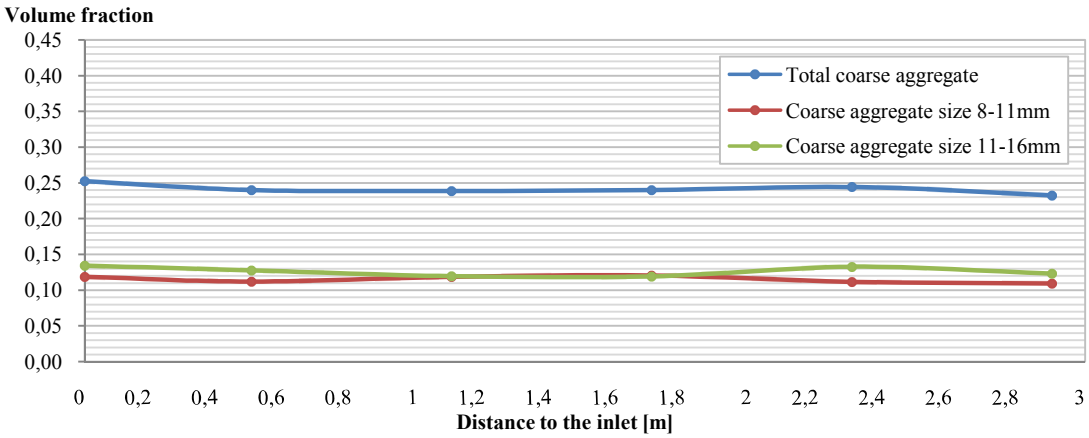

Figure 30. Coarse aggregate distribution by volume fraction for SegC2.3

As the results show, no considerable segregation was observed. The total volume fraction of aggregate was approximately constant with the distance to the casting point and just a slightly lower value is achieved for the furthest sub region respect with the first one.

The segregation experiment with the large mould was tested for the SegC group before the decision about testing the SCC group was made. The reason of this fact was that results of this test, for SegC2.3, were significant enough to predict the behaviour of SCC mix. While SCC7 was a more stable mix than SegC2.3, a uniform distribution of the coarse aggregate could be expected.

3.6.3. Results for the fibre reinforced self compacting concrete

We performed the segregation experiment with the LCPC-box for the $FIB3_{0,25}$.2 mix. The following results concerning the shape of the concrete after flow stoppage, the distribution of the coarse aggregates 8-16 mm and the fibres shown in Figure 31, Figure 32 and Figure 33 were obtained.

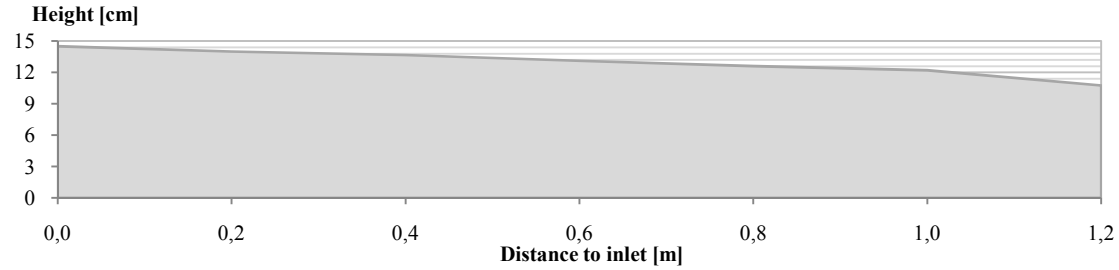

Figure 31. Shape of the concrete after casting for $FIB3_{0,25}$

The rheological properties shown for this mix on the previous section (Table 13) and the shape represented in Figure 32, with a minimum height of 10,75 cm, show that this concrete was considerably flowable.

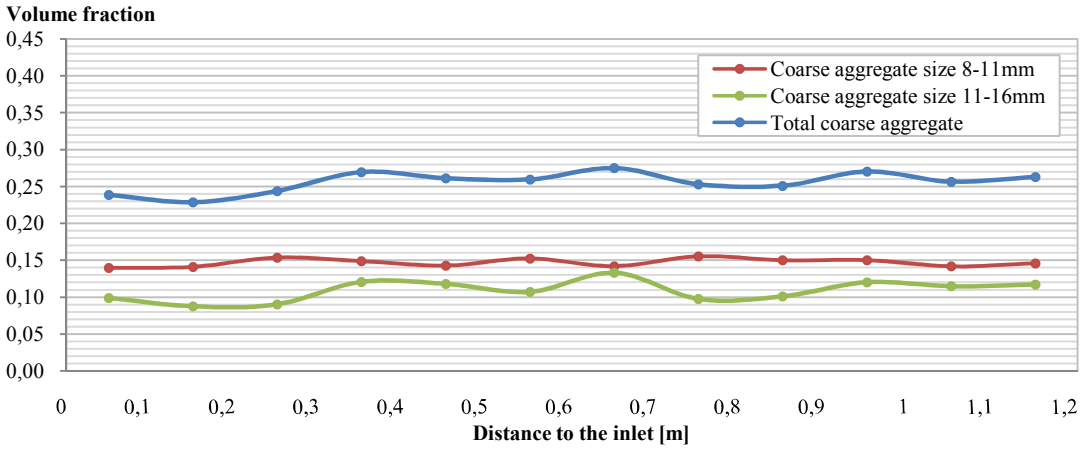

Figure 32. Aggregate distribution by volume fraction for $FIB3_{0,25}$

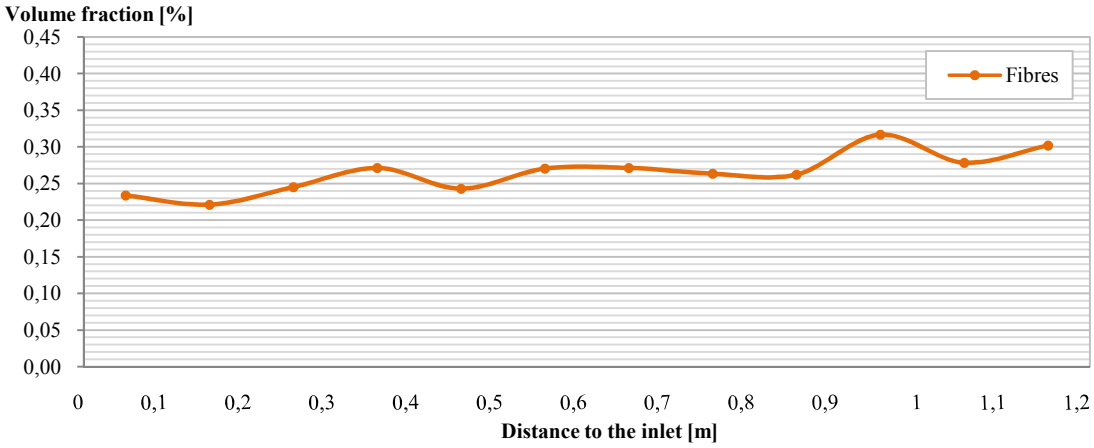

Figure 33. Fibre distribution by volume for $FIB3_{0,25}$

As the results show, no segregation was observed. The total volume fraction of aggregates was approximately constant with the distance to the casting point. A similar behaviour was observed for fibres, for which the volume ratio was slightly higher in the further sub regions, but close, for the major part of the sub regions, to the dosage volume, i.e. 0,25%.

Again, we decided to investigate about the possibility of the dynamic segregation of the coarse aggregate increasing the distance of flow. The segregation experiment described in section 3.5.2 was realized with the mix FIB4 and the distribution of the coarse aggregates 8-16 mm was studied in 6 sub regions of 0,10 m long distributed at different distances from the casting point. Figure 34 and Figure 35 shows the results obtained.

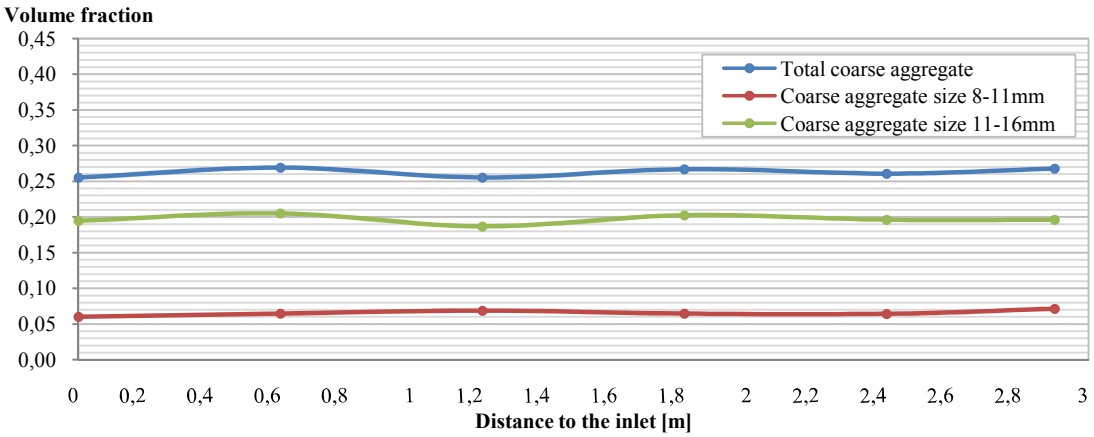

Figure 34. Coarse aggregate distribution by volume for FIB4

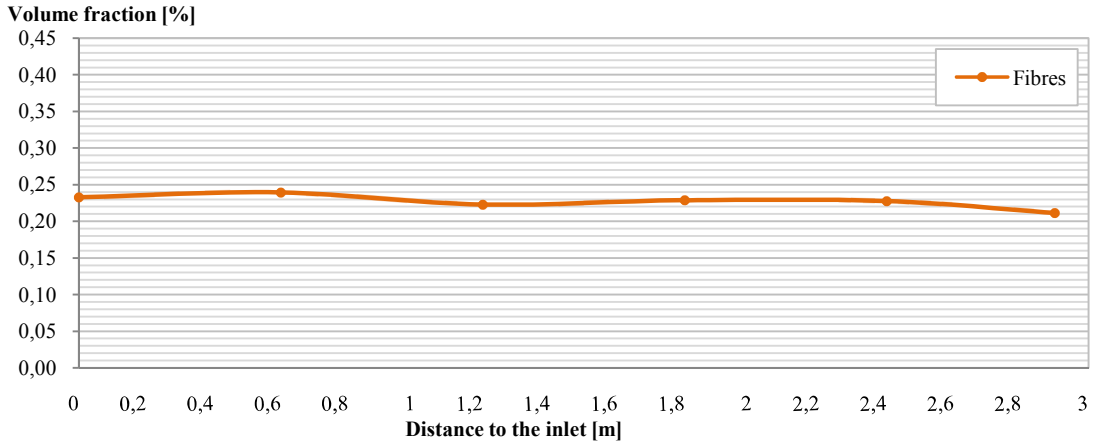

Figure 35. Fibre distribution by volume for FIB4

As the results show, no segregation was observed. The total volume fraction of aggregate was approximately constant with the distance to the casting point. A similar behaviour was observed for fibres, for which the volume ratio was slightly lower in the further sub regions, but close, for the major part of the sub regions, to the dosage volume of 0,25%.

3.7. Conclusions

This experimental research had the aim to investigate the possible non-uniform distribution of aggregates and fibres in the flowable concrete, due to a process of dynamic segregation. The results of the segregation experiments showed that the three mixes studied in this research had a constant distribution of aggregate and fibres. In consequence, the mixes exhibited no segregation due to concrete flow.

Chapter 4

Fibre distribution

4.1. Introduction

The homogenous dispersion of fibres within SFRSCC elements is crucial for a reliable structural performance. The presence of nests or lower fibre content zones could alert us to a non uniform distribution of fibres. Fibre distribution concerns a homogenous distribution over the cross-section, but also within the length of the element. A structural element like a beam would not be acceptable for a symmetric load distribution if it showed a non uniform distribution of the fibre reinforcement.

In this chapter, the fibre distribution in a hardened beam is analyzed and results of the influence of flow on it are concluded for that case.

4.2. Research parameters

The research parameter for this chapter is the number of fibres over the sawn surfaces of a long specimen (beam), whom concrete has flowed along its length. This number of fibres refers to the fibres crossing a specific section, and may be an approximation of the number of fibres in a volume close to that section.

4.3. Properties of the materials and preparation of the specimens

4.3.1. Concrete

The fibre reinforced self compacting concrete used for this test was based on the mix proportioning identified as FIB4 for previous tests (Table 12).

The concrete was mixed on a vertical axis mixer of 700 litres capacity. A batch of 540 l was performed, although only 150 l were needed for this test. The following mixing protocol was adopted. First, aggregates, cement, filler and silica were dried-mixed for one minute. Then, water was added and mixed further for one minute. After two minutes rest, fibres and superplasticizer were added and, finally, concrete was mixed for one additional minute.

Slump-flow test, air content and density of concrete measurements were performed for characterization of the concrete. Table 15 shows the results of these tests.

Table 15. Characterization of FIB4 mix

Date of manufacturing	19.11.2010
Spread for the slump-flow test [mm]	455
Density [kg/m^3]	2338
Air content [%]	2,8

4.3.2. Casting and curing processes

A single large beam was performed for studying the fibre distribution due to flow. A framework with the following dimensions was used:

Table 16. Dimensions of the beam

Length [m]	2,96
Height [m]	0,25
Width [m]	0,20

The concrete was poured into the framework from one end. This way, concrete could flow along the length of the mould a longer distance than if casting from the central point. This fact is of special importance because our study deals with the different properties of concrete induced by flow.

For the curing process, the beam was kept in its mould covered with a plastic sheet for 24 and, then, demoulded. A moisture curing process was followed, keeping the specimen at 22°C and approximately 100% relative humidity until the age of 7 days. Thereafter, the specimens were kept at a constant room temperature.

4.3.3. Preparation of the specimens

Three specimens were obtained from this initial 2,96 m long beam, consisting in sawn slices of 10 cm thick. Table 17 and Figure 36 summarize the dimensions and distance to the casting end for both samples.

Table 17. Location and dimensions of the specimens

Slice identification	**A**	**B**	**C**
Distance to the casting end [m]	0,50	1,48	2,47
Dimensions [m]	0,25x0,20x0,10		

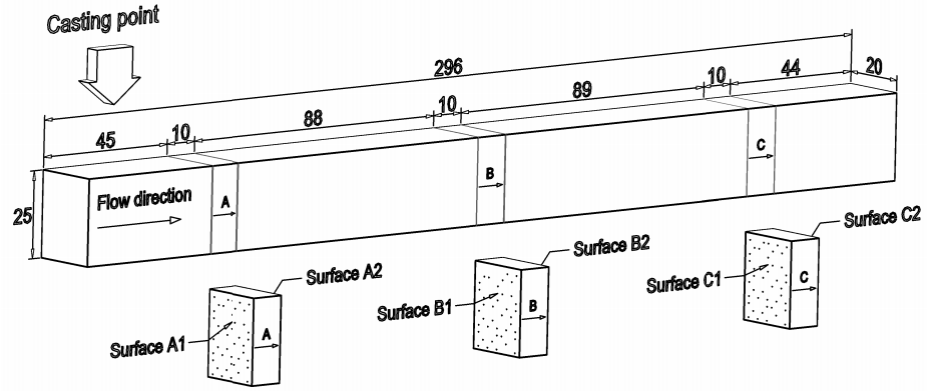

Figure 36. Definition of the specimens for the fibre distribution. Dimensions in cm

4.4. Method and testing procedure

The number of fibres over the concrete cross-section was determined by manual counting over each sawn surface of the slices. Over every counting surface, different sub regions where defined for the registration of the number of fibres depending on the height. Also an outer crown of a fibre length thick was considered for studying the wall effect in the study of the fibre orientation (Chapter 5). Figure 37 represents a sketch of the sub regions considered.

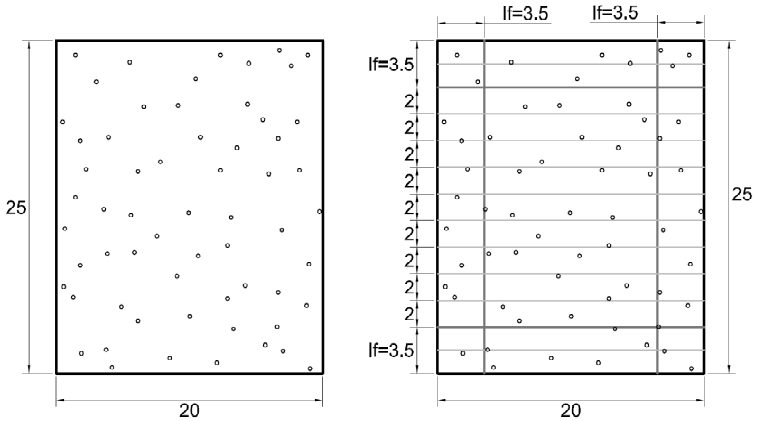

Figure 37. Defined areas for the fibre counting

Figure 38. Fibre counting process

A plastic adhesive paper was used for covering the counting surfaces and defining the sub regions on top. Moreover, each fibre was marked with a permanent marker, so that double counting was avoided. After removing this paper a picture of the fibres dispersion could be easily analyzed (Figure 39). Further information is found in Appendix 3.

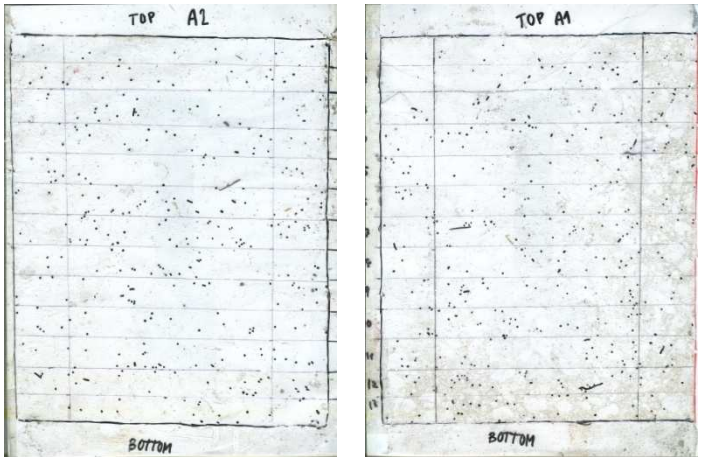

Figure 39. Plastic adhesive after removing from the specimen A

4.5. Results, analysis and discussion

The results of this experimental part are organized in three sections, depending if the distribution refers to the cross-section or to the beam length.

4.5.1. Fibre distribution on the cross-section

Thirteen rows were considered for obtaining the vertical distribution of fibres in the cross-section. The number of fibres in each line was registered and subsequently referred to the area of the line. Figure 40 and Figure 41 represent the results grouped for counting surfaces belonging to the same slice.

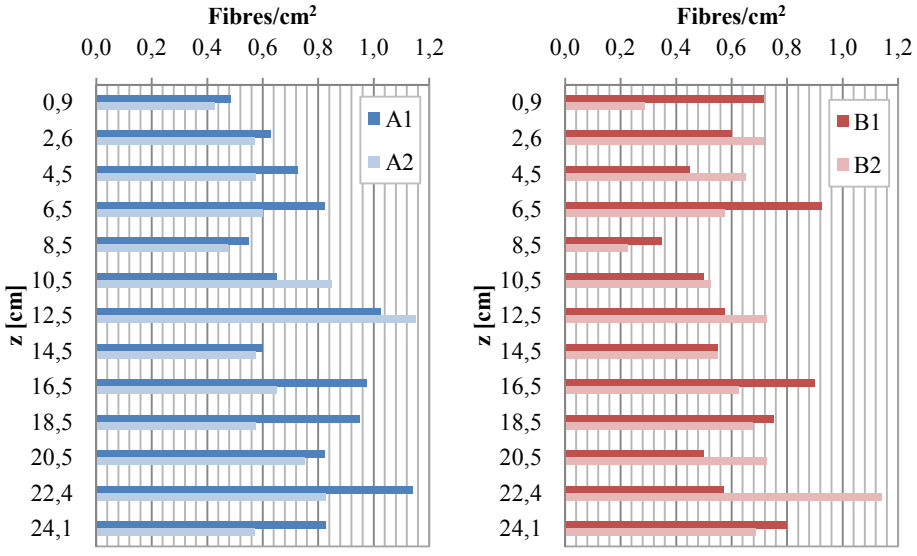

Figure 40. Vertical distribution of fibres in the specimens A (left) and B (right)

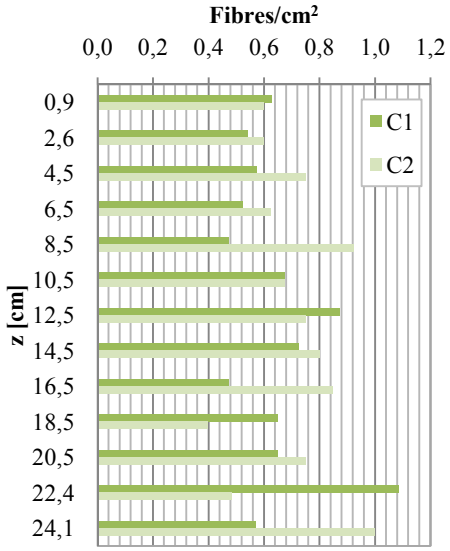

Figure 41. Vertical distribution of fibres in the specimen C

Fibres were generally well distributed over the beam cross-section. Just a slight tendency to distribute fewer fibres on the top of the cross-section and more fibres on the bottom part was observed. This is generally observed for the three slices, i.e. for different distances to the casting point. Because of that, these slight differences in distribution should not be connected with the flow effect and could appear due to static segregation.

4.5.2. Fibre distribution along the length of the beam

For this section, the total number of fibres counted on the surfaces was evaluated for the three slices. Figure 42 shows the number of fibres per unit surface for the six counting surface and its respective position on the beam. Mean values for each slice are shown to be representative of the number of fibres in the vicinity of the slice.

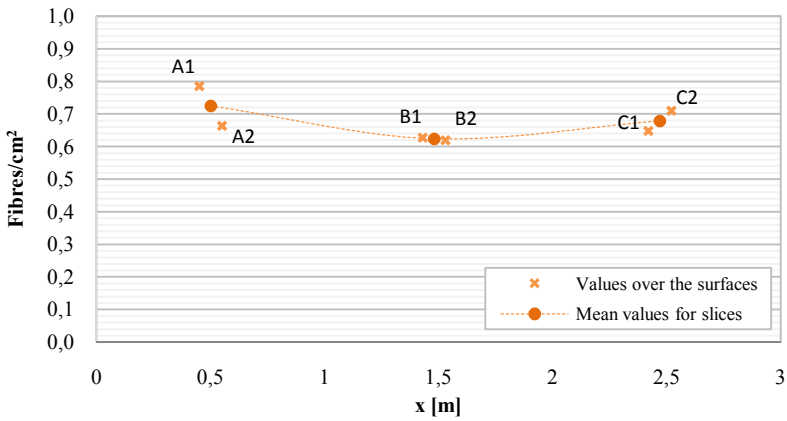

Figure 42. Fibre distribution along the length of the beam

The number of fibres per unit surface had its highest value for the slice A, the closest to the casting point. The last slice, C, the furthest from the casting point and the one whose concrete had flowed more, had a slightly lower value of fibres per unit surface respect with the slice A. The slice B, which represented the middle of the beam, had an even

lower value of fibres. This result would seem unusual if we misunderstood the scale of variation. For example, the variation between the mean values for slice A and B was lower than the variation between the values within the same slice, i.e. variation between A1 and A2. This fact reflects that slices A, B and C showed no considerable differences for number of fibres far from the intrinsic scatter of analyzing different samples. In conclusion, the total number of fibres along the length of the beam was constant.

A second part of this experimental test tried to investigate if any differences on the number of fibres were observed for the top third of the cross-section height, the middle third or the bottom third, along the length of the beam. In despite that the previous results showed no significant variations on the total number of fibres, dynamic segregation could have occurred if the number of fibres for each of these regions was different depending on the distance to the casting point.

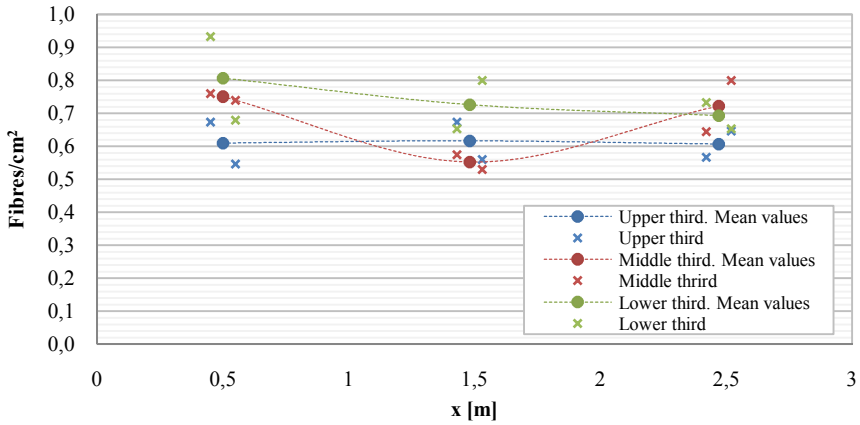

Figure 43. Fibre distribution along the length of the beam for the upper, middle and lower third of the cross section

According to the results (Figure 43) the number of fibres per unit surface was constant for the upper third. Therefore, the more flowed concrete, placed the furthest to the casting point, had not suffered any loss of fibres due to flow for that top third of the cross-section. On the other hand, the lower third decreased the value of fibres per unit surface while increasing the distance to the inlet. If dynamic segregation was present, the opposite had been registered: an increase of the lower third for the last slice (C) would mean than fibres had migrated from the upper part to the bottom part for that segregation effect. However, the results were not so clear for the middle third, which exhibited quite variable number of fibres along the beam length. No causes for that low number of fibres were found for the middle slice (B). Again, the scale of variation between slices was quite reduced compare with variation within the two surfaces measured within the same slice. Consequently, the general behaviour of the three thirds of the beam was that no significant differences of the number of fibres along the length of the beam are found.

A general overview of the graph give us the idea that, as we saw for section 4.5.1, the number of fibres slightly decreased with the height of the sample, i.e. the lower third had higher number of fibres while the upper third had a lower number. But it is worth to emphasize that this fact occurred all over the length of the beam, and not differentially with the distance to the casting point.

4.6. Conclusions

The manual counting showed that fibres are generally uniformly dispersed over the beam cross-section. No appreciable nests or regions without reinforcement are frequently found.

The results showed a distribution of fibres slightly higher on the bottom region of the beam than on the top. This fact occurred along the length of the beam without significant differences with the distance to the casting point. The static segregation is pointed as a possible cause.

Finally, the total number of fibres on the cross-section is constant along the beam. Therefore, the specimen shows no differences on the fibre distribution caused by the flow of the material.

Chapter 5

Fibre orientation

5.1. Introduction

The study of the fibre orientation has a special interest for the engineering properties in the hardened state. Firstly, because the anisotropy due to flow induced orientation of fibres may cause to exhibit significantly different mechanical properties in two orthogonal directions. This has to be carefully evaluated and taken into account in the design. And secondly, because this flow induced orientation of fibres can be taken advantage for an intended application, which is along the anticipated directions of the principal stresses within the structural element when in service.

What is the fibre orientation expected for our case of study and how this fibre orientation may vary in different distances from the casting point are the objectives of this experimental part.

5.2. Research parameters

Several methods for dealing with the fibre orientation have been found in literature (sections 2.3.4.1). Most of these methods are based on the evaluation of a non-dimensional parameter known as orientation factor, α, that we previously defined in section 2.3.4.3. The parameters needed to assess its value are: the number of fibres over the concrete cross-section, N; the fibre volume fraction, v_f; the fibre cross-section, A_f; and the concrete cross-section, A_c.

The number of fibres over the concrete cross-section was obtained by manual counting as reported in section 4.4. On the other hand, from the two different methods generally used to determine the fibre volume fraction (section 2.3.4.3), the direct method was selected. This method, far from theoretical assumptions, is based on crushing the element and manually separating the fibres.

5.3. Properties of the materials and preparation of the specimens

5.3.1. Concrete

The fibre reinforced self compacting concrete used for this test was based on the mix proportioning identified as FIB4 (Table 12).

The concrete was mixed on a vertical axis mixer of 700 l capacity. A batch of 540 l was performed, although only 150 l were needed for this test. The following mixing protocol was adopted. First aggregates, cement, filler and silica were dried-mixed for one minute. Then, water was added and mixed further for one minute. After two minutes rest, fibres and superplasticizer were added and, finally, concrete was mixed for one additional minute.

The slump-flow test, air content and density of concrete measurements were performed for characterization of the concrete. Table 18 shows the results of these tests.

Table 18. Characterization of the concrete properties

Date of manufacturing	19.11.2010
Spread for the slump-flow test [mm]	455
Density [kg/m^3]	2338
Air content [%]	2,8

5.3.2. Casting and curing processes

A single large beam was performed for studying the fibre orientation due to flow. A framework with the following dimensions was used:

Table 19. Dimension of the initial beam for slices A and C

Length [m]	2,96
Height [m]	0,25
Width [m]	0,20

The concrete was poured into the framework from one end. This way, concrete could flow along the length of the mould a longer distance than if casting from the central point. This fact is of special importance because our study deals with the different properties of concrete induced by flow.

For the curing process, the beam was kept in its mould covered with a plastic sheet for 24 and, then, demoulded. A moisture curing process was followed, keeping the specimen at 22°C and approximately 100% relative humidity until the age of 7 days. Thereafter, the specimens were kept at a constant room temperature.

5.3.3. Preparation of the specimens

Two specimens were obtained from this initial 2,96 m long beam, consisting in sawn slices of 10 cm thick. Table 20 summarizes the dimensions and distance to the casting end for both samples.

Table 20. Location and dimensions of the specimens

Slice identification	**A**	**C**
Distance to the casting end [m]	0,50	2,47
Dimensions [m]	0,25x0,20x0,10	

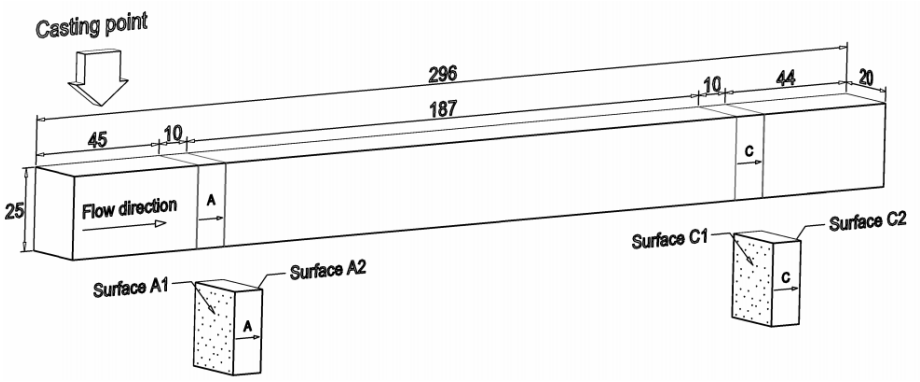

Figure 44. Definition of the specimens for the fibre distribution. Dimensions in cm

5.4. Method and testing procedure

The measure of the fibre orientation through the orientation factor requires the determination of two main parameters: the number of fibres over the concrete cross-section (N) and the fibre volume fraction (v_f).

The number of fibres over the concrete cross-section was determined by manual counting over each sawn surface. As every slice had two sawn surfaces, the mean value for the number of fibres could be taken. Alternatively, two values of the orientation factor could be calculated corresponding to the number of fibres obtained for each sawn surface and, afterwards, mean value could be estimated. This last process allowed to have an idea of the variation of this factor within the same slice, i.e. at approximately the same distance to the casting end.

Figure 45. Crushing process of the slices and isolation of the fibres

The fibre volume fraction was determined by crushing the slice into small fragments. Afterwards, manual crushing together with the help of a magnet enabled to isolate the steel fibres from the crushed concrete. The weight of fibres, correlated with its density and the volume of the slice, provides the result of the fibre volume fraction.

Once all the information required was obtained, the orientation factor was assessed from equation (6).

5.5. Results

The results for the manual counting of the sawn surfaces are collected in Table 21, as well as the weight of fibres within each slice and its corresponding volume fraction. The surfaces are identified as Xi, where X refers to the slice identification and $i = 1$ means the sawn surface of the slice closest to the casting point and $i = 2$ the furthest surface to this point.

Table 21. Results of the fibre counting for slices A and C

Slice	**A**		**B**	
Fibre weight [g]	99,0		89,5	
Volume of fibres [l]	0,0127		0,0115	
v_f [%]	0,254		0,229	
Surface	A1	A2	C1	C1
N	393	332	324	355

Other necessary parameters to obtain the value of the orientation factor are shown in Table 22.

Table 22. Geometry of fibres and area of concrete for the slices

d_f [mm]	0,54
A_f [mm^2]	0,228
A_c [mm^2]	50000

The results for the orientation factor, calculated with the values referred above are shown in Table 23.

Table 23. Results for the orientation factor for slices A and C

	Slice A		**Slice C**	
Surface where fibres counted	A1	A2	C1	C2
Orientation factor for the surface	0,71	0,60	0,64	0,70
Mean orientation factor for the slice	**0,65**		**0,67**	
C.V. [%]	8,4		4,6	
Mean orientation factor for the beam	0,66			
C.V. [%]	1,77			

5.6. Analysis and discussion

The slice A is a specimen from the initial beam placed at 0,50 m from the casting point, while slice C is placed 2,47 m from the same point. That means that the constituent concrete of each slice has a different degree of flow, which could induce differences in the orientation of fibres if flow actually has an influence on the uniformity of concrete.

Table 23 shows that the mean value of the orientation factor for the slice A was 0,65, while the value was 0,67 for slice C. The immediate idea is that both slices have the same orientation factor, because the variation between them was lower than the variation between the orientation factors within the same slice. As a result, the specimens showed no differences in fibre orientation and a mean value of 0,66 can be understood as representative of the beam. Considering the values of this factor correlated with the three ideal orientation situations (previously in section 2.3.4.3):

- Uni-directed fibres: $\alpha = 1{,}00$
- Plane orientation: $\alpha = 0{,}64$
- Isotropic orientation: $\alpha = 0{,}50$

The value of 0,66 reflects that the specimen is featured by a plane orientation of fibres.

5.7. Conclusions

The study of the fibre orientation was carried out with a beam casted from one end with a fibre reinforced self compacting concrete defined as FIB4, allowing the concrete to flow in order to fill the framework. Two slices of this beam were studied for the orientation factor measurement. Results showed similar values of this factor. In consequence, no differences of the fibre orientation along the beam were found due to flow. On the other hand, the general predominant orientation of the specimen was planar.

Chapter 6

Bending test

6.1. Introduction

FRSCC has numerable advantages respect with the use of a vibration compacted concrete and ordinary reinforced concrete. But the better working conditions and the increase of productivity that this concrete represents are only considerable if the final behaviour of the material performs reliable mechanical properties. A main feature of this material, the ability of flowing during the casting process without need of vibration, could have an effect on the mechanical properties if the concrete was no stable during flow. A minor amount of fibres or aggregates on a particular region of a structural element could cause a lower strength on the hardened state that should, at least, be studied.

This research has investigated the variation of the mechanical properties of a FRSCC long element, consisting on a 2,96 m long beam casted from one end, without vibration. The hardened element was sawed into three parts, so that three specimens composed of concrete with potentially different flow effects, according to its proximity to the casting point, were obtained. The mechanical properties of these specimens were studied through bending tests. Moreover, three standard specimens not subjected to flow conditions and three subjected to flow conditions were tested in order to characterize the concrete and compare them with the sawn specimens.

6.2. Research parameters

A common use of FRSCC is the production of beams and slabs. Beams are the structural element studied in that research and its mechanical properties were studied through the bending test. Bending tests are often performed to obtain the theoretical maximum tensile stress reached on the bottom fibre of the test beam, known as the *modulus of rupture*. However, fibres have not considerable influence on that value due to two main factors. First, the elongations at break of fibres are two or three orders of magnitude greater than the strain at failure of the matrix and, hence, the matrix will usually crack long before the fibre strength is approached. Secondly, the modulus of elasticity of the fibre is generally less than five times that of the matrix and this, combined with the low fibre volume fraction, means that the modulus of the composite is not greatly different from that of the matrix (Hannant, 2003). Then, as it is been mentioned before, the main benefits of the inclusion of fibres in hardened concrete relate to the post-cracking state, where the fibres bridging the crack contribute to the

increase of the strength of the composite. As a result, the major attention will be focused on the study of the residual flexural strength.

During bending tests the relationship between the load applied and the deflection, or vertical displacement (δ), at a specific point of the element are registered. Once the maximum load is reached, the specimen breaks and a crack begins to progress with the increase of load. The parameter known as *crack mouth opening displacement* ($CMOD$) refers to the horizontal displacement between the two cracked walls while the crack is progressing due to the application of the load. Consequently, deflection and $CMOD$ are alternatively used for exhibiting most of the bending test results.

However, if specimens with different sizes are tested and the comparison between them is required, the load applied is usually referred to its corresponding value of flexural strength. The correlation load-flexural strength needs the moment distribution of the element, the geometry of the specimen and an assumption of the stress distribution on the cross section. In conclusion, the research parameters that will allow us to draw conclusions will be the flexural tensile strength and its corresponding deflection or, alternatively, $CMOD$ value.

6.3. Properties of the materials and preparation of the specimens

6.3.1. Concrete

The fibre reinforced self compacting concrete used for that test was based on the mix proportioning identified as FIB4 for previous tests (Table 12).

Concrete was mixed on a vertical axis mixer of 700 l capacity. A batch of 540 l was performed, although only 150 l were needed for this test. The following mixing protocol was adopted. First aggregates, cement, filler and silica were dried-mixed for one minute. Then, water was added and mixed further for one minute. After two minutes rest, fibres and superplasticizer were added and, finally, concrete was mixed for one additional minute.

The slump-flow test, air content and density of concrete measurements were performed for the characterization of concrete. Table 24 shows the results of these tests.

Table 24. Characterization of FIB4 mix

Date of manufacturing	19.11.2010
Spread for the slump-flow test [mm]	455
Density [kg/m^3]	2338
Air content [%]	2,8

6.3.2. Preparation of the specimens: casting and curing processes

An initial long beam was prepared with the dimensions shown in Figure 46. The casting point was placed at one end, so that concrete could flow until it completely filled the framework. No vibration was required due to its self-compacting feature. This initial

long beam was sawn into three equal specimens, identified as *First*, *Middle* and *Last*, being *First* the closest to the casting point.

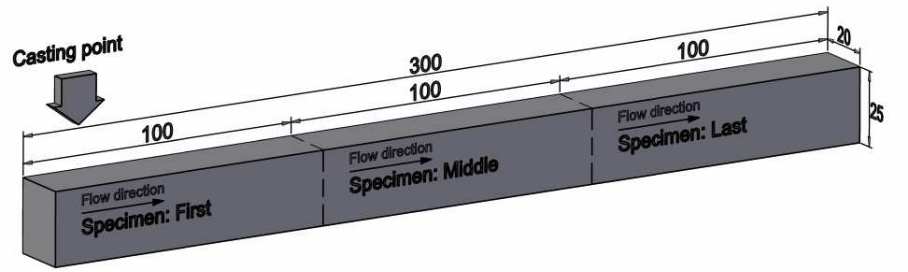

Figure 46. Origin of the sawn specimens. Dimensions in cm

Parallel, six standard beams were casted with the dimensions shown in Figure 47. Three of them were casted with concrete directly after the mixing process. The other three beams were casted with the concrete used for the segregation experiment. This concrete came from the furthest end to the casting point, which means that it had approximately flown the length of the mould, i.e. 3 m. This way, we had three standard beams filled with concrete without any flow effect and three more with possible flow effects. Table 25 summarizes the dimensions and identification of the specimens.

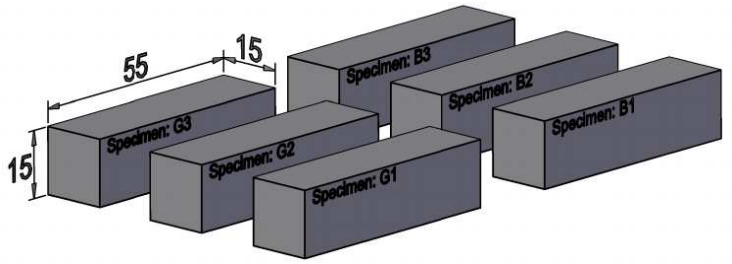

Figure 47. Standard beams. Dimensions in cm

Table 25. Dimensions of the specimens and origin of their concrete

Group of specimens	Identification of the specimen	Dimensions			Origin of the concrete
		Length [m]	Height [m]	Width [m]	
Sawn beams	First, Middle and Last	1,00	0,25	0,20	Directly from the mixer
Standard beams	G1, G2 and G3	0,55	0,15	0,15	Directly from the mixer
	B1, B2 and B3	0,55	0,15	0,15	After flow for the segregation experiment

For the curing process, the beam was kept in its mould covered with a plastic sheet for 24 and, then, demoulded. A moisture curing process was followed, keeping the specimen at 22°C and approximately 100% relative humidity until the age of 7 days. Thereafter, the specimens were kept at a constant room temperature.

6.3.3. Compressive strength test

In order to characterize the potential quality of the concrete, three standard cubes were tested for the compressive strength test. The specimens were casted in steel moulds (Figure 48), 100 mm cubes, with its surfaces covered with oil to prevent the bond between the mould and the concrete.

Figure 48. Moulds for the compressive strength cubes

Due to the lack of time during the last stage of the experimental research, the cubes were tested 19 days after the casting date, instead of 28 days as generally prescribed. Results are summarized in Table 26.

Table 26. Results for the compressive strength test

Date of the casting		19.11.2010
Date of the test		07.12.2010
Days after casting		19
Compressive strength [MPa]	Specimen 1	57,13
	Specimen 2	58,02
	Specimen 3	59,19
Mean value [MPa]		58,11

6.4. Method and testing procedure

Two different methods were used for determining the flexural tensile strength depending on the tested specimens.

6.4.1. Bending test for standard beams

The group of specimens denoted as *standard beams* was tested according to the European Standard test described in EN 14651. This test is widely used to characterize the flexural tensile strength of concrete, and its standardized conditions allow the comparison with specimens tested for other researches.

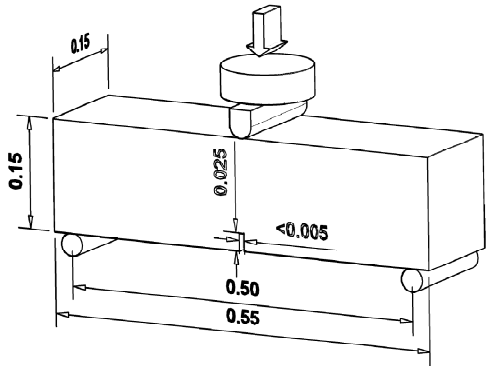

Figure 49. Loading and supporting system for the bending test with the standard beams. Dimensions in m

Before the test, the three beams were notched through their width at mid-span section. Afterwards, they were placed in the testing machine with a 0,50 m span and the loading roller perfectly centred at the mid-span section (Figure 49). Afterwards, two displacement transducers were mounted on two rigid frames that were fixed to the specimen at mid-height over the supports, one on each side (Figure 50). These transducers were connected to a data recording system capable to record loads and deflections. The load was applied at a constant rate of increase of deflection of 0,2 mm/min. This can be considered as a deviation from the standard test method, due to it specifies that the machine should firstly be operated at a lower rate until the deflection reaches the value of $\delta = 0{,}13$ mm. Unfortunately, the testing machine at the NTNU concrete laboratory is not able to be programmed to increase the deflection rate at a specified value. However, no other deviations from the standard test methods were followed.

Figure 50. Bending test equipment for the standard beams

Figure 51. Crack located at the notched section for the standard beams

During the test the recording system registered continuous information of time, load, deflection of the left side and deflection of the right side. These two last measurements provided a higher accuracy of results for the deflection, obtained as the mean value of both sides. Finally, the load was applied until a deflection value not less than 3,44 mm was achieved, as it is specified in EN 14651.

In this test the mid-span section was the section where the load was applied, i.e. the more stressed section, and, on the same time, the notched section, i.e. the smallest cross section. The combination of both facts made that for this test the crack was always located at this point. This is one of the features of the Standard test.

6.4.2. Bending test for the sawn beams

The four point bending test is the commonly used bending test described by the Norwegian guidelines (NSBT). The group of *sawn beams* (First, Middle and Last) was tested with this method.

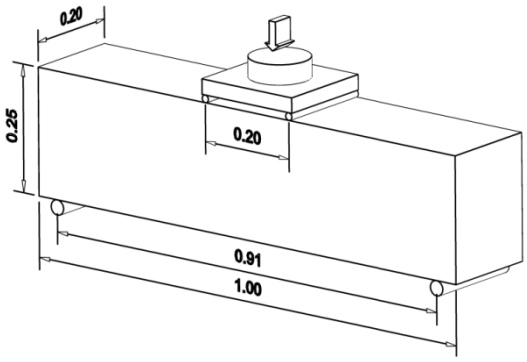

Figure 52. Loading and supporting system for the bending test with the sawn beams. Dimensions in m

The beams were placed in the same loading machine. On that occasion, the beams could not be lifted manually by a single person due to its weight of approximately 117 kg. The help of a crane and a forklift was required. The spam between the simple supports was 910 mm and the loading element, formed by two loading rollers at a distance of 200 mm, was perfectly centred at the mid-span section. Contrarily to the three points-bending test, for that current test the testing direction was parallel to the casting direction. For that reason, two elastic elements were placed between the loading rollers and the specimens, in order to avoid a non-uniform contact due to the rough surface. Afterwards, two displacement transducers were mounted on two rigid frames that were fixed to the specimen at mid-height over the supports, one on each side. These transducers were connected to a data recording system capable to record loads and deflections. The load was applied at a constant rate of increase of deflection of 0,5 mm/min. Finally, the load was applied until the fixed value of $\delta = 3{,}44$ for the Standard test was largely exceeded.

Figure 53. Bending test equipment for the sawn beams

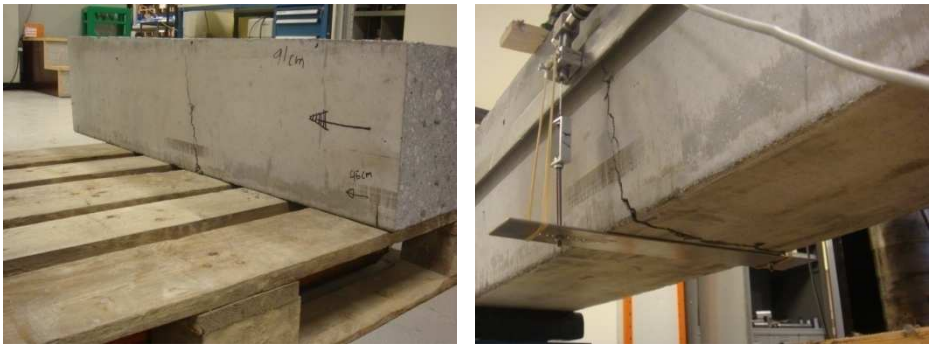

Figure 54. Crack located at the weakest section for the sawn beams

In this case, the beams were not notched. That meant that the location of the crack was not previously known and it would appear on the weakest section where the maximum concrete strength was firstly reached.

Again, time, load, deflection on the left side and deflection on the right side were registered for each test.

6.4.3. Fibre counting close to the cracked section

As we have seen in section 6.2, the residual flexural tensile strength is very much dependant on the fibre content. A lower number of fibres in the more stressed section could mean a limited residual flexural strength. In order to compare the number of fibres with the results from the bending tests, all the specimens tested were sawn at a distance of 50 mm from the cracked section and fibres were counted. The distance of 50 mm was considered to be enough for avoiding effects induced by the failure, for what generally a minimum of a fibre length is recommended. Figure 55 and Figure 56 show the sawn section for the fibre counting.

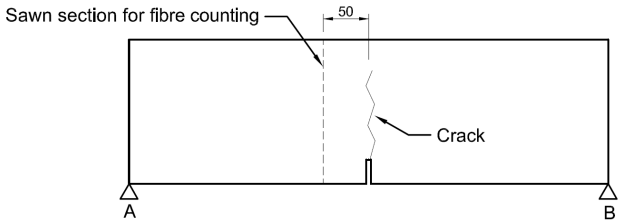

Figure 55. Sawn section for fibre counting for a Standard specimen. Dimensions in mm

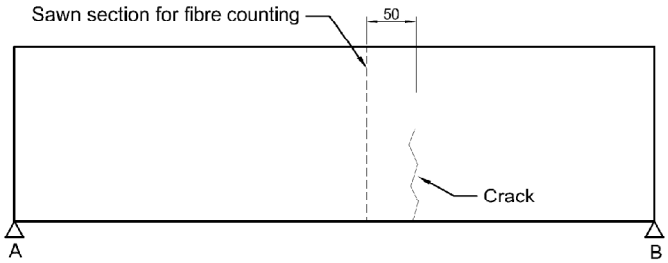

Figure 56. Sawn section for fibre counting for a Sawn specimen. Dimensions in mm

6.5. Results

The results obtained directly from the recording system machine during the bending test were treated differently and previous calculations need to be reported.

6.5.1. Previous calculations for the standard beams

6.5.1.1. Correlation between deflection and CMOD

Several expressions can be used to correlate the measured deflection with its alternative parameter defined as crack mouth opening displacement ($CMOD$), which refers to the horizontal displacement between the two sides of the crack while it is progressing due to the application of the load. The EN 14651 establishes the relationship between them with the following equation:

$$\delta = 0{,}85CMOD + 0{,}04 \quad (15)$$

where both parameters are in mm.

However, the use of this expression is limited to the specific conditions described by the standard, and, therefore, the expression will not be applicable to the *sawn beams*. As a result, for the comparison of results between standard beams and sawn beams a different expression based on the same theoretical principles is required. The following proposed expressions are developed and described in (Sandbakk 2010).

As we saw in the last section, due to the notch, all the standard beams cracked at the mid-span section. Figure 57 represents a simplified sketch of the initial and cracked beam, where once the specimen has broken the two parts divided by the crack behave like a rigid solid, with only a rotating movement.

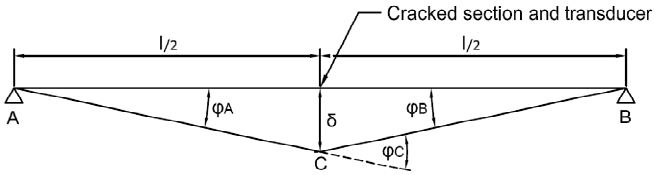

Figure 57. Sketch of the breaking mechanism for a standard beam

Due to the symmetry, the rotation of the two parts divided by the crack (φ_A, φ_B) will be equal and the deflection will be maximum at the central point. Assuming low angles, the rotation at the crack (φ_C) can be expressed as:

$$\varphi_A = \varphi_B = \frac{2\delta}{l} \quad (16)$$

$$\varphi_C = \varphi_A + \varphi_B = \frac{4\delta}{l} \quad (17)$$

On the other hand, Figure 58 helps us to define the link between rotation and $CMOD$.

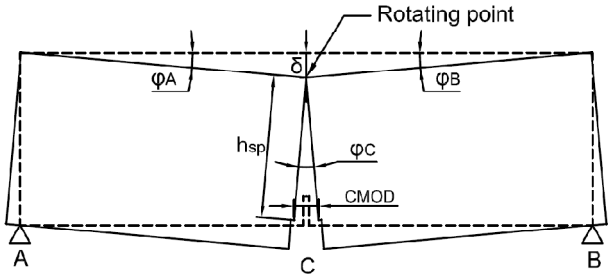

Figure 58. Breaking mechanism for a standard beam

$$CMOD = h_{sp}\varphi_B \quad (18)$$

where h_{sp} is the distance between the tip of the notch and the top of the specimen. Joining the relations rotation- deflection and rotation- $CMOD$, defined by equations (17) and (18), the expression that connects CMOD and deflection is written as:

$$CMOD = \frac{4\delta h_{sp}}{l} \quad (19)$$

6.5.1.2. LOP and residual flexural tensile strength

The expression of the results according to the Standard EN 14651 is given by two strength parameters: the *limit of proportionality* (LOP or $f_{ct,L}^{f}$) and the *residual flexural tensile strength* ($f_{R,j}$). The LOP is defined as the stress at the tip of the notch which is assumed to act in the uncracked mid-span section of the beam subjected to its maximum load (F_L). On the other hand, the *residual flexural tensile strength* is defined as the stress at the same point after the maximum load is reached. The *Standard* only demands the calculation of $f_{R,j}$ corresponding to δ_j or $CMOD_j$ ($j = 1,2,3,4$), being these $CMOD$ values 0,5, 1,5, 2,5 and 3,5, respectively. Of course, the residual flexural tensile strength can be obtained for all the range of loads corresponding to the deflections measured.

As we have mentioned before, correlating load and strength needs to know the moment distribution of the element, the geometry of the specimen and an assumption of the stress distribution on the cross section. The moment distribution is, according to the supporting conditions and the load, shown in Figure 59, where F_j is the load applied.

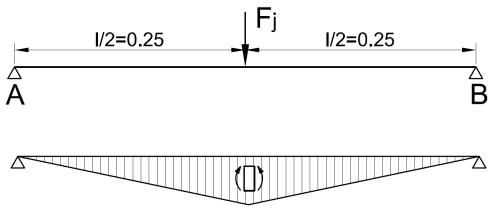

Figure 59. Loading sketch and moment distribution for a standard beam. Dimensions in cm

The geometry is measured at the mid-span section before every test, so that deviations from the prescribed dimensions can be considered. And, finally, the EN 14651 assumes a linear stress distribution as shown in Figure 60.

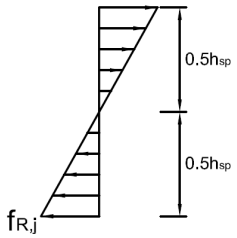

Figure 60. Simplified linear stress distribution for a standard beam

Gathering these conditions, the LOP and the residual flexural tensile strength are given by the expressions:

$$f_{ct,L}^{f} = \frac{6M_L}{bh_{sp}^2} = \frac{3F_L l}{2bh_{sp}^2} \quad (20)$$

$$f_{R,j} = \frac{6M_j}{bh_{sp}^2} = \frac{3F_j l}{2bh_{sp}^2} \quad (21)$$

where:
F_L is the maximum load, corresponding to the LOP
F_j is the load applied for a corresponding value of $CMOD$
M_L is the bending moment corresponding to the load at LOP
M_j is the bending moment corresponding to the load applied F_j
l is the span length
b is the width of the specimen

6.5.2. Previous calculations for the sawn beams

6.5.2.1. Correlation between deflection and CMOD

The deflection measured for this test corresponds to the point where the transducer was placed Figure 61. However, comparing the results between the three specimens (First, Middle and Last) requires correlating this deflection with the maximum deflection, placed at the cracked section. Moreover, as we have seen before, the specimens were not notched and, consequently, the crack would appear in the weakest section. For that reason, the distance between the transducer and the cracked section (x) needed to be measured after the end of every test.

The correlation between deflection and CMOD for this section follows the same theoretical principles exposed on the previous section 6.5.1.1 and studied in depth in (Sandbakk 2010).

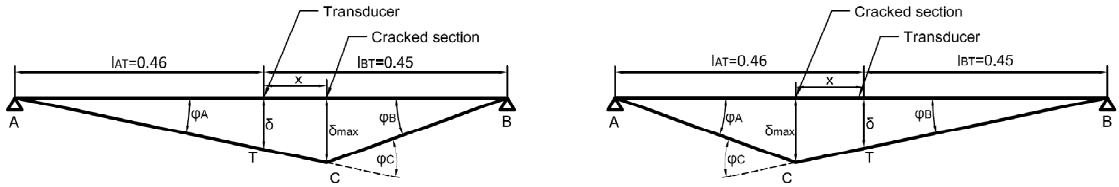

Figure 61. Sketch of the breaking mechanism for the sawn beams. Diemensions in m

Because of the transducer was not placed at mid-span ($l_{AT} \neq l_{BT}$), the maximum deflection is calculated with the expression (22)-(23), where $i = A$ if the crack is closer to the support B and, otherwise, $i = B$.

$$\varphi_i = \frac{\delta}{l_{iT}} = \frac{\delta_{max}}{l_{iT} + x} \quad (22)$$

$$\delta_{max} = \left(1 + \frac{x}{l_{iT}}\right)\delta \quad (23)$$

Where:

δ is the measured deflection

δ_{max} is the maximum deflection

x is the distance between the transducer (T) and the cracked section

l_{AT} is the distance between the support A and the transducer (T), with a value of $0{,}46\ m$

l_{BT} is the distance between the support B and the transducer (T), with a value of $0{,}45\ m$

When the crack is closer to the support B, the rotation at the crack (φ_C) can be expressed as $\varphi_C = \varphi_A + \varphi_B$, where:

$$\varphi_A = \frac{\delta_{max}}{l_{AT} + x} = \frac{\delta}{l_{AT}} \quad (24)$$

$$\varphi_B = \frac{\delta_{max}}{l_{BT} - x} = \frac{l_{AT} + x}{l_{AT}(l_{BT} - x)}\delta \quad (25)$$

On the other hand, Figure 62 helps us to define the link between rotation and $CMOD$.

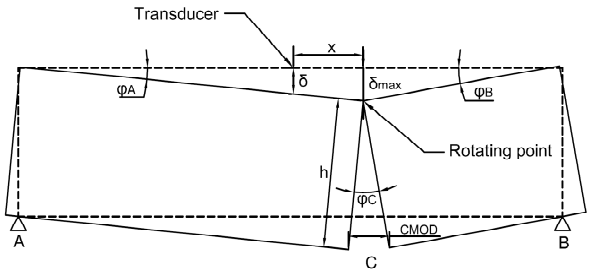

Figure 62. Breaking mechanism for a sawn beam

$$CMOD = h\varphi_C \quad (26)$$

where h is the height of the beam. Joining the relations rotation- deflection and rotation-$CMOD$, defined by equations (24)-(26), $CMOD$ is expressed as a function of δ_{max}:

$$CMOD = \left(\frac{1}{l_{AT} + x} + \frac{1}{l_{BT} - x}\right) h \cdot \delta_{max} \quad (27)$$

Or as a function of the measured deflection δ:

$$CMOD = \frac{\delta hl}{l_{AT}(l_{BT} - x)} \quad (28)$$

6.5.2.2. Residual flexural tensile strength

Again, correlating load and strength needs to know the moment distribution of the element, the geometry and an assumption of the stress distribution on the cross section. However, the load distribution is different to the standard test and, consequently, the moment distribution will also be.

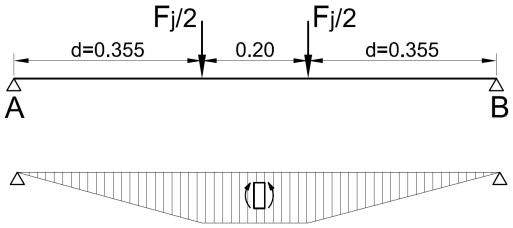

Figure 63. Loading sketch and moment distribution. Dimensions in m

If the crack is located between the two loading points, the bending moment (M_j) corresponding to the load F_j for the cracked section can be expressed as:

$$M_j = \frac{F_j d}{2} \quad (29)$$

Where d is the distance between the support and the closest loading point section, with value $0{,}355\ m$.

The geometry is measured at the cracked section at the end of every test, so that deviations from the prescribed dimensions can be considered. Finally, the flexural tensile strength has been determined with the assumption of a linear stress distribution as shown in Figure 64. This is the same assumption used for the expression of the residual strength according to the Standard and, consequently, results will be comparable.

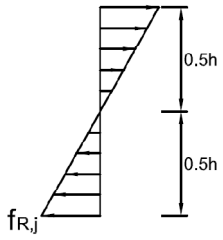

Figure 64. Simplified linear stress distribution for a sawn beam

Gathering these conditions, the residual flexural tensile strength is given by the expression:

$$f_{R,j} = \frac{6M_j}{bh^2} = \frac{3F_j d}{bh^2} \quad (30)$$

Where:
F_j is the load applied for a corresponding value of $CMOD$
M_j is the bending moment corresponding to the load applied F_j
b is the width of the specimen at the cracked section
h is the height of the specimen at the cracked section

6.5.3. Results

The recording system connected to the testing machine provided results of time, load and deflection. In the previous section, we have described the treatment of this initial data in order to obtain the flexural tensile strength versus CMOD diagrams. Moreover, as we have mentioned, the main benefit of the inclusion of fibres relate to the post-cracking state and, then, a special attention will be focused on the residual flexural strength, more than the modulus of rupture.

▪ *Standard beams* casted with concrete directly from the mixer: *G1*, *G2* and *G3*

The flexural tensile strength-CMOD diagram of the three beams *G1*, *G2* and *G3* and its mean curve is shown in Figure 65. Table 27 reports the calculated results according to the Standard.

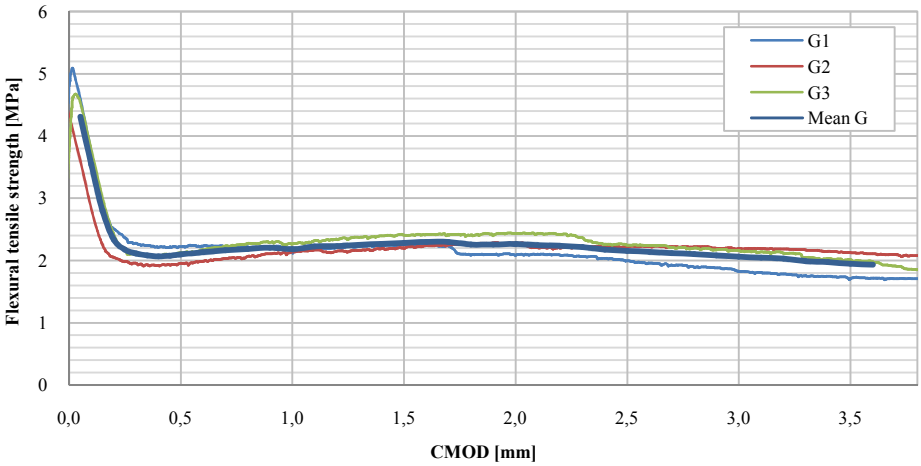

Figure 65. Flexural tensile strength variation with CMOD for the G specimens

Table 27. LOP and residual flexural tensile strength for the G specimens

	G1	G2	G3	Mean value	Coef. of variation [%]
$f_{ct,L}$ [Mpa]	5,09	4,49	4,67	4,75	5,3
$f_{R,1}$ [Mpa]	2,22	1,95	2,13	2,10	5,3
$f_{R,2}$ [Mpa]	2,25	2,19	2,41	2,28	4,0
$f_{R,3}$ [Mpa]	1,99	2,22	2,25	2,15	5,3
$f_{R,4}$ [Mpa]	1,71	2,13	2,01	1,95	9,0

The three beams showed the same behaviour and a low variation of the results was observed. A mean value of 4,75 MPa corresponded to the LOP and it decreased close to

half of this value, 2,15 MPa, for the residual flexural tensile strength corresponding to a 2,5 mm $CMOD$.

The results of the fibre counting for the three specimens are reported in Table 28.

Table 28. Results of the fibre counting for specimens G1, G2 and G3

	G1	G2	G3
Upper half [fibres/cm^2]	0,55	0,84	0,86
Lower half [fibres/cm^2]	0,55	0,90	0,67
Average for cross-section [fibres/cm^2]	0,55	0,87	0,76
Average [fibres/cm^2]	0,73		

The specimen G2 exhibited the higher number of fibres, especially in the lower half, where higher tensile stresses are concentrated. However, this higher value was not reflected in a higher residual flexural strength according to Figure 65.

▪ *Standard beams* casted with concrete from the segregation experiment: *B1*, *B2* and *B3*

The flexural tensile strength-CMOD diagram of the three beams *B1*, *B2* and *B3* and its mean curve is shown in Figure 66. Table 29 reports the calculated results according to the Standard.

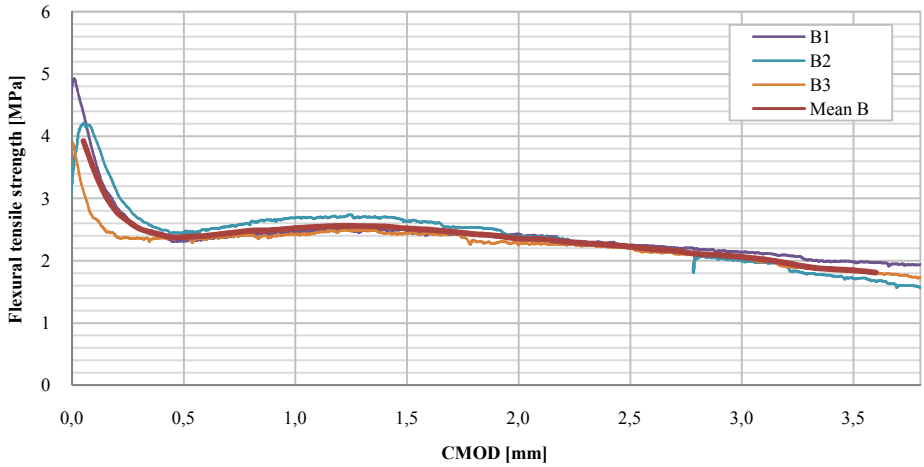

Figure 66. Flexural tensile strength variation with CMOD for the B specimens

Table 29. LOP and residual flexural tensile strength for the B specimens

	B1	B2	B3	Mean value	Coef. of variation [%]
$f_{ct,L}$ [Mpa]	4,92	4,21	3,90	4,34	9,9
$f_{R,1}$ [Mpa]	2,32	2,45	2,37	2,38	2,3
$f_{R,2}$ [Mpa]	2,48	2,63	2,43	2,52	3,3
$f_{R,3}$ [Mpa]	2,25	2,23	2,20	2,23	0,8
$f_{R,4}$ [Mpa]	1,98	1,72	1,83	1,84	5,9

Again, the three beams showed the same behaviour and a low variation of the results was observed. A mean value of 4,34 MPa corresponded to the LOP and it decreased close to half of this value, 2,23MPa, for the residual flexural tensile strength corresponding to a 2,5 mm $CMOD$.

The results of the fibre counting for the three specimens are reported in Table 30.

Table 30. Results of the fibre counting for specimens B1, B2 and B3

	B1	**B2**	**B3**
Upper half [fibres/cm^2]	0,57	0,64	0,55
Lower half [fibres/cm^2]	0,58	0,59	0,69
Average for cross-section [fibres/cm^2]	0,57	0,61	0,62
Average [fibres/cm^2]	0,60		

The specimen B3 exhibited a slightly higher number of fibres, especially in the lower half. Again, this higher value was not reflected in a higher residual flexural strength according to Figure 66.

- *Sawn beams*: *First*, *Middle* and *Last*

The flexural tensile strength-CMOD diagram of the three beams *First*, *Middle* and *Last* is shown in Figure 67.

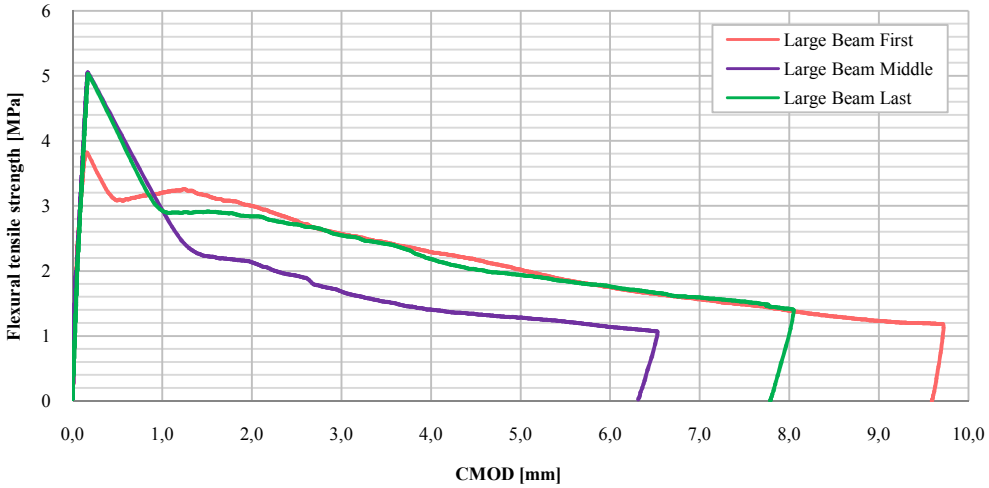

Figure 67. Flexural tensile strength variation with CMOD for the sawn specimens

From Figure 67 some observations are worth to emphasize. Firstly, specimens Middle and Last cracked at almost the same value of flexural tensile strength, 5,05 and 5,03 MPa, respectively. Contrarily, the specimen *First* cracked at a lower value of 3,82 MPa. The cause of that fact can not be attributed to fibres because, as we have previously seen, fibres have its main effect on the post-cracking behaviour, which is in that specimen comparable to the others.

More outstanding is the post-cracking behaviour of the beam identified as *Middle*, which has lower strengths for all the $CMOD$ values registered, while *First* and *Last* have almost identical results. The fact that the specimen closer to the casting point and the specimen further to this point have the same residual flexural strengths prove that no difference in that mechanical property is found due to the flow of concrete. For that reason, the different behaviour observed for the *Middle* beam can not be associated to the flow influence.

This last statement is, moreover, supported by the results of the fibre counting.

Table 31. Results of the fibre counting for specimens First, Middle and Last

	First	Middle	Last
Upper half [fibres/cm^2]	0,74	0,55	0,40
Lower half [fibres/cm^2]	0,69	0,70	0,80
Average for cross-section [fibres/cm^2]	0,71	0,83	0,79
Average [fibres/cm^2]	0,78		

Table 31 shows that specimen named *Last* have same total number of fibres compared with specimen *First*. However, a considerable decrease of fibres in the upper half is observed. This could mean that fibres tend to migrate towards the bottom part. In despite of this, a higher repeatability would be necessary to state that phenomenon. What is clearly demonstrated is that the residual flexural strength is not altered by any effect derived from flow.

On the other hand, a second conclusion from Table 31 is that the lower residual strength of the specimen *Middle* is clearly not connected to lower fibre content.

6.6. Analysis and discussion

A first analysis is given by the comparison of the specimens *G* and *B*. *G* represents the group of the three standard beams filled with concrete without any previous flow (*G1*, *G2* and *G3*), while *B* represents the three Standard beams with possible flow effects (*B1*, *B2* and *B3*). Figure 68 and Table 32 show the results of the mean curves obtained for the flexural tensile strength-CMOD diagram.

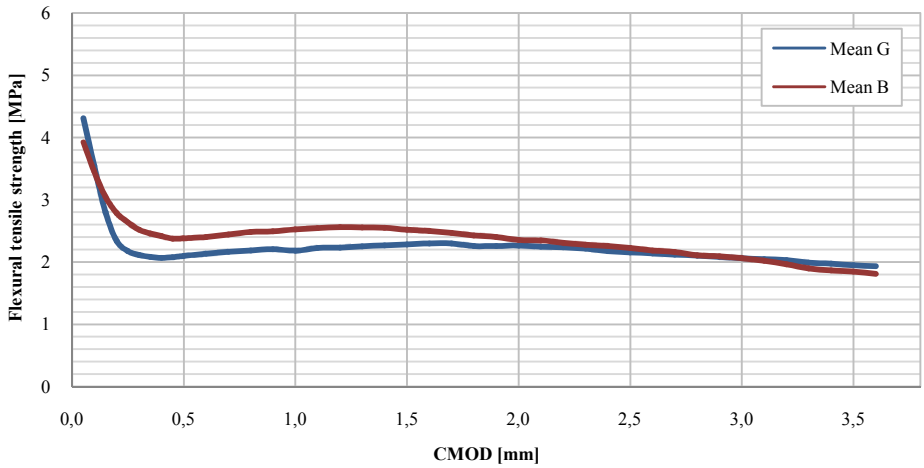

Figure 68. Comparison of the flexural tensile strength between specimens G and B

Table 32. LOP and residual flexural tensile strength comparison between specimens G and B

	Mean G	Mean B	Mean value	Coef. of variation [%]
$f_{R,1}$ [Mpa]	2,10	2,38	2,24	6,3
$f_{R,2}$ [Mpa]	2,28	2,52	2,40	4,8
$f_{R,3}$ [Mpa]	2,15	2,23	2,19	1,7
$f_{R,4}$ [Mpa]	1,95	1,84	1,90	2,8

In the post-cracking behaviour, a maximum variation of 4,8% was obtained for the flexural tensile strength corresponding to a $0{,}5\,mm\,CMOD$. That means that both groups, *G* and *B,* had a very similar response to that test. Consequently, no influence of the previous flow that specimens *B* had before casting is reflected in the flexural strength.

A second and last analysis concerns the comparison between the standard beams and the sawn beams. Figure 69 shows the flexural tensile strength-CMOD diagram with the resulting curves of all the specimens tested for the bending test.

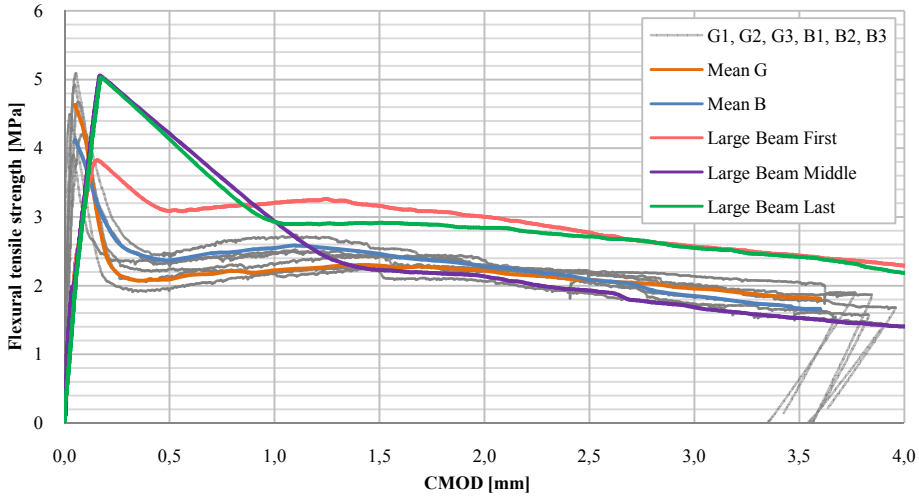

Figure 69. Comparison of the flexural tensile strength variation with the CMOD between standard and sawn beams

Considering as untypical the behaviour of the sawn beam *Middle*, higher residual flexural strengths are observed for the sawn beams compared to the standard beams. This scale effect would have been expected to be opposed if the fibre reinforcement was missing. As we have seen in section 2.3.3.2, steel fibre reinforced elements have a residual flexural strength proportionally dependant on the height of the specimen, which is exactly what the results of Figure 69 show.

A second explanation why higher residual flexural strengths are observed for the sawn beams compared to the standard beams is not connected with the scale effect but with a difference in the testing conditions. As we mentioned during the description of the methods used for each group of specimens, sawn beams were tested parallel to the casting direction while standard beams were tested perpendicularly. Some researches (Toutanji and Bayasi 1998) have studied how the flexural behaviour of SFRC is strongly affected by testing direction, concluding that specimens with relatively high flowabilty, tested in the direction perpendicular to the casting direction, exhibited reductions in the flexural ultimate strength of a 22%, compared to those tested in the direction parallel to casting direction (section 2.3.3.1). A combination of both facts, and probably other more factors, will be responsible of the increased strengths for the group of the sawn beams.

6.7. Conclusions

This experimental part had the aim to investigate if the flow of concrete had an influence on the mechanical properties, more particularly; on the residual flexural tensile strength for steel fibre reinforced self compacting concrete. After testing the thirds of a 3 meter long specimen casted from one end, the lack of differences on the flexural tensile strength between the third closer and the third further to the casting point proved that no influence of the flow of concrete was found in that mechanical property. Additionally, a maximum variation of only 4,8% was obtained for the flexural tensile strength of the post-cracking behaviour between a group of standard specimens without any flow and a group of standard specimens casted with concrete which had flown a distance of 3 m.

The consideration of all the results obtained in that section points in the direction that concrete had the enough stability during the flow to exhibit uniform mechanical properties in the hardened state, unaffected by this flow.

Chapter 7

Conclusions and future perspectives

7.1. Conclusions

Self compacting concrete is often defined as a composite that possesses not only a very high workability, which results in a not necessary compaction, but also that resists segregation and maintains stable composition throughout transport and placing. However, two of the inner properties of SCC, fluidity and stability, seem, in a primary analysis, to be opposed. That research has tried to investigate how these two properties interact. More particularly, what is the influence of the flow of concrete in its stability. However, this potential instability caused by flow could transcend further than the fresh state, affecting also the hardened properties. This research has carried out a main experimental part, divided into four parts.

The first part (Chapter 3) had the aim to investigate the possible segregation of the concrete due to flow during the casting process and its consequent loss of uniformity by means of the segregation experiment. Three mixes were studied representing each mix one of the three groups: a self compacting concrete, a self compacting concrete with the aggregate grading modified for a potential higher segregation and, finally, a steel fibre reinforced self compacting concrete. Almost identically results were assessed for the three mixes: the coarse aggregate distribution was constant along the mould length. In the case of the SFRSCC, also the fibre volume fraction exhibited a uniform distribution. Therefore, no segregation was observed for the three mixes studied, neither when the mix flowed into a 1,2 m long mould, nor when a longer mould of 2,96 m was used.

The second part (Chapter 4) dealt with the distribution of fibres within SFRSCC elements. The study of the fibre distribution concerned not only the investigation of the cross-section dispersion of fibres, but also within the length of the element. A uniform distribution of fibres is of crucial interest to guarantee, until a certain degree, a constant response of the element and the absence of weakest section that could cause structural problems. A 2,96 m long beam, with 0,25% fibre content, was casted from one end of the formwork. Three slices were sawn from this original specimen. The three slices exhibited a general good distribution over the beam cross-section. Just a slight common tendency to distribute more fibres on the bottom part was observed. The number of fibres per unit surface of the slice closest to the casting point and the slice furthest from this point showed no considerable differences far from the intrinsic scatter of analyzing different samples.

In third part (Chapter 5), the study of the fibre orientation was carried out. The alignment of fibres has a special interest for the engineering properties in the hardened state. Firstly, because the anisotropy due to flow induced orientation of fibres may cause to exhibit significantly different mechanical properties in two orthogonal directions. This has to be carefully evaluated and taken into account in the design. And secondly, because this flow induced orientation of fibres can be taken advantage for an intended application, which is along the anticipated directions of the principal stresses within the structural element when in service. In this research we tried to assess the orientation factor for different distances from the casting point and compare the results obtained. A long beam was casted from one end, allowing the concrete to flow in order to fill the framework. Two slices of this beam were studied for the orientation factor measurement. Results showed similar values of this factor, 0,65 for the slice closest to the casting point and 0,67 for the furthest, i.e. no differences of the fibre orientation along the beam were found due to flow. The general predominant orientation of the specimens was planar.

Finally, the fourth part (Chapter 6) studied how this previous analysis, the possible segregation, the fibre distribution and the fibre orientation, concluded with an effect on the mechanical properties, more particularly, on the residual flexural strength, for SFRSCC elements. This research investigated the variation of the mechanical properties of a SFRSCC long element, consisting of a 2,96 m long beam casted from one end. The hardened element was sawn into three parts, so that three specimens composed of concrete with potentially different flow effects, according to its proximity to the casting point, were obtained. The mechanical properties of these specimens were studied through bending tests. Moreover, three standard specimens not subjected to flow conditions and three subjected to flow conditions were tested in order to characterize the concrete and compare them with the sawn specimens. After testing the thirds, the lack of differences on the flexural tensile strength between the third closer and the third further to the casting point proved that no influence of the flow of concrete was found in that mechanical properties. Additionally, a maximum variation of only 4,8% was obtained for the flexural tensile strength of the post-cracking behaviour between a group of specimens without any flow and a group of specimens casted with concrete which had flown a distance of 3 m. The consideration of all the results points in the direction that concrete had the enough stability during the flow to exhibit uniform mechanical properties in the hardened state, unaffected by flow.

To sum up, the three mixes used in this research proved to be stable in despite of their fluidity. In accordance with this, the mechanical properties of the mix tested (SFRSCC mix) showed to be unaffected.

The scope covered by this research, through its four experimental parts, comes to a main conclusion: fluidity and stability of self compacting concrete are not necessary confronted terms. Thanks to great technological advances like, among others, superplasticizers, or thanks to large investigations on the rheological properties, it is possible to embrace these two properties that together make SCC and also FRSCC technologically efficient materials.

7.2. Future perspectives

Several are the future perspectives I could suggest for this field. The scope of this research represents only a particular case within the SCC and FRSCC, featured by their mix proportioning. Any other mix, characterized by its rheological properties, could contribute to make this a more consistent research. A special interest would be studying how the aggregate distributes when increasing the fluidity of the mix.

But also a larger research about the mechanical properties could be included in a future larger investigation. With the same procedure we used, cubes could be sawn from different distances to the casting point in order to compare their compressive strength. The numerical analysis developed in (Spangenberg, et al. 2010) showed that drying shrinkage strain was the most affected mechanical property with variations of the order of 25%. Experimental researches would complement this numerical analysis results about shrinkage.

References

Collepardi, M. (1997). *Symposium on Advances in Concrete Science and Technology.* P.K. Mehta Editor.

De Schutter, G., Bartos, P., Domone, P., & Gibbs, J. (2008). *Self-Compacting Concrete.* Dunbeath, Scotland: Whittles Publishing.

Døssland, Å. L. (2008). *Fibre Reinforcement in Load Carrying Concrete Structures.* Trondheim: NTNU.

Felekoglu, B., Türkel, S., & Baradan, B. (2007). Effect of water/cement ratio on the fresh and hardened properties of self-compacting concrete. *Building and Environment 42* , 1795-1802.

Ferrara, L., Grünewald, S., & Dehn, F. (2010). Design with highly flowable fibre-reinforced concrete: Overview of the activity of fib TG 8.8. *Design, Production and Placement of Self-Consolidating Concrete* (pp. 395-406). Montreal: Springer.

Ferrara, L., Park, Y., & Shah, S. P. (2007). A method for mix-design of fiber-reinforced self-compacting concrete. *Cement and Concrete Research 37* , 957-971.

Ferrara, L., Tregger, N., & Shah, S. P. (2010). Flow-induced fiber orientation in SCSFRC: monitoring and prediction. *Design, production and placement of self-compacting concrete* (pp. 417-428). Montreal: Springer.

Flatt, R., & Houst, Y. (2001). A simplified view on chemical effects perturbing the action of superplasticizers. *Cement and Concrete Research 31* , 1169-1176.

Gaimster, R., & Dixon, N. (2003). 9 Self-compacting concrete. In *Advanced Concrete Technology. Processes* (pp. 9/1-9/21). Amsterdam : Elsevier Butterworth-Heinemann.

Geiker, M. (2008). Chapter 9 Self-compacting concrete (SCC). In *Developments in the formulation and reinforcement of concrete* (pp. 187-207). Cambridge: Woodhead Publishing Limited.

Ghanbari, A., & Karihaloo, B. L. (2009). Prediction of the plastic viscosity of self-compacting steel fibre reinforced concrete. *Cement and Concrete Research 39* , 1209-1216.

Hannant, D. (2003). 6 Fibre-reinforced concrete. In *Advance Concrete Technology. Processes* (pp. 6/1-6/17). Amsterdam: Elsevier Butterworth-Heinemann.

Hegseth, I., Kanstad, T., & Sandbakk, S. (2008). *Fibre reinforced structures: Comparison test methods.* Trondheim: NTNU Institutt for Bygg, Anlegg og Transport.

Laranjeira, F. (2010). *Design-oriented contitutive model for steel fibre reinforced concrete.* Barcelona: Universitat Politècnica de Catalunya.

Martinie, L., & Roussel, N. (2010). Fiber-reinforced cementitious materials: from intrinsic isotropic behavior to fiber alignement. *Design, production and placement of self-compacting concrete* (pp. 407-415). Montreal: Springer.

Martinie, L., Rossi, P., & Roussel, N. (2010). Rheology of fiber reinforced cementitious materials: classification and prediction. *Cement and Concrete Research 40* , 226-234.

Neville, A. M. (2003). *Properties of Concrete. Fourth Edition.* Essex: Pearson Education Limited.

Nguyen, T., Roussel, N., & Coussot, P. (2006). Correlation between L-box test and rheological parameters of a homogeneous yield stress fluid. *Cement and Concrete Research 36* , 1789-1796.

Roussel, N. (2007). The LCPC BOX: a cheap and simple technique for yield stress measurements of SCC. *Materials and Structures 40* , 889-896.

Roussel, N., & Coussot, P. (2005). Fifty-cent rheometer for yield stress measurements: From slump to spreading flow. *Journal of rheology 49(3)* , 705-718.

Roussel, N., Lemaitre, A., Flatt, R., & Coussot, P. (2010). Steady state flow of cement suspensions: A micromechanical state of the art. *Cement and Concrete Research 40* , 77–84.

Sandbakk, S. (2010). *Beam test methods for fibre reinforced concrete beams. Draft version of chapter to be published in PhD-thesis in 2011.* Trondheim: Sintef, Structures and material, NTNU Department of Structural Engineering.

Spangenberg, J., Roussel, N., Hattel, J. H., Thorborg, J., Geiker, M. R., Stang, H., et al. (2010). *Prediction of flow induced heterogeneities and their consequences in Self Compacting Concrete (SCC). Draft version.*

Toutanji, H., & Bayasi, Z. (1998). Effects of manufacturing techniques on the flexural behavior of steel fiber-reinforced concrete. *Cement and Concrete Research 28* , 115-124.

Vikan, H. (2008). Fresh Fibre Reinforced Concrete- A state of the art report. *International Workshop & Nordic Miniseminar: Fibre Reinforced Concrete* (pp. 69-79). Trondheim, Norway: The Nordic Concrete Federation.

Appendixes: overview

Appendix 1. Characterization of aggregates

A1.1. Grading of aggregates

A1.2. Moisture content of aggregate

A1.3. Maximum packing density

Appendix 2. Mixes and results of the segregation experiment

Appendix 3. Fibre counting over the slices A, B and C

Appendix 4. Fibre counting over sections close to the cracked sections

Appendix 5. Results of the bending test

A5.1. Results for the sawn specimens

A5.2. Results for the sawn specimens

Appendix 1

Characterization of aggregates

This appendix summarizes the basic information concerning aggregate: the grading distributions, the measurements of the moisture content in order to adjust the water content of the concrete mixes and, finally, the maximum packing density, necessary to obtain the minimum paste content.

A1.1. Grading of aggregates

	% Passing				
Opening [mm]	Årdal 0-4 mm	Årdal 0-8 mm	Årdal 8-11,2 mm	Årdal 11,2-16 mm	Årdal 8-16
32	100,0	100,0	100,0	100,0	100,0
16	100,0	100,0	100,0	87,9	82,8
11,2	100,0	100,0	100,0	6,0	28,3
8	100,0	97,1	7,0	1,3	4,4
4	99,2	82,5	0,4	0,2	0,7
2	88,0	66,6	0,2	0,0	0,0
1	69,3	47,6	0,0	0,0	0,0
0,5	40,2	28,1	0,0	0,0	0,0
0,25	14,2	14,4	0,0	0,0	0,0
0,125	3,7	6,3	0,0	0,0	0,0

A1.2. Moisture content of aggregate

Identification of the sample	0-8 mm aggregate for SCC1-SCC11 and FIB1-FIB3, exception SCC7.3
Date of the test	19/10/2010
Mass of the moist aggregate [g]	500,0
Mass of the dried aggregate [g]	491,7
Moisture content [%]	1,7

Identification of the sample	0-8 mm aggregate for SCC7.3
Date of the test	29/10/2010
Mass of the moist aggregate [g]	500,0
Mass of the dried aggregate [g]	489,9
Moisture content [%]	2,0

Identification of the sample	0-4 mm aggregate for SegC1, SegC2.1 and SegC2.2
Date of the test	05/11/2010
Mass of the moist aggregate [g]	984,4
Mass of the dried aggregate [g]	955,2
Moisture content [%]	3,0

Identification of the sample	0-4 mm aggregate for SegC2.3
Date of the test	26/11/2010
Mass of the moist aggregate [g]	500,0
Mass of the dried aggregate [g]	481,0
Moisture content [%]	3,0

Identification of the sample	0-8 mm aggregate for FIB4
Date of the test	19/11/2010
Mass of the moist aggregate [g]	-
Mass of the dried aggregate [g]	-
Moisture content [%]	3,2

A1.3. Maximum packing density

Identification of the sample	0-8 mm aggregate		
Date of the test	27/10/2010		
Volume of the container [ml]	1524,3		
Mass of the compacted aggregate [g]	3059,1	3043,0	3087,5
Maximum packing density [kg/m^3]	2009,6		
Percentage of voids [%]	24,2		

Appendix 2

Mixes and results of the segregation experiment

This appendix contains information about the mix proportioning of all the mixes tested. Also results about density, air content and LCPC-box test for 6 litres are shown. Finally, results of the segregation experiments, for the mixes that were tested, are included.

A2.1. Group of SCC mixes

SCC1

Date of the test	19/10/2010
Volume of the mix [l]	22

Comments
The SP was added on the same time as water. The mix was unstable.

Mix proportioning

Water/binder	by wt	0,52
Silica/concrete	% by wt	6,0
Filler/concrete	% by wt	5,0
Paste content	l/m^3	380
Water/powder	by wt	0,42
Powder	kg/m^3	511,6
Water/cement	by wt	0,58

Cement	kg/m^3	368,7
Microsilica	kg/m^3	22,1
Filler	kg/m^3	18,4
Free water	kg/m^3	214,8
Absorbed water	kg/m^3	11,0
Aggregate 0 - 8 mm	kg/m^3	975,0
Aggregate 8 - 16 mm	kg/m^3	650,0
Superplastizicer	kg/m^3	3,7
	% from C	1,00

Slump-flow test

Spread [cm]	53/53
Measured t_{500} [s]	0,9

LCPC-box test 6l

Lateral wall spread length [cm]	49,0/49,5
Maximum spread length [cm]	53,0
Height at the inlet end, h_0 [cm]	8
Mass of the concrete [g]	13852,3
Yield stress [MPa]	82,22

Density

Mass of concrete [kg]	18,720
Volume of the container [l]	8,002
Density of concrete [kg/m^3]	2339

SCC2

Date of the test	25/10/2010
Volume of the mix [l]	9

Comments
The mix was unstable.

Mix proportioning

Water/binder	by wt	0,52
Silica/concrete	% by wt	6,0
Filler/concrete	% by wt	5,0
Paste content	l/m^3	400
Water/powder	by wt	0,42
Powder	kg/m^3	534,8
Water/cement	by wt	0,58

Cement	kg/m^3	389,5
Microsilica	kg/m^3	23,4
Filler	kg/m^3	19,5
Free water	kg/m^3	226,8
Absorbed water	kg/m^3	11,0
Aggregate 0 - 8 mm	kg/m^3	975,0
Aggregate 8 - 16 mm	kg/m^3	650,0
Superplastizicer	kg/m^3	1,6
	% from C	0,41

Slump-flow test

Spread [cm]	-
Measured t_{500} [s]	<1,0

LCPC-box test 6l

Lateral wall spread length [cm]	51,5/61,3
Maximum spread length [cm]	62,0
Height at the inlet end, h_0 [cm]	7,5
Mass of the concrete [g]	14010
Yield stress [MPa]	69,31

Density

Mass of concrete [kg]	2,335
Volume of the container [l]	1,0
Density of concrete [kg/m^3]	2335

SCC3

Date of the test	25/10/2010
Volume of the mix [l]	9

Comments
Bleeding was not observed. The mix was apparently stable. The yield stress was too hight.

Mix proportioning

Water/binder	by wt	0,45
Silica/concrete	% by wt	6,0
Filler/concrete	% by wt	5,0
Paste content	l/m^3	400
Water/powder	by wt	0,37
Powder	kg/m^3	572,7
Water/cement	by wt	0,50

Cement	kg/m^3	423,7
Microsilica	kg/m^3	25,4
Filler	kg/m^3	21,2
Free water	kg/m^3	213,6
Absorbed water	kg/m^3	11,0
Aggregate 0 - 8 mm	kg/m^3	975,0
Aggregate 8 - 16 mm	kg/m^3	650,0
Superplastizicer	kg/m^3	3,3
	% from C	0,78

Slump-flow test

Spread [cm]	59,0/59,0
Measured t_{500} [s]	1,0

LCPC-box test 6l

Lateral wall spread length [cm]	56,5/57,5
Maximum spread length [cm]	60,5
Height at the inlet end, h_0 [cm]	7,5
Mass of the concrete [g]	14220
Yield stress [MPa]	70,3

Density

Mass of concrete [kg]	2,370
Volume of the container [l]	1,0
Density of concrete [kg/m^3]	2370

SCC4

Date of the test	25/10/2010
Volume of the mix [l]	9

Comments
Bleeding was not observed. The mix was apparently stable. The mix needed to be more flowable.

Mix proportioning

Water/binder	by wt	0,40
Silica/concrete	% by wt	6,0
Filler/concrete	% by wt	5,0
Paste content	l/m^3	400
Water/powder	by wt	0,34
Powder	kg/m^3	604,3
Water/cement	by wt	0,45

Cement	kg/m^3	452,2
Microsilica	kg/m^3	27,1
Filler	kg/m^3	22,6
Free water	kg/m^3	202,6
Absorbed water	kg/m^3	11,0
Aggregate 0 - 8 mm	kg/m^3	975,0
Aggregate 8 - 16 mm	kg/m^3	650,0
Superplastizicer	kg/m^3	3,1
	% from C	0,69

Slump-flow test

Spread [cm]	55,0/56,0
Measured t_{500} [s]	3,0

LCPC-box test 6l

Lateral wall spread length [cm]	44,0/49,0
Maximum spread length [cm]	52,5
Height at the inlet end, h_0 [cm]	8,0
Mass of the concrete [g]	13980
Yield stress [MPa]	82,0

Density

Mass of concrete [kg]	2,330
Volume of the container [l]	1,0
Density of concrete [kg/m^3]	2330

SCC5

Date of the test	26/10/2010
Volume of the mix [l]	8

Comments
The flowability increased. The plastic viscosity was too high.

Mix proportioning

Water/binder	by wt	0,40
Silica/concrete	% by wt	6,0
Filler/concrete	% by wt	5,0
Paste content	l/m^3	400
Water/powder	by wt	0,34
Powder	kg/m^3	604,3
Water/cement	by wt	0,45

Cement	kg/m^3	452,2
Microsilica	kg/m^3	27,1
Filler	kg/m^3	22,6
Free water	kg/m^3	202,6
Absorbed water	kg/m^3	11,0
Aggregate 0 - 8 mm	kg/m^3	975,0
Aggregate 8 - 16 mm	kg/m^3	650,0
Superplastizicer	kg/m^3	4,5
	% from C	1,00

Slump-flow test

Spread [cm]	57,0/57,0
Measured t_{500} [s]	2,7

LCPC-box test 6l

Lateral wall spread length [cm]	49,0/50,0
Maximum spread length [cm]	53,0
Height at the inlet end, h_0 [cm]	7,5
Mass of the concrete [g]	14394
Yield stress [MPa]	71,2

Density

Mass of concrete [kg]	2,399
Volume of the container [l]	1,0
Density of concrete [kg/m^3]	2399

SCC6

Date of the test	26/10/2010
Volume of the mix [l]	8

Comments
The mix was quite flowable and the plastic viscosity decreased.

Mix proportioning

Water/binder	by wt	0,40
Silica/concrete	% by wt	6,0
Filler/concrete	% by wt	5,0
Paste content	l/m^3	390
Water/powder	by wt	0,33
Powder	kg/m^3	592,2
Water/cement	by wt	0,45

Cement	kg/m^3	439,7
Microsilica	kg/m^3	26,4
Filler	kg/m^3	22,0
Free water	kg/m^3	197,0
Absorbed water	kg/m^3	11,2
Aggregate 0 - 8 mm	kg/m^3	991,5
Aggregate 8 - 16 mm	kg/m^3	661,0
Superplastizicer	kg/m^3	3,9
	% from C	0,90

Slump-flow test

Spread [cm]	59,0/60,0
Measured t_{500} [s]	1,2

LCPC-box test 6l

Lateral wall spread length [cm]	53,0/53,5
Maximum spread length [cm]	57,0
Height at the inlet end, h_0 [cm]	7,5
Mass of the concrete [g]	14025
Yield stress [MPa]	69,4

Density

Mass of concrete [kg]	2,338
Volume of the container [l]	1,0
Density of concrete [kg/m^3]	2338

SCC7.1

Date of the test	27/10/2010
Volume of the mix [l]	8

Comments
The mix was stable and flowable.

Mix proportioning

Water/binder	by wt	0,426
Silica/concrete	% by wt	6,0
Filler/concrete	% by wt	5,0
Paste content	l/m^3	393
Water/powder	by wt	0,35
Powder	kg/m^3	579,0
Water/cement	by wt	0,48

Cement	kg/m^3	428,2
Microsilica	kg/m^3	25,7
Filler	kg/m^3	21,4
Free water	kg/m^3	204,3
Absorbed water	kg/m^3	11,2
Aggregate 0 - 8 mm	kg/m^3	987,0
Aggregate 8 - 16 mm	kg/m^3	658,0
Superplastizicer	kg/m^3	4,3
	% from C	1,0

Slump-flow test

Spread [cm]	67,0/72,0
Measured t_{500} [s]	0,9

LCPC-box test 6l

Lateral wall spread length [cm]	65,0/74,7
Maximum spread length [cm]	75,5
Height at the inlet end, h_0 [cm]	6,5
Mass of the concrete [g]	13543
Yield stress [MPa]	49,0

Density

Mass of concrete [kg]	2,338
Volume of the container [l]	1,0
Density of concrete [kg/m^3]	2338

SCC7.2

Date of the test	28/10/2010
Volume of the mix [l]	8

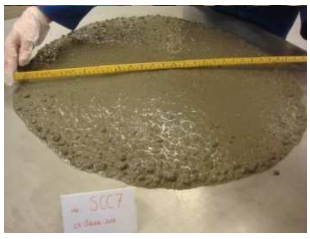

Comments
The mix was unstable and flowable.

Mix proportioning

Water/binder	by wt	0,426
Silica/concrete	% by wt	6,0
Filler/concrete	% by wt	5,0
Paste content	l/m^3	393
Water/powder	by wt	0,35
Powder	kg/m^3	579,0
Water/cement	by wt	0,48

Cement	kg/m^3	428,2
Microsilica	kg/m^3	25,7
Filler	kg/m^3	21,4
Free water	kg/m^3	204,3
Absorbed water	kg/m^3	11,2
Aggregate 0 - 8 mm	kg/m^3	987,0
Aggregate 8 - 16 mm	kg/m^3	658,0
Superplastizicer	kg/m^3	4,3
	% from C	1,0

Slump-flow test

Spread [cm]	67,0/70,0
Measured t_{500} [s]	1,0

LCPC-box test 6l

Lateral wall spread length [cm]	64,0/66,8
Maximum spread length [cm]	69,2
Height at the inlet end, h_0 [cm]	6,5
Mass of the concrete [g]	13832
Yield stress [MPa]	48,1

Density

Mass of concrete [kg]	2,339
Volume of the container [l]	1,0
Density of concrete [kg/m^3]	2339

SCC7.3

Date of the test	29/10/2010
Volume of the mix [l]	46

Comments
The mix was stable, but a bit less flowable than the previous mixes denoted with SCC7.

Mix proportioning

Water/binder	by wt	0,42
Silica/concrete	% by wt	6,0
Filler/concrete	% by wt	5,0
Paste content	l/m^3	390
Water/powder	by wt	0,35
Powder	kg/m^3	579,4
Water/cement	by wt	0,47

Cement	kg/m^3	428,2
Microsilica	kg/m^3	25,7
Filler	kg/m^3	21,4
Free water	kg/m^3	201,4
Absorbed water	kg/m^3	11,2
Aggregate 0 - 8 mm	kg/m^3	991,5
Aggregate 8 - 16 mm	kg/m^3	661,0
Superplastizicer	kg/m^3	4,3
	% from C	1,0

Slump-flow test

Spread [cm]	57,5/57,5
Measured t_{500} [s]	2,3

LCPC-box test 6l

Lateral wall spread length [cm]	53,5/55,0
Maximum spread length [cm]	58,0
Height at the inlet end, h_0 [cm]	7,0
Mass of the concrete [g]	13389
Yield stress [MPa]	61,3

Density

Mass of concrete [kg]	18,824
Volume of the container [l]	8,002
Density of concrete [kg/m^3]	2352
Air content [%]	1,7

Segregation experiment with the LCPC-box

Distance to inlet [m]	0,0	0,2	0,4	0,6	0,8	1,0	1,2
Height wall 1 [cm]	15,0	14,0	13,0	12,0	11,0	10,0	8,4
Height wall 2 [cm]	15,0	13,0	12,0	10,5	10,5	10,0	7,5

Sub regions	Weight subregion [g]	Weight of aggregate 8-11 [g]	Weight of aggregate 11-16 [g]
1 (inlet)	6517,0	1249,5	661,4
2	6742,0	1142,1	599,5
3	6561,0	1137,5	761,8
4	6441,0	1116,0	720,1
5	6072,1	1042,6	740,5
6	5612,9	982,1	706,7
7	5698,5	957,8	708,1
8	5138,0	781,6	779,1
9	5033,9	827,6	694,8
10	4979,2	882,4	623,3
11	4835,0	768,5	651,0
12	4196,0	730,3	460,0

SCC8

Date of the test	27/10/2010
Volume of the mix [l]	8

Comments
The mix was stable, but less flowable than SCC7.1.

Mix proportioning

Water/binder	by wt	0,40
Silica/concrete	% by wt	6,0
Filler/concrete	% by wt	5,0
Paste content	l/m^3	380
Water/powder	by wt	0,33
Powder	kg/m^3	580,1
Water/cement	by wt	0,45

Cement	kg/m^3	427,3
Microsilica	kg/m^3	25,6
Filler	kg/m^3	21,4
Free water	kg/m^3	191,4
Absorbed water	kg/m^3	11,4
Aggregate 0 - 8 mm	kg/m^3	1008,0
Aggregate 8 - 16 mm	kg/m^3	672,0
Superplastizicer	kg/m^3	4,3
	% from C	1,0

Slump-flow test

Spread [cm]	59,0/61,0
Measured t_{500} [s]	1,3

LCPC-box test 6l

Lateral wall spread length [cm]	56,5/57,0
Maximum spread length [cm]	61,0
Height at the inlet end, h_0 [cm]	7,0
Mass of the concrete [g]	13633
Yield stress [MPa]	59,0

Density

Mass of concrete [kg]	2,330
Volume of the container [l]	1,0
Density of concrete [kg/m^3]	2330

SCC9

Date of the test	27/10/2010
Volume of the mix [l]	8

Comments
A bit of segregation was observed. The mix did not flow enough.

Mix proportioning

Water/binder	by wt	0,42
Silica/concrete	% by wt	6,0
Filler/concrete	% by wt	5,0
Paste content	l/m^3	380
Water/powder	by wt	0,34
Powder	kg/m^3	567,7
Water/cement	by wt	0,47

Cement	kg/m^3	416,1
Microsilica	kg/m^3	25,0
Filler	kg/m^3	20,8
Free water	kg/m^3	195,7
Absorbed water	kg/m^3	11,4
Aggregate 0 - 8 mm	kg/m^3	1008,0
Aggregate 8 - 16 mm	kg/m^3	672,0
Superplastizicer	kg/m^3	4,2
	% from C	1,0

Slump-flow test

Spread [cm]	50,0/56,0
Measured t_{500} [s]	3,0

LCPC-box test 6l

Lateral wall spread length [cm]	44,0/48,0
Maximum spread length [cm]	49,5
Height at the inlet end, h_0 [cm]	7,5
Mass of the concrete [g]	13492
Yield stress [MPa]	74,0

Density

Mass of concrete [kg]	2,368
Volume of the container [l]	1,0
Density of concrete [kg/m^3]	2368

SCC10

Date of the test	28/10/2010
Volume of the mix [l]	8

Comments
The mix was unstable

Mix proportioning

Water/binder	by wt	0,40
Silica/concrete	% by wt	6,0
Filler/concrete	% by wt	5,0
Paste content	l/m^3	420
Water/powder	by wt	0,34
Powder	kg/m^3	628,5
Water/cement	by wt	0,45

Cement	kg/m^3	477,2
Microsilica	kg/m^3	28,6
Filler	kg/m^3	23,9
Free water	kg/m^3	213,8
Absorbed water	kg/m^3	10,7
Aggregate 0 - 8 mm	kg/m^3	941,9
Aggregate 8 - 16 mm	kg/m^3	627,9
Superplastizicer	kg/m^3	4,8
	% from C	1,0

Slump-flow test

Spread [cm]	65,0/65,0
Measured t_{500} [s]	1,3

LCPC-box test 6l

Lateral wall spread length [cm]	56,0/58,5
Maximum spread length [cm]	60,5
Height at the inlet end, h_0 [cm]	7,0
Mass of the concrete [g]	13731
Yield stress [MPa]	60,1

Density

Mass of concrete [kg]	2,360
Volume of the container [l]	1,0
Density of concrete [kg/m^3]	2360

SCC11

Date of the test	28/10/2010
Volume of the mix [l]	8

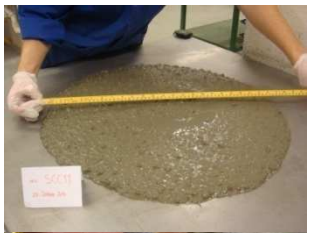

Comments
The mix was flowable but with a slight tendency to bleed.

Mix proportioning

Water/binder	by wt	0,45
Silica/concrete	% by wt	6,0
Filler/concrete	% by wt	5,0
Paste content	l/m^3	420
Water/powder	by wt	0,38
Powder	kg/m^3	595,2
Water/cement	by wt	0,50

Cement	kg/m^3	447,1
Microsilica	kg/m^3	26,8
Filler	kg/m^3	22,4
Free water	kg/m^3	225,3
Absorbed water	kg/m^3	10,7
Aggregate 0 - 8 mm	kg/m^3	941,9
Aggregate 8 - 16 mm	kg/m^3	627,9
Superplastizicer	kg/m^3	3,0
	% from C	0,7

Slump-flow test

Spread [cm]	62,0/64,0
Measured t_{500} [s]	0,8

LCPC-box test 6l

Lateral wall spread length [cm]	53,5/56,3
Maximum spread length [cm]	59,5
Height at the inlet end, h_0 [cm]	7,7
Mass of the concrete [g]	13542
Yield stress [MPa]	76,0

Density

Mass of concrete [kg]	2,322
Volume of the container [l]	1,0
Density of concrete [kg/m^3]	2322

A2.2. Group of SCC mixes with a gap in the aggregate grading 4-8 mm

SegC1

Date of the test	05/11/2010
Volume of the mix [l]	8

Comments
The mix was completely thick.

Mix proportioning

Water/binder	by wt	0,42
Silica/concrete	% by wt	6,0
Filler/concrete	% by wt	11,0
Paste content	l/m^3	390
Water/powder	by wt	0,33
Powder	kg/m^3	604,3
Water/cement	by wt	0,47

Cement	kg/m^3	429,0
Microsilica	kg/m^3	25,7
Filler	kg/m^3	47,2
Free water	kg/m^3	201,8
Absorbed water	kg/m^3	6,2
Aggregate 0 - 4 mm	kg/m^3	959,0
Aggregate 8 - 16 mm	kg/m^3	666,4
Superplastizicer	kg/m^3	4,3
	% from C	1,0

Slump-flow test

Spread [cm]	48,0/51,0
Measured t_{500} [s]	4,5

LCPC-box test 6l

Lateral wall spread length [cm]	35,0/38,0
Maximum spread length [cm]	41,0
Height at the inlet end, h_0 [cm]	13,5
Mass of the concrete [g]	13260
Yield stress [MPa]	326,4

Density

Mass of concrete [kg]	2,305
Volume of the container [l]	1,0
Density of concrete [kg/m^3]	2305

SegC2.1

Date of the test	05/11/2010
Volume of the mix [l]	8

Comments
The mix was stable and flowable.

Mix proportioning

Water/binder	by wt	0,42
Silica/concrete	% by wt	6,0
Filler/concrete	% by wt	5,0
Paste content	l/m^3	390
Water/powder	by wt	0,35
Powder	kg/m^3	590,9
Water/cement	by wt	0,47

Cement	kg/m^3	440,1
Microsilica	kg/m^3	26,4
Filler	kg/m^3	22,0
Free water	kg/m^3	207,0
Absorbed water	kg/m^3	6,2
Aggregate 0 - 4 mm	kg/m^3	959,0
Aggregate 8 - 16 mm	kg/m^3	666,4
Superplastizicer	kg/m^3	4,4
	% from C	1,0

Slump-flow test

Spread [cm]	68,0/68,0
Measured t_{500} [s]	1,3

LCPC-box test 6l

Lateral wall spread length [cm]	58,0/58,0
Maximum spread length [cm]	62,0
Height at the inlet end, h_0 [cm]	7,0
Mass of the concrete [g]	13545
Yield stress [MPa]	58,0

Density

Mass of concrete [kg]	2,303
Volume of the container [l]	1,0
Density of concrete [kg/m^3]	2303

SegC2.2

Date of the test	05/11/2010
Volume of the mix [l]	54

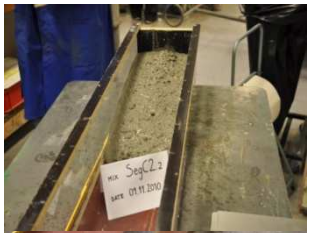

Comments
The mix was stable although less flowable than expected.

Mix proportioning

Water/binder	by wt	0,42
Silica/concrete	% by wt	6,0
Filler/concrete	% by wt	5,0
Paste content	l/m^3	390
Water/powder	by wt	0,35
Powder	kg/m^3	590,9
Water/cement	by wt	0,47

Cement	kg/m^3	440,1
Microsilica	kg/m^3	26,4
Filler	kg/m^3	22,0
Free water	kg/m^3	207,0
Absorbed water	kg/m^3	6,2
Aggregate 0 - 4 mm	kg/m^3	959,0
Aggregate 8 - 16 mm	kg/m^3	666,4
Superplastizicer	kg/m^3	4,4
	% from C	1,0

Slump-flow test

Spread [cm]	57,0/60,0
Measured t_{500} [s]	2,0

LCPC-box test 6l

Lateral wall spread length [cm]	46,0/50,0
Maximum spread length [cm]	52,0
Height at the inlet end, h_0 [cm]	8,0
Mass of the concrete [g]	13077
Yield stress [MPa]	85,5

Density

Mass of concrete [kg]	18,412
Volume of the container [l]	8,002
Density of concrete [kg/m^3]	2301
Air content [%]	2,7

Segregation experiment with the LCPC-box

Distance to inlet [m]	0,0	0,1	0,2	0,3	0,4	0,5	0,6	0,7	0,8	0,9	1,0	1,1	1,2
Height wall 1 [cm]	14,3	15,0	14,0	13,0	12,6	12,0	11,0	10,5	9,5	8,5	7,5	5,5	4,0
Height wall 2 [cm]	14,5	15,0	14,0	13,5	12,5	12,0	11,2	10,6	9,7	8,8	6,4	6,4	3,5

Sub regions	Weight subregion [g]	Weight of aggregate 8-11 [g]	Weight of aggregate 11-16 [g]
1 (inlet)	6493,1	494,3	978,9
2	6639,5	801,2	1246,5
3	6544,9	981,2	1099,0
4	5911,3	739,3	1123,2
5	5752,7	848,1	969,9
6	5279,8	835,8	852,8
7	5023,2	703,6	845,4
8	4712,6	698,0	788,1
9	4154,9	606,3	718,7
10	3847,2	549,0	657,3
11	3251,5	398,0	632,9
12	2253,1	267,8	458,1

SegC2.3

Date of the test	29/11/2010
Volume of the mix [l]	159

Comments
The mix was stable but a bit thicker than what expected.

Mix proportioning

Water/binder	by wt	0,42
Silica/concrete	% by wt	6,0
Filler/concrete	% by wt	5,0
Paste content	l/m^3	390
Water/powder	by wt	0,35
Powder	kg/m^3	590,9
Water/cement	by wt	0,47

Cement	kg/m^3	440,1
Microsilica	kg/m^3	26,4
Filler	kg/m^3	22,0
Free water	kg/m^3	207,0
Absorbed water	kg/m^3	6,2
Aggregate 0 - 4 mm	kg/m^3	959,0
Aggregate 8 - 16 mm	kg/m^3	666,4
Superplastizicer	kg/m^3	3,5
	% from C	0,8

Slump-flow test

Spread [cm]	47,0/52,0
Measured t_{500} [s]	3,1

Density

Mass of concrete [kg]	18,718
Volume of the container [l]	8,002
Density of concrete [kg/m^3]	2339
Air content [%]	2,0

Segregation experiment with the large mould

Sub regions	Weight subregion [g]	Weight of aggregate 8-11 [g]	Weight of aggregate 11-16 [g]
1 (inlet)	13374,2	1794,9	2031,7
2	12626,2	1602,8	1828,0
3	12713,9	1709,6	1723,5
4	9990,8	1365,3	1350,0
5	9797,8	1239,0	1471,6
6	9061,6	1120,4	1263,8

A2.3. Group of FRSCC mixes

FIB1

Date of the test	10/11/2010
Volume of the mix [l]	8

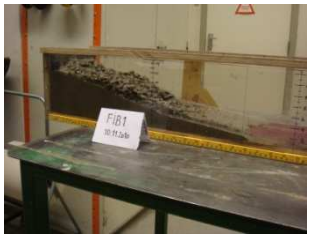

Comments
The mix was completely unstable.

Mix proportioning

Water/binder	by wt	0,52
Silica/concrete	% by wt	6,0
Filler/concrete	% by wt	5,0
Paste content	l/m^3	380
Water/powder	by wt	0,42
Powder	kg/m^3	511,0
Water/cement	by wt	0,58

Cement	kg/m^3	368,9
Microsilica	kg/m^3	22,1
Filler	kg/m^3	18,4
Free water	kg/m^3	214,9
Absorbed water	kg/m^3	11,0
Aggregate 0 - 4 mm	kg/m^3	966,7
Aggregate 8 - 16 mm	kg/m^3	644,5
Superplastizicer	kg/m^3	1,7
	% from C	0,46
Fibres	kg/m^3	39

Slump-flow test

Spread [cm]	58,5/58,7
Measured t_{500} [s]	1,9

LCPC-box test 6l

Lateral wall spread length [cm]	51,0/52,5
Maximum spread length [cm]	52,2
Height at the inlet end, h_0 [cm]	13,0
Mass of the concrete [g]	13449
Yield stress [MPa]	308,1

Density

Mass of concrete [kg]	2,365
Volume of the container [l]	1,0
Density of concrete [kg/m^3]	2365

FIB2

Date of the test	10/11/2010
Volume of the mix [l]	8

Comments
The mix was stable enough.

Mix proportioning

Water/binder	by wt	0,45
Silica/concrete	% by wt	6,0
Filler/concrete	% by wt	5,0
Paste content	l/m^3	380
Water/powder	by wt	0,37
Powder	kg/m^3	547,1
Water/cement	by wt	0,50

Cement	kg/m^3	401,5
Microsilica	kg/m^3	24,1
Filler	kg/m^3	20,1
Free water	kg/m^3	202,3
Absorbed water	kg/m^3	11,0
Aggregate 0 - 4 mm	kg/m^3	966,7
Aggregate 8 - 16 mm	kg/m^3	644,5
Superplastizicer	kg/m^3	3,6
	% from C	0,91
Fibres	kg/m^3	39

Slump-flow test

Spread [cm]	59,5/62,5
Measured t_{500} [s]	2,1

LCPC-box test 6l

Lateral wall spread length [cm]	55,5/58,5
Maximum spread length [cm]	59,2
Height at the inlet end, h_0 [cm]	7,5
Mass of the concrete [g]	13510
Yield stress [MPa]	71,3

Density

Mass of concrete [kg]	2,325
Volume of the container [l]	1,0
Density of concrete [kg/m^3]	2325

$FIB3_{0,25}.1$

Date of the test	
Volume of the mix [l]	

Comments
The mix was stable and flowable.

Mix proportioning

Water/binder	by wt	0,426
Silica/concrete	% by wt	6,0
Filler/concrete	% by wt	5,0
Paste content	l/m^3	393
Water/powder	by wt	0,35
Powder	kg/m^3	578,9
Water/cement	by wt	0,48

Cement	kg/m^3	428,6
Microsilica	kg/m^3	25,7
Filler	kg/m^3	21,4
Free water	kg/m^3	204,5
Absorbed water	kg/m^3	11,1
Aggregate 0 - 4 mm	kg/m^3	982,4
Aggregate 8 - 16 mm	kg/m^3	654,9
Superplastizicer	kg/m^3	4,3
	% from C	1,00
Fibres	kg/m^3	19,5

Slump-flow test

Spread [cm]	62,5/63,5
Measured t_{500} [s]	1,4

LCPC-box test 6l

Lateral wall spread length [cm]	59,5/64,5
Maximum spread length [cm]	64,5
Height at the inlet end, h_0 [cm]	7,5
Mass of the concrete [g]	13658
Yield stress [MPa]	72,2

Density

Mass of concrete [kg]	2,354
Volume of the container [l]	1,0
Density of concrete [kg/m^3]	2354

This mix was also tested for other fibre conents. Although only the slump-flow test was performed, the decrese of the workabilty was observed with the results shown in Table X.

	Fibre conent[%vol]	Fiber content [kg/m^3]	Spread [cm]	Measured t_{500} [s]
$FIB3_{0,35}$	0,35	27,3	54,0/57,0	2,3
$FIB3_{0,50}$	0,50	39,0	52,6/55,0	3,4
$FIB3_{0,75}$	0,75	58,5	44,0/50,0	4,8

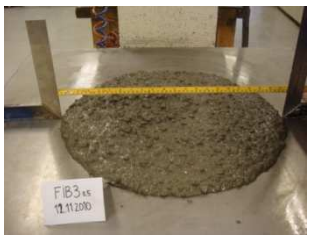

$FIB3_{0,25}.2$

Date of the test	16/11/2010
Volume of the mix [l]	54

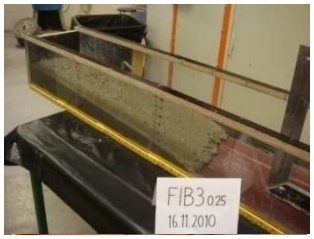

Comments
The mix was stable and considerably flowable.

Mix proportioning

Water/binder	by wt	0,426
Silica/concrete	% by wt	6,0
Filler/concrete	% by wt	5,0
Paste content	l/m^3	393
Water/powder	by wt	0,35
Powder	kg/m^3	578,9
Water/cement	by wt	0,48

Cement	kg/m^3	428,6
Microsilica	kg/m^3	25,7
Filler	kg/m^3	21,4
Free water	kg/m^3	204,5
Absorbed water	kg/m^3	11,1
Aggregate 0 - 8 mm	kg/m^3	982,4
Aggregate 8 - 16 mm	kg/m^3	654,9
Superplastizicer	kg/m^3	4,3
	% from C	1,00
Fibers	kg/m^3	19,5

Slump-flow test

Spread [cm]	65,0/70,0
Measured t_{500} [s]	1,0

LCPC-box test 6l

Lateral wall spread length [cm]	67,0/70,5
Maximum spread length [cm]	71,5
Height at the inlet end, h_0 [cm]	6,5
Mass of the concrete [g]	13520
Yield stress [MPa]	49,3

Density

Mass of concrete [kg]	18,729
Volume of the container [l]	8,002
Density of concrete [kg/m^3]	2340
Air content [%]	1,7

Segregation experiment with the LCPC-box

Distance to inlet [m]	0,0	0,2	0,4	0,6	0,8	1,0	1,2
Height wall 1 [cm]	14,5	14,0	13,7	13,2	12,7	12,2	10,5
Height wall 2 [cm]	14,5	14,0	13,6	13,0	12,5	12,2	11,0

Sub regions	Weight subregion [g]	Weight of aggregate 8-11 [g]	Weight of aggregate 11-16 [g]	Weight of fibres [g]
1 (inlet)	6655,8	1052,6	746,9	51,8
2	6529,3	1043,8	646,9	48,1
3	6503,8	1131,2	663,8	53,1
4	6320,6	1064,0	864,0	57,1
5	6323,1	1023,1	845,5	51,2
6	6365,3	1098,2	773,0	57,4
7	6096,5	978,7	918,5	55,1
8	6055,8	1065,2	668,3	53,2
9	5766,5	979,0	659,0	50,4
10	5582,8	949,4	759,0	58,9
11	5399,0	867,0	701,5	50,1
12	5212,0	861,4	691,2	52,4

FIB4

Date of the test	19/11/2010
Volume of the mix [l]	540

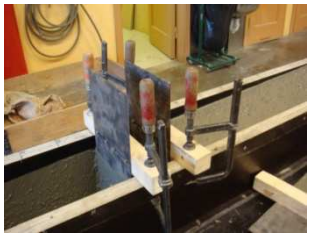

Comments
The mix was too thick.

Mix proportioning

Water/binder	by wt	0,42
Silica/concrete	% by wt	6,0
Filler/concrete	% by wt	5,0
Paste content	l/m^3	390
Water/powder	by wt	0,35
Powder	kg/m^3	590,9
Water/cement	by wt	0,47

Cement	kg/m^3	428,3
Microsilica	kg/m^3	25,7
Filler	kg/m^3	21,4
Free water	kg/m^3	201,5
Absorbed water	kg/m^3	11,2
Aggregate 0 - 8 mm	kg/m^3	987,3
Aggregate 8 - 16 mm	kg/m^3	658,2
Superplastizicer	kg/m^3	4,3
	% from C	1,0
Fibers	kg/m^3	19,5

Slump-flow test

Spread [cm]	43,0/48,0
Measured t_{500} [s]	No reached 500mm

Density

Mass of concrete [kg]	18,705
Volume of the container [l]	8,002
Density of concrete [kg/m^3]	2338
Air content [%]	2,8

Segregation experiment with the LCPC-box

Sub regions	Weight subregion [g]	Weight of aggregate 8-11 [g]	Weight of aggregate 11-16 [g]	Weight of fibres [g]
1 (inlet)	11357,0	777,7	2508,5	88,3
2	13120,2	959,7	3047,6	104,9
3	12781,8	992,6	2708,4	95,1
4	10861,4	793,7	2493,7	82,9
5	8879,0	648,1	1975,4	67,5
6	10814,8	876,2	2405,8	76,3

Appendix 3

Fibre counting over the slices A, B and C

The fibre counting over the three slices was carried out counting over the two sawn surfaces of each slice. Results of the six surfaces A1, A2, B1, B2, C1 and C2, are shown in the tables below. A previous sketch is presented in order to make easier the understanding of the results.

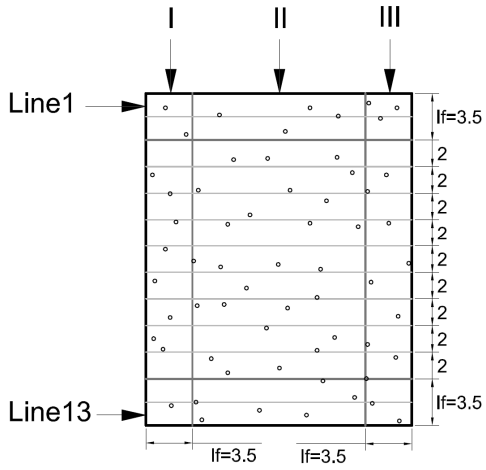

	A1			A2			B1		
Line	I	II	III	I	II	III	I	II	III
1	0	11	6	4	7	4	4	17	4
2	0	19	3	3	13	4	3	13	5
3	4	13	12	5	16	2	3	14	1
4	3	22	8	3	19	2	5	30	2
5	8	11	3	5	7	7	3	9	2
6	9	13	4	7	24	3	2	10	8
7	7	30	4	9	34	3	5	14	4
8	2	19	3	3	17	3	2	18	2
9	7	28	4	8	14	4	11	15	10
10	5	29	4	3	14	6	8	18	4
11	6	21	6	6	21	3	6	10	4
12	5	31	4	6	18	5	4	7	9
13	3	21	5	4	15	1	6	16	6
Total	393			332			314		

	B2			C1			C2		
Line	I	II	III	I	II	III	I	II	III
1	1	8	1	4	14	4	6	14	1
2	3	21	1	3	13	3	5	16	0
3	3	14	9	5	14	4	7	21	2
4	3	19	1	6	15	0	6	18	1
5	2	4	3	4	13	2	4	23	10
6	2	16	3	7	16	4	6	14	7
7	7	20	2	11	20	4	7	17	6
8	2	16	4	6	16	7	6	22	4
9	8	10	7	4	11	4	6	25	3
10	3	20	4	2	21	3	1	10	5
11	3	20	6	4	16	6	3	21	6
12	3	30	7	5	29	4	5	10	2
13	1	20	3	7	7	6	2	29	4
Total	310			324			355		

During the fibre counting a plastic adhesive paper was used for covering the surfaces, defining the sub regions on top and marking with a permanent marker the fibres. After removing this paper from each slice, a picture of the fibre dispersion could be easily analyzed. All these papers are presented in this appendix.

Surface A1

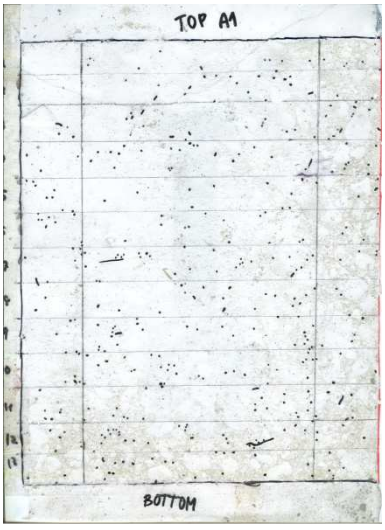

Surface A2

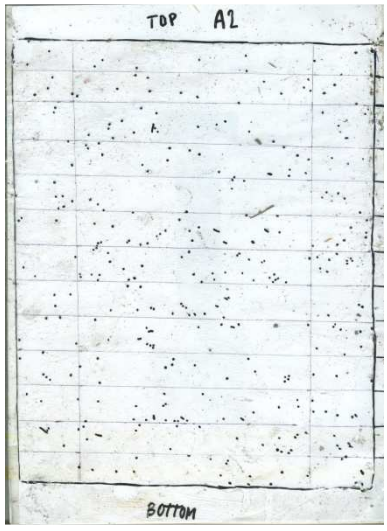

Surface B1

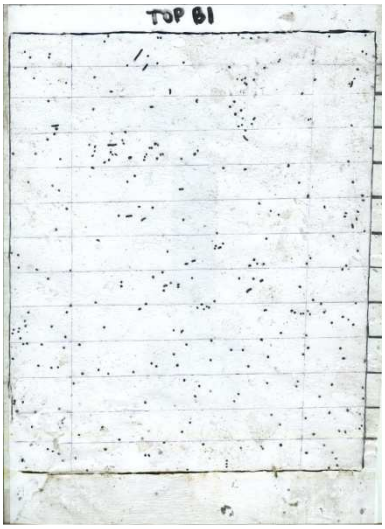

Surface B2

Surface C1

Surface C2

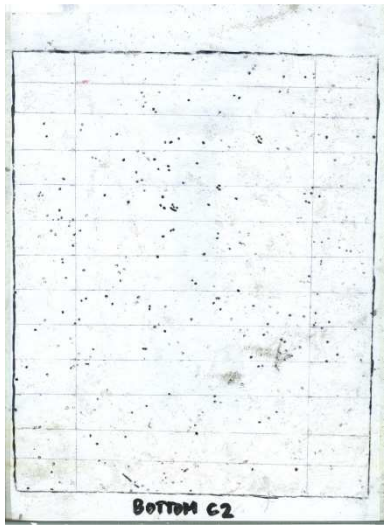

Appendix 4

Fibre counting over sections close to the cracked sections

All the specimens tested for the bending test were sawn at a distance of 50 mm from the cracked section. The fibres were counted over the sawn section. The results are reported in the tables below. Previous sketches are presented in order to make easier the understanding of the results for the sawn specimens and the standard specimens.

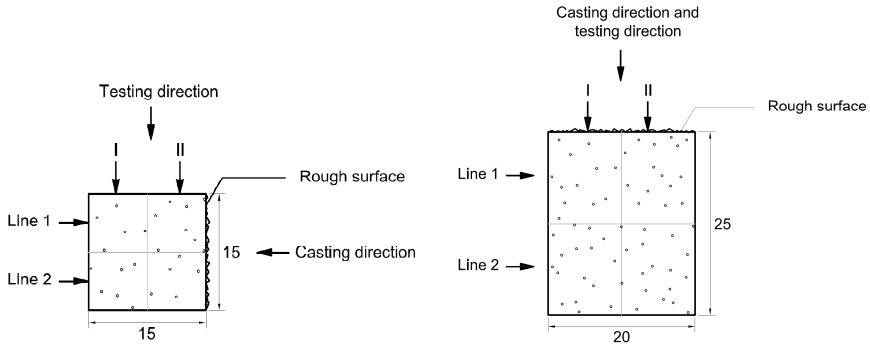

	G1		G2		G3		B1		B2		B3	
	I	II	I	II	I	II	I	II	I	II	I	II
Line 1	38	24	53	42	48	49	30	34	35	37	33	29
Line 2	23	39	50	51	42	33	33	32	34	32	37	41

	First		Middle		Last	
	I	II	I	II	I	II
Line 1	111	73	69	68	45	54
Line 2	74	98	86	88	95	104

Appendix 5

Results of the bending test

This appendix collects all the information that was registered during the development of the bending test and that was relevant for the subsequent preparation of the results exposed in Chapter 6.

A5.1. Results for the sawn specimens

Specimen First

Identification of the test specimen	First	
Identification of the concrete composition	FIB4	
Date of manufacture	19.11.2010	
Date of testing	03.12.2010	
Width of specimen, b [mm]	198	206
Height of specimen, h_{sp} [mm]	254	252
Distance between bottom and transducer, y [mm]	125	
Span length, l [mm]	910	
Specimen length, L [mm]	980	
Rate of increase of deflection [mm/min]	0,5	
Distance between transducer and crack [mm]	15	

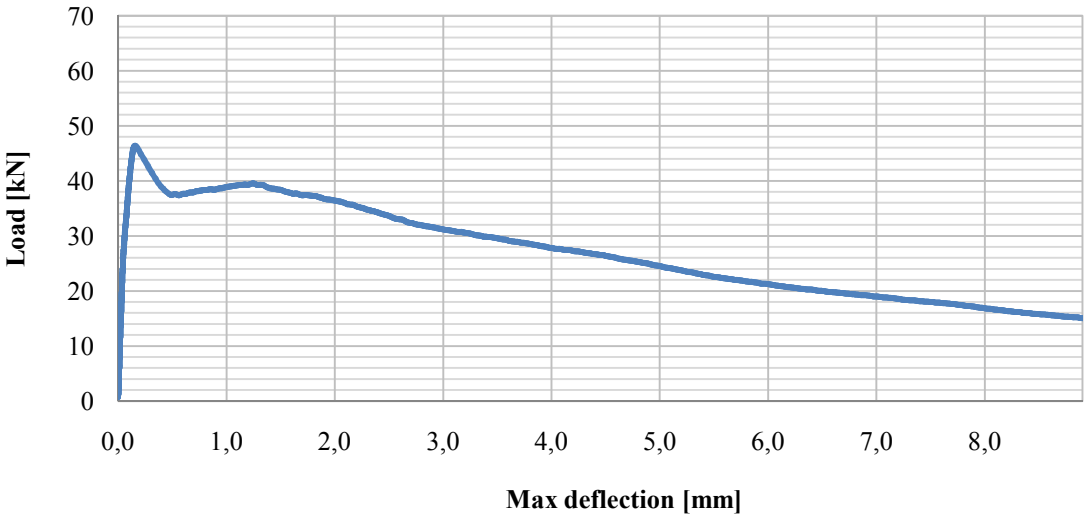

Specimen Middle

Identification of the test specimen	Middle	
Identification of the concrete composition	FIB4	
Date of manufacture	19.11.2010	
Date of testing	03.12.2010	
Width of specimen, b [mm]	215	200
Height of specimen, h_{sp} [mm]	253	251
Distance between bottom and transducer, y [mm]	125	
Span length, l [mm]	910	
Specimen length, L [mm]	980	
Rate of increase of deflection [mm/min]	0,2-0,5	
Distance between transducer and crack [mm]	35	

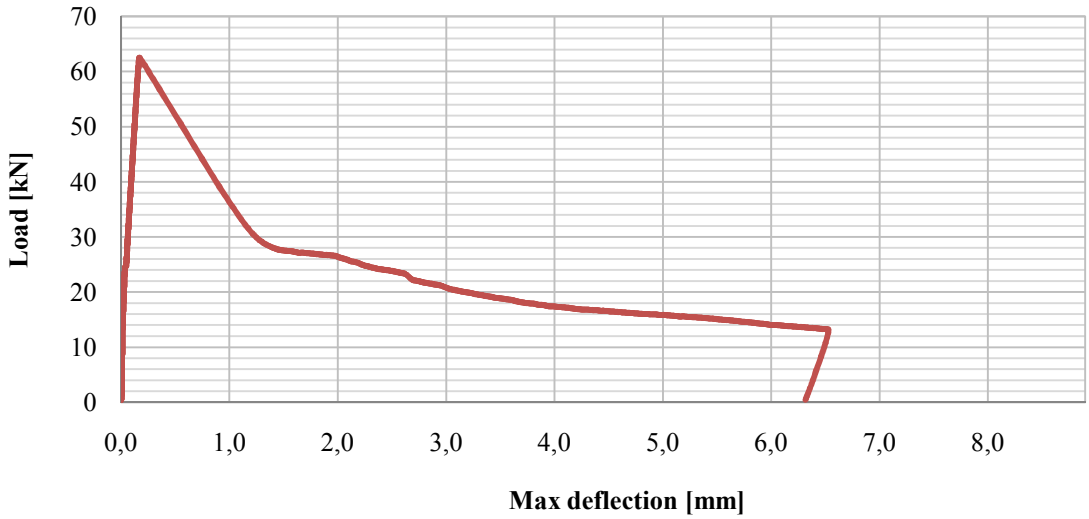

Specimen Last

Identification of the test specimen	Last	
Identification of the concrete composition	FIB4	
Date of manufacture	19.11.2010	
Date of testing	03.12.2010	
Width of specimen, b [mm]	205	198
Height of specimen, h_{sp} [mm]	253	253
Distance between bottom and transducer, y [mm]	125	
Span length, l [mm]	910	
Specimen length, L [mm]	980	
Rate of increase of deflection [mm/min]	0,5	
Distance between transducer and crack [mm]	30	

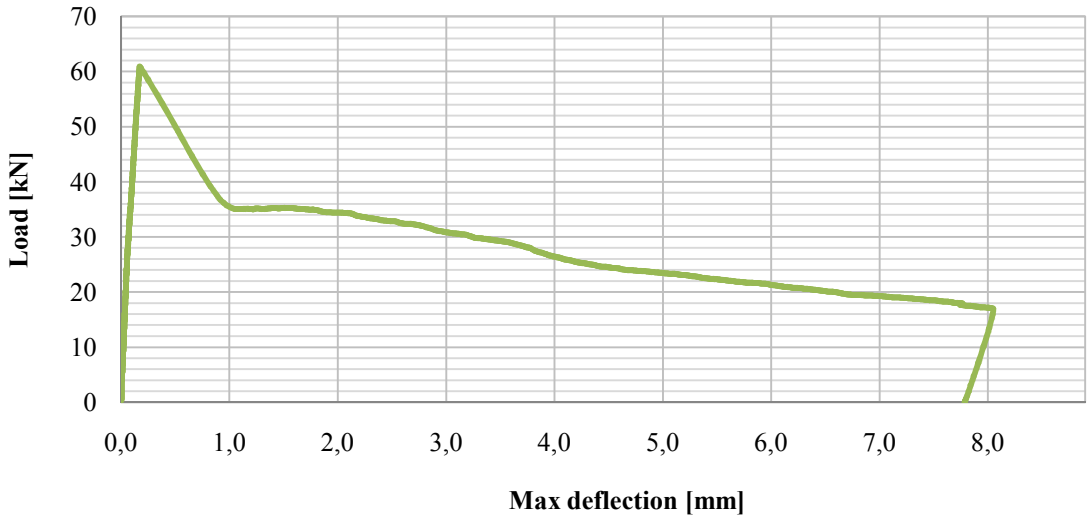

A5.2. Results for the sawn specimens

Specimen G1

Identification of the test specimen	G1	
Identification of the concrete composition	FIB4	
Date of manufacture	19.11.2010	
Date of notching	03.12.2010	
Date of testing	03.12.2010	
Width of specimen, b [mm]	152,8	154,7
Distance between the tip of the notch and the top, h_{sp} [mm]	125,0	125,2
Distance between bottom and transducer, y [mm]	75	
Span length, l [mm]	500	
Specimen length, L [mm]	550	
Rate of increase of deflection [mm/min]	0,2	

Maximum load, F_L [kN]	16,32
Limit of proportionality, LOP [MPa]	5,09

CMOD [mm]	Load [kN]	Residual flexural tensile strength [MPa]
0,5	7,12	2,22
1,5	7,22	2,25
2,5	6,39	1,99
3,5	5,48	1,70

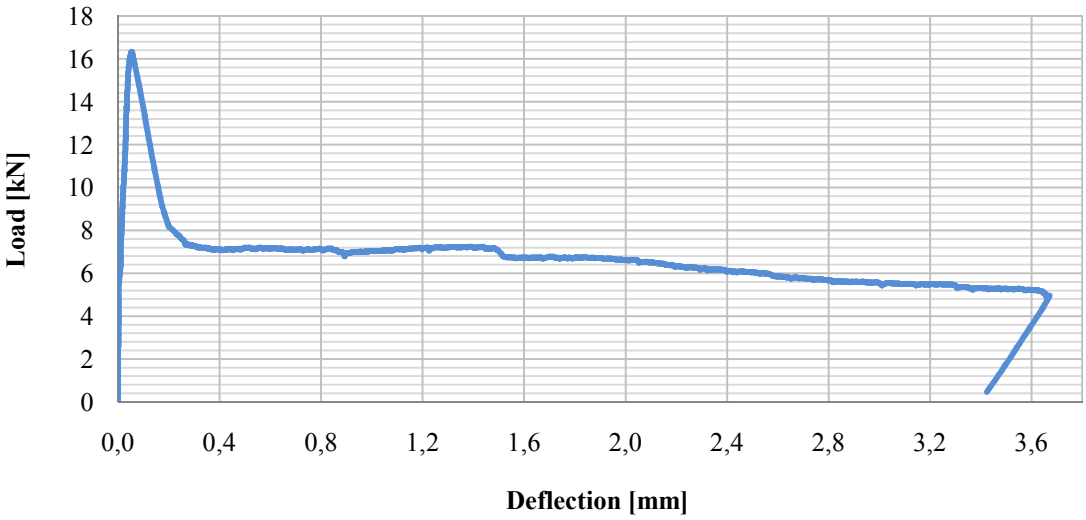

Specimen G2

Identification of the test specimen	G2	
Identification of the concrete composition	FIB4	
Date of manufacture	19.11.2010	
Date of notching	03.12.2010	
Date of testing	03.12.2010	
Width of specimen, b [mm]	152,0	153,3
Distance between the tip of the notch and the top, h_{sp} [mm]	125,5	126,0
Distance between bottom and transducer, y [mm]	75	
Span length, l [mm]	500	
Specimen length, L [mm]	550	
Rate of increase of deflection [mm/min]	0,2	

Maximum load, FL [kN]	14,46
Limit of proportionality, LOP [MPa]	4,49

CMOD [mm]	Load [kN]	Residual flexural tensile strength [MPa]
0,5	6,28	1,953
1,5	7,05	2,192
2,5	7,16	2,223
3,5	6,84	2,126

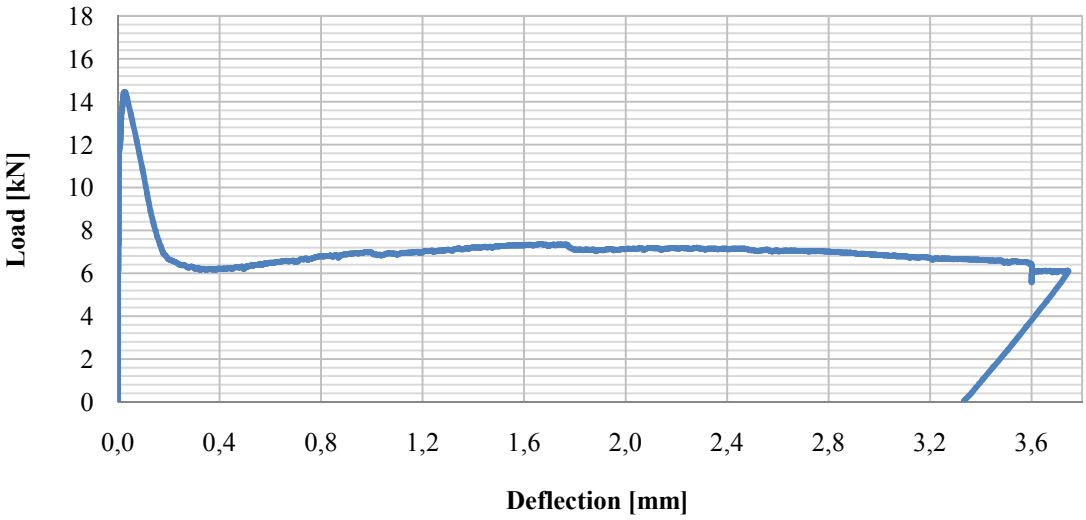

Specimen G3

Identification of the test specimen	G3	
Identification of the concrete composition	FIB4	
Date of manufacture	19.11.2010	
Date of notching	03.12.2010	
Date of testing	03.12.2010	
Width of specimen, b [mm]	154,0	151,0
Distance between the tip of the notch and the top, h_{sp} [mm]	126,0	125,0
Distance between bottom and transducer, y [mm]	75	
Span length, l [mm]	500	
Specimen length, L [mm]	550	
Rate of increase of deflection [mm/min]	0,2	

Maximum load, FL [kN]	14,97
Limit of proportionality, LOP [MPa]	4,67

CMOD [mm]	Load [kN]	Residual flexural tensile strength [MPa]
0,5	6,81	2,13
1,5	7,71	2,41
2,5	7,20	2,25
3,5	6,44	2,01

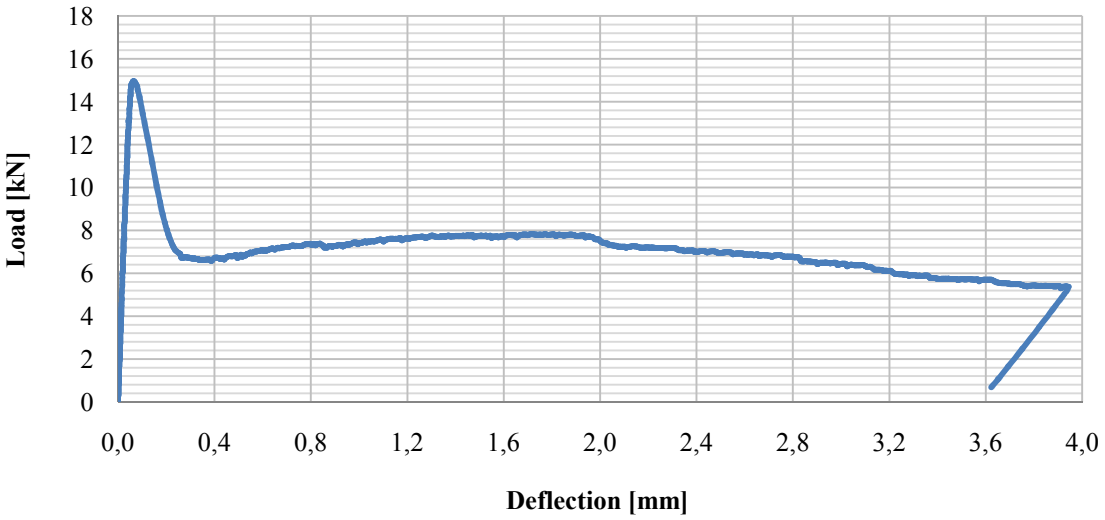

Specimen B1

Identification of the test specimen	B1	
Identification of the concrete composition	FIB4	
Date of manufacture	19.11.2010	
Date of notching	03.12.2010	
Date of testing	03.12.2010	
Width of specimen, b [mm]	151,0	151,0
Distance between the tip of the notch and the top, h_{sp} [mm]	125,2	125,4
Distance between bottom and transducer, y [mm]	75	
Span length, l [mm]	500	
Specimen length, L [mm]	550	
Rate of increase of deflection [mm/min]	0,2	

Maximum load, FL [kN]	15,56
Limit of proportionality, LOP [MPa]	4,92

CMOD [mm]	Load [kN]	Residual flexural tensile strength [MPa]
0,5	7,32	2,32
1,5	7,85	2,48
2,5	7,10	2,25
3,5	6,26	1,98

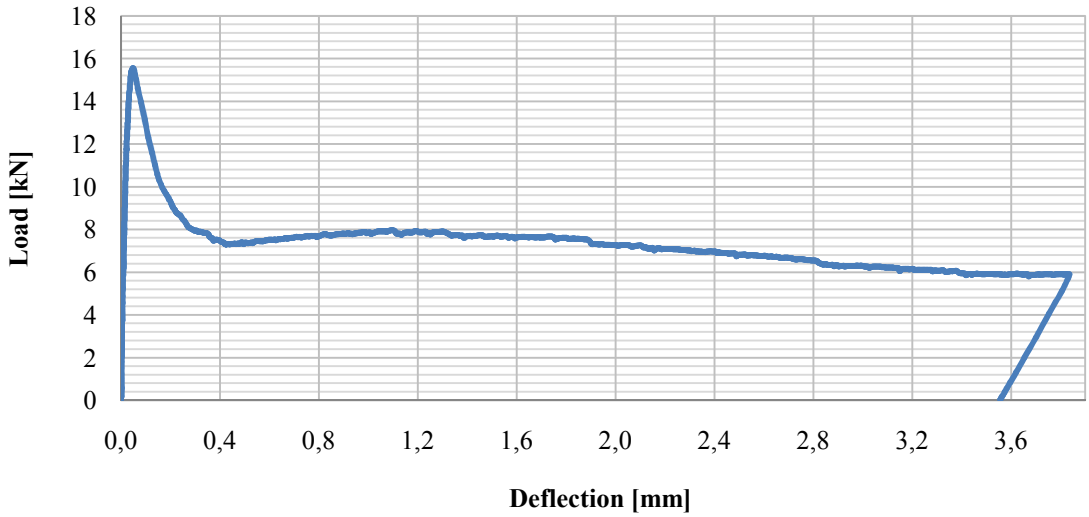

Specimen B2

Identification of the test specimen	B2	
Identification of the concrete composition	FIB4	
Date of manufacture	19.11.2010	
Date of notching	03.12.2010	
Date of testing	03.12.2010	
Width of specimen, b [mm]	151,0	150,5
Distance between the tip of the notch and the top, h_{sp} [mm]	125,5	124,7
Distance between bottom and transducer, y [mm]	75	
Span length, l [mm]	500	
Specimen length, L [mm]	550	
Rate of increase of deflection [mm/min]	0,2	

Maximum load, FL [kN]	13,24
Limit of proportionality, LOP [MPa]	4,21

CMOD [mm]	Load [kN]	Residual flexural tensile strength [MPa]
0,5	7,71	2,45
1,5	8,27	2,63
2,5	7,02	2,23
3,5	5,40	1,72

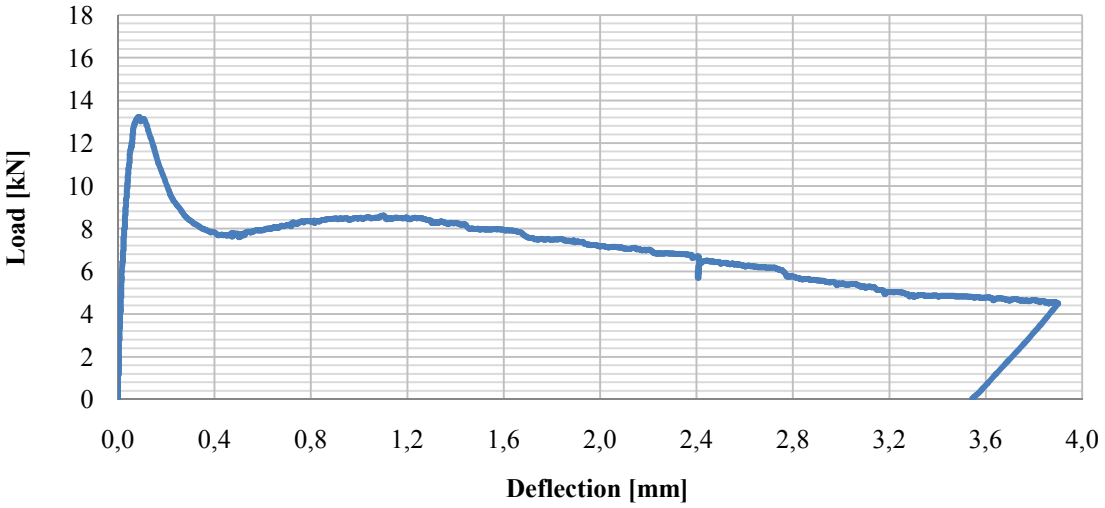

Specimen B3

Identification of the test specimen	B3	
Identification of the concrete composition	FIB4	
Date of manufacture	19.11.2010	
Date of notching	03.12.2010	
Date of testing	03.12.2010	
Width of specimen, b [mm]	150,5	150,7
Distance between the tip of the notch and the top, h_{sp} [mm]	125,7	125,5
Distance between bottom and transducer, y [mm]	75	
Span length, l [mm]	500	
Specimen length, L [mm]	550	
Rate of increase of deflection [mm/min]	0,2	

Maximum load, FL [kN]	12,34
Limit of proportionality, LOP [MPa]	3,90

CMOD [mm]	Load [kN]	Residual flexural tensile strength [MPa]
0,5	7,52	2,37
1,5	7,71	2,43
2,5	6,98	2,20
3,5	5,81	1,83

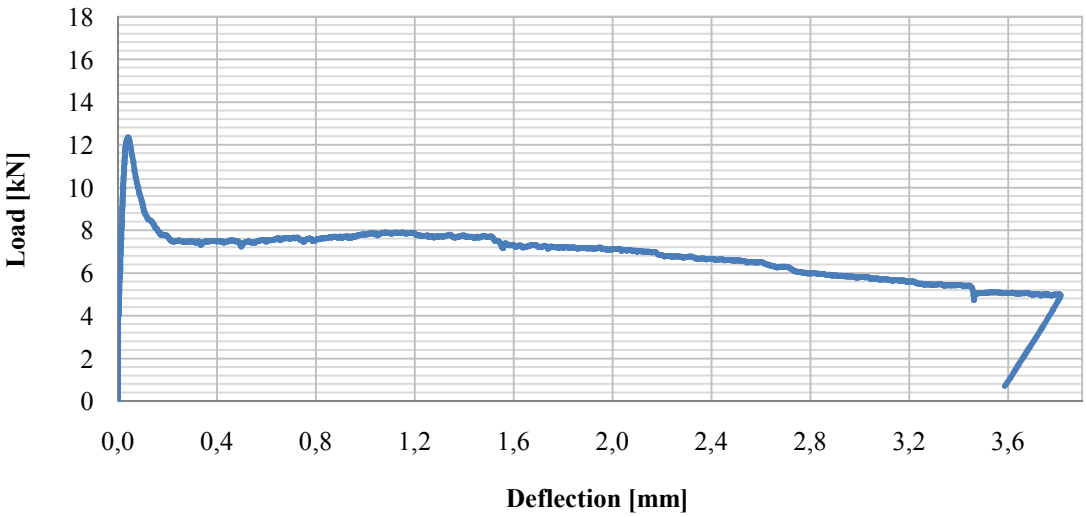

List of symbols

A_c	concrete cross-section
A_f	cross-section of a fibre
b	width of the specimen at the cracked section
$CMOD$	crack mouth opening displacement
d	distance between the support and the closest loading point section for the bending test
d_f	fibre diameter
$f_{ct,L}^{f}$	limit of proportionality LOP
$f_{ct,residual}$	residual flexural tensile strength
$f_{R,j}$	residual flexural tensile strength for a corresponding value of δ_j, $j = 1,2,3,4$
$f_{t,eq}$	residual flexural tensile strength of a standard test specimen
$f_{t,res}$	residual flexural tensile strength of the structural element
F_j	load applied during the bending test for a corresponding value of δ_j, $j = 1,2,3,4$
F_L	maximum load reached during the bending test, corresponding to the LOP
g	earth gravity
h	height of the specimen at the cracked section
h_0	thickness of the sample at the extremity of the LCPC-box
h_{sp}	distance between the tip of the notch and the top of a standard beam
H	final height of the sample in (Roussel and Coussot 2005)
K	adjusted coefficient
l	span length of the specimen
l_{iT}	distance between the support i and the transducer (T)
l_0	width of the LCPC-box
L	spread length in the LCPC-box
M_j	bending moment corresponding to the load applied F_j, $j = 1,2,3,4$
M_L	bending moment corresponding to F_L
n_f	number of fibres per concrete unit surface
N	number of fibres over the concrete cross-section

N_i	number of fibres on each surface i of a sawn block, with $i = 1,2,3$
R	final radius of the sample in (Roussel and Coussot 2005)
t_{500}	time taken during the slump-flow test from the moment the mould is being lifted to the flowing concrete to reach a circle of 500 mm in diameter
v_f	fibre volume fraction
$v_{f,struct}$	fibre volume of the structural element
V_{paste}	paste content
w/b	water-binder ratio
w/c	water-cement ratio
x	distance between the transducer and the cracked section for the bending test
z_c	critical distance from the wall for the plug flow area
α	orientation factor
α_{struct}	orientation factor for the structural element
$\dot{\gamma}$	shear rate
δ	measured deflection at the section where the transducer is placed
δ_{max}	maximum deflection at the cracked section
η	capacity factor
η_{struct}	capacity factor of the structural element
μ	plastic viscosity
ρ	density of the concrete
$\sigma_{f,average}$	average post-cracking fibre stress
τ	stress
τ_0	yield stress
φ_i	rotation at the point i, where $i = A, B$ for the supports and $i = C$ for the cracked section
ϕ_{perc}	critical solid fraction value
Ω	volume of the sample in (Roussel and Coussot 2005)

Abbreviations

FRSCC	fibre reinforced self compacting concrete
FRVCC	fibre reinforced vibrated compacted concrete
SCC	self compacting concrete
SFRC	steel fibre reinforced concrete
SFRSCC	steel fibre reinforced self compacting concrete
VCC	vibrated compacted concrete
VMA	viscosity modifying admixtures

Subscripts

C	concrete
f	fibre
max	maximum
$struct$	structural element
T	transducer